Multifunctional and Multi-Staged Reactors for Liquid Fuel Generation from Renewable Feedstocks

A DISSERTATION SUBMITTED TO THE FACULTY OF THE
GRADUATE SCHOOL OF THE UNIVERSITY OF MINNESOTA
BY

Hui Sun

IN PARTIAL FULFILLMENT OF THE REQUIREMENTS FOR THE
DEGREE OF DOCTOR OF PHILOSOPHY

Adviser: Lanny D. Schmidt

September, 2012

© Hui Sun 2012
ALL RIGHTS RESERVED

ACKNOWLEDGMENTS

The completion of this thesis would not have been possible without assistance from a number of people. Firstly, I would like to thank my advisor, Professor Lanny D. Schmidt, for giving me the opportunity to be a part of his group. I highly appreciate his patience, and beneficial insightful discussions. I turned out to be a very independent researcher because of my advisor's "hands-off" management. Secondly, I would like to take this opportunity to thank Mark Huberty, who helped me to start my project in methanol synthesis. I am deeply indebted to him for his guidance and discussions. I would like to thank Reetam Chakrabarti and Samuel Blass for many suggestions on experiments, data analysis and writing. I want to thank Jeremy Bedard and Alex Marvin, for providing me with many good ideas during discussions and group meetings. I want to thank Christine for the delicious food she brought to the office, which provided us energy to work harder in the lab. I wish to offer thanks to all the undergraduate researchers for experimental assistance: Tyler Josephson, Richard Hermann, Edward Michor, and Corey Rosenthal.

I am also sincerely grateful to my husband, Ken-Hsuan Liao (Kirby), for constant support, for encouraging me to try out my own ideas, for interesting discussion about politics, entertainment, for all small things that happened in our lives, and for making a promising future picture and planning every detail in it. I want to thank my parents for cheering me up and encouraging me through graduate school. Last, but not the least, I would like to thank all my friends, Yanfei, Varoon, Nandita and Aruna, who shared happiness and difficulties with me in these 4 years of graduate school.

ABSTRACT

With fast depletion of fossil fuel, finding alternative and sustainable energy sources is one of the largest problems we currently face. Alternative energy sources, such as biomass and plastic waste, are good starting materials to potentially reduce our dependence on fossil fuel. Biomass is a sustainable feed stock, but it requires densification due to lower energy density. Biomass is also a distributed energy source; hence processing biomass continuously in a small-scale reactor with short residence time may be highly profitable. Plastic wastes derived from petroleum products are also a good replacement, since they can be recovered or processed to synthetic crude oil for use in transportation.

Catalytic partial oxidation (CPO) of biomass or plastics over a noble metal catalyst which convert the solids (or liquids) into syngas and then to light hydrocarbons, is a promising technique to generate suitable liquid fuels. The CPO product, syngas, can be used to produce methanol over a $Cu/ZnO/Al_2O_3$ catalyst under elevated pressure. Alternatively, the CPO technique could be integrated with a dehydration reaction to produce densified liquid fuel (DME and butene) from biomass-derived alcohols.

Methanol, one important product generated from biomass-derived syngas, is a platform for production of higher hydrocarbons. Chapter 2 describes small-scale methanol synthesis in a multifunctional reactor over a $Cu/ZnO/Al_2O_3$ catalyst. Conversion is increased by using *in situ* condensation with water as a coolant. Parallel hydrogenation of CO, CO_2 produces the largest amount of methanol in the shortest period of time, and is closest to equilibrium in a fixed-bed reactor. A multifunctional reactor with

water coolant is able to increase the conversion by a factor of two.

Chapter 3 discusses methanol synthesis with *in situ* adsorption using nanocomposites (salt inside a porous matrix). $CaCl_2$ inside silica gel has high capacity to uptake a significant amount of methanol at the synthesis operating conditions, resulting in equilibrium shift towards the product (methanol) and increase in the single-pass conversion of the reactants (CO). Multiple multifunctional reactors were built and their single-pass conversions were investigated. An integration of *in situ* condensation and *in situ* adsorption is proposed to further increase conversion.

Chapter 4 and 5 describe the combination the CPO reaction and the dehydration reaction in an autothermal staged reactor to deoxygenate biomass-derived alcohols. The novelty of this reactor is that it integrates exothermic and endothermic reactions in a single reactor tube. Chapter 4 investigates the integration of the CPO reaction and methanol dehydration reaction to produce dimethyl ether (DME). Reactor configurations were compared, showing that a side feed of methanol between the two stages have the similar performance as those in an isothermal reactor with the dehydration reaction. Top feed methanol to the CPO stage results in decreasing in DME yield since part of the methanol consumed in the top stage is used to generate heat and drive the second stage endothermic reaction. Chapter 5 describes the use of a similar concept and reactor configuration with butanol as feed, since butanol is a next generation transportation fuel derived from biomass. The effect of isomers (n-butanol, 2-butanol, iso-butanol, and tert-butanol) and catalysts (HZSM-5, HFER, and γ-Al_2O_3) were studied in a systematic way. Butenes are the desirable dehydration product, which is the intermediate to produce transportation fuel or other chemicals. The integration of the CPO reaction and alcohol dehydration reaction also provides a potential way to reduce the capital cost of the process since it is not necessary to employ a fired heater or combustion chamber to preheat the butanol.

The fast oxidative pyrolysis of polystyrene (PS) waste in an autothermal fixed-bed reactor is discussed in chapter 6. The PS particle is fed in the reactor by an auger, which then reacted on the catalyst particle surface, and converted into styrene monomers and other minor products. The temperature of oxidative pyrolysis was varied from 600 ^{o}C to 900 ^{o}C. Production of styrene dimers and trimers was not observed. The styrene yield was 75% at high C/O ratio (2.2-2.4) and was 85% with H_2 as sacrificial fuel. The results of oxidative prolysis of PS provide valuable insights regarding the capabilities of catalyst for oxidative pyrolysis of other plastic wastes, e.g. polypropylene (PP), polymethyl methacrylate (PMMA), and etc.

In chapter 7, several experiments are proposed to explore more efficient ways to generate liquid fuel from biomass-derived syngas, including a multifunctional reactor with baffles and spinning catalyst baskets, one-step DME synthesis and one-step gasoline ranged hydrocarbon synthesis from syngas. Additionally, process integrations are also proposed to generate long chain hydrocarbons for transportation purposes. Methanol (generated from syngas) can be reacted with hyoxymethylfurfural (HMF) to obtain an acetal or hemiacetal product. A CPO reaction on the top stage with Guerbet reaction on the second stage is proposed to generate butanol from ethanol. Finally, more oxidative pyrolysis of plastic wastes is proposed with more complex feedstocks, such as PE, PP, and PMMA.

The diversity of applications suggests that biomass (or plastic waste) upgradation; involving reactor design, process integration and CPO reactions; are an important area of research. This thesis offers preliminary insights to understand the production of liquid fuel from sustainable energy sources with multifunctional or multi-staged reactors.

CONTANTS

7. Future Work

LIST OF TABLES

LIST OF FIGURES

CHAPTER
ONE

INTRODUCTION

SUMMARY

This chapter discusses the urgency of finding alternative energy sources due to the fast depletion of fossil fuels. Potential uses, problems and challenges of biomass and plastics, which are sustainable energy alternatives, are also discussed. Results in this thesis can be used to reduce the current energy dependence on fossil fuels by making liquid fuel from renewable and sustainable alternative energy sources. The techniques to synthesize liquid fuels involve multifunctional reactor, thermochemical reforming (e.g. steam reforming, catalytic partial oxidation, and water-gas shift reaction) in a millisecond contact time reactor. The potential catalysts are noble metal catalysts, such as Rh and Pt loaded on solid-acid supports. These supports can have different geometries and different metal loadings. Zeolite catalysts can also act as solid-acid catalysts to deoxygenate biomass and biomass-derived alcohols, and to increase their energy density. At the end of this chapter, a thesis overview provides an outline of experiments performed, and discusses results and their impact on the current energy infrastructure.

1.1 Introduction

We are facing tremendous challenges in the form of soaring global energy demand, diminishing fossil fuel resources and ever increasing industrial waste. This chapter serves to describe the need for sustainable alternative energy sources, with an emphasis on the role that biofuels will likely fulfill in the near future. This chapter introduces biomass and plastics as alternative energy sources, as well as noble metals and zeolite as catalysts. This chapter also presents technologies for generating liquid fuels, such as methanol in a multifunctional reactor, and thermochemical reforming process in a millisecond short contact time reactor. The research presented in this thesis aims to discover more pathways leading to the development of new technologies to produce sustainable biofuels and to recycle plastics.

1.2 Fossil Fuel Consumption

With the depletion of fossil fuels, the energy crisis has become one of the most important technological challenges of the near future. Fossil fuels consist of oil, natural gas and coal, which will last approximately for 40 years, 75 years and 200 years, respectively, at current consumption rates [1]. In 2007, sources of energy consisted of petroleum (36.0%), coal (27.4%), natural gas (23.0%), totaling 86.4% of the world's primary energy consumption [2]. World energy consumption is growing about 2.3% per year. The global energy supply is roughly 12 terawatts for human consumption annually, which is equivalent to 2000 barrels of oil every second [3].

Fossil fuels are non-renewable resources since their generation require millions of years. Fuel reserves are being depleted much faster than they are created. The world's liquid fuels supply meets demand at 87 million barrels per day prior to 2012. By 2030, the world's liquid fuels supply will decrease to 43 million barrel per day, while the demand is

expected to rise to 105 barrels per day [4]. More than 50% of world's fuels will have to be supplied by unidentified sources [4].

Furthermore, the production and use of fossil fuels raise environmental problems and concerns. The consumption of fossil fuels produces around 21.3 billion tons of CO_2 per year. There is a net increase of 10.65 billion tons of atmospheric CO_2 per year. It is estimated that natural processes can only absorb about half of the CO_2 released into the atmosphere [5]. The amount of CO_2 released into the air increases substantially every year. CO_2 is one of the greenhouse gases that greatly contributes to global warming, causing the average surface temperature of the Earth to rise. This emphasizes the need of finding alternative carbon natural fuel.

In addition, coal consumption generates waste products that also contain mercury, uranium, thorium, arsenic, and other heavy metals. Therefore, sustainable and environmental friendly energy sources urgently need to be investigated.

1.3 Alternative Energy Source – Biomass

1.3.1 Composition of Biomass

Non-fossil fuel sources include biomass, hydroelectric, nuclear, geothermal, solar, tidal, wind, etc. Among these, biomass is abundantly available. Biomass is mainly derived from wood (forest and agriculture), garbage, waste, and alcohol fuels as shown in Fig 1.1. The biggest source for biomass is wood. Most of the wood energy is derived from lignocellulose. Lignocellulose consists of cellulose, lignin and hemicellulose. Those three components comprise nearly 90% of all plants. The lignocellulosic energy is derived either from harvested wood or from wood waste streams. The second largest energy source from biomass is waste energy, such as municipal solid waste (MSW), manufacturing waste, and landfill gas. Alcohol fuels are also an important energy source

from biomass. The alcohols are derived from sugars or oils. Alcohol fuels can be used directly, like other fuels, or as an additive to gasoline.

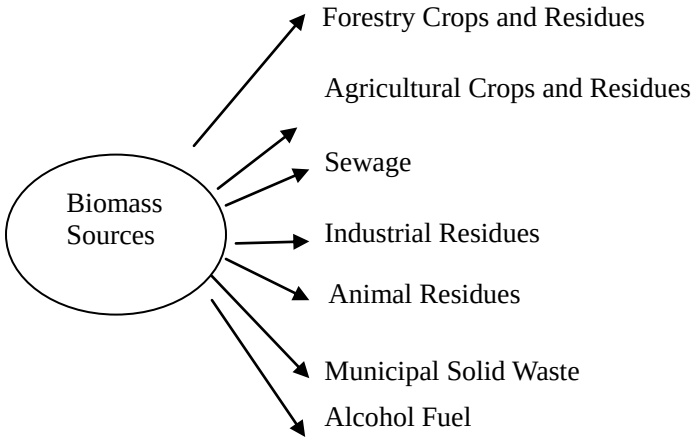

Figure1.1 Different sources of biomass.

1.3.2 Converting Biomass to Power

Historically biomass utilization involved heat generation from direct combustion and anaerobic digestion processes. More recently, biomass energy is extracted by combined heat and power (CHP) and gasification processes. The CHP process has higher energy efficiency than direct combustion. In the gasification process, biomass is combusted with controlled amount of oxygen to produce syngas (CO/H_2). Syngas is then passed through a gas or a steam turbine to produce electricity. This process is much cleaner than traditional coal combustion for electricity generation as it only produces water and CO_2 as waste products. Syngas can also be further processed to make liquid biofuels or other chemicals. The first U.S. commercial scale biomass gasification demonstration plant began in 1998 at the McNeil Power Station in Burlington, Vermont. This power station is capable of generating 50 MW of power from local wood waste products [6].

Until 2009, biomass was the largest source of renewable electricity. In the United States, 50 billion KWH of electricity is generated from biomass. This is nearly 1.5 % of nation's total electricity uses [6]. The Energy Information Administration (EIA)

estimated that ~600 million tons of biomass would be available and that would meet 12% of the nation's electricity needs by 2025.

1.3.3 Advantages of Biomass

One advantage of biomass is that it is relatively abundant. Jenkins *et al.* [7] reported an estimate of forest biomass for the mid-Atlantic region of the United States. Maximum forest biomass averaged 248 and 200 $Mg \cdot ha^{-1} \cdot yr^{-1}$ in hardwood and softwood forest types, respectively.

Another major advantage of using biomass as an energy source is that it is carbon neutral and does not contribute to the process of global warming. In a typical biomass life cycle, plants convert atmospheric CO_2 into biomass. The CO_2 is released back into the atmosphere when biomass energy is harvested. The CO_2 is again converted to biomass by plants during the next crop's growth cycle [8].

Another advantage of choosing biomass as an energy source is that it helps in solid waste management. Millions of tons of solid wastes, including hazardous waste, recyclable waste and construction waste, are produced by human activities. These wastes could be utilized as biomass, so that it simultaneously solves the problems of pollution and increasing demand of energy.

1.3.4 Disadvantages of Biomass

Besides the above mentioned advantages of using biomass for energy generation, there are two major problems associated with it. Firstly, biomass being a highly distributed resource, transporting bulky biomass over long distances to a central processing facility is a key barrier to its utilization. Ruan *et al*. [9] reported the cost of transporting biomass over different distances (Table 1.1). The cost for transporting 1 dry ton of biomass for 35 km is $43, which is 20% ($52) less than the cost for transporting it for 3 times the distance (100 km). Hence, the financial advantage provided by a large processing capacity is potentially offset by the high delivery costs of the feedstock, and suggests that biorefining should adopt small-scale facilities to become economically viable. Therefore,

in terms of utilizing biomass as an energy source, highest profit may not be associated with a large-scale process but with a small-scale system. Secondly, the energy density of biomass is relatively small compared to other liquid fuels (e.g. gasoline, diesel, and butanol, etc) as shown in Table 1.2 due the presence of oxygen atoms in biomass. Much research has been focused on oxygen removal and increasing carbon-carbon chain length by dehydration reactions [10], aldol condensation reactions [11], and esterification reactions [12] to increase the energy density of biomass.

Based on the above mentioned disadvantages of biomass, a small-scale biomass processing facility, such as small-scale a biorefinery, is a more viable alternative for biomass utilization as an energy source. A smaller size biorefinery might offer multiple advantages, such as- significantly reduce transportation cost for feedstock, non-catastrophic accidents, simpler start up/shut down processes, and lower capital investment and operating cost. In contrast, disadvantages of large plants include risk of accidents on an industrial scale, large capital investment, difficulty in modifying the infrastructure once it has been constructed, and complex start up/shut down procedures, etc.

The research presented in this thesis includes the generation of high energy density liquid fuels on a small-scale (e.g. bench-scale or farm-scale) with new technologies, such as multifunctional reactor or multi-staged reactors.

Table 1.1 Biomass delivery cost [9]

Facility capacity (dry ton/day)	Delivery cost ($/dry ton)	Hauling distance (one-way, km)
500	43	35
4000	52	100

Table 1.2 Energy densities of various materials in their natural states

	Energy density (MJ/kg)	**Energy density (MJ/L)**
H_2	123	5.6
coal	24	-
Natural gas	53.6	0.00364
Gasoline	47.2	34
Diesel	45.4	38.6
Methanol	19.7	15.6
Ethanol	30	24
Butanol	36.6	29.2
Biomass	15	18

1.4 Alternative Energy Source-Plastic Waste

Plastic materials are polymeric materials consisting of monomer units, which repeat the chemical structure throughout the chain. Most of plastics are derived from petrochemicals. Representative plastic materials are polyethylene (PE), polypropylene (PP), polystyrene (PS), polyethylene terephthalate (PET), and poly(methyl methacrylate) (PMMA).

Plastic wastes create many problems, and the largest one comes from that fact that they are not biodegradable. The chemical bonds in plastic make it durable and difficult to degrade naturally because micro-organisms do not possess the enzymes required to break them down. The amount of plastic waste generated all over the world is enormous every year. Since the 1950s, one billion tons of plastic waste has been discarded and may persist for hundreds or thousands of years [13]. Thirty one million tons of plastic waste was generated in 2010, which consisted of 12.4% of total Municipal Solid Wastes (MSW). In that year, the United States generated almost 14 million tons of plastic as packaging and containers, and only 8% of them were recovered for recycling [14]. Besides that, nurdles, the tiny pre-plastic pellets, kill a significant number of fish and birds that mistake them for food [15]. Traditional waste management methods such as landfill disposal, incineration and recycling have failed to provide an opportunity to resolve all these problems. Incineration of plastic waste is not environmentally friendly due to the production of toxic gases as by-products. Inadequate levels of recycling aggravate the waste problem.

Plastic recycling is one of the most environmentally friendly solutions to the plastic waste problem. Across the United States, there are about 1,800 businesses or post-consumer plastics recycling according to the American Chemistry Council's estimation. Plastics from MSW are usually collected from recycling bins or drop-off sites. The plastic waste is sorted out by plastic type and sent to a reclaiming facility. At the facility, plastic is washed and ground into small pieces. The small pieces are then dried, melted, filtered, and formed into pellets, which are shipped to the manufacturing plants for new plastic production [14].

The most popular recycled plastic material is PET and HDPE (high density PE). The recycled PET is used in the carpet and textiles industry, while the primary market for recycled HDPE is the bottle manufacturing. According to American Chemistry Council, the market demand for recycled plastics exceeds the supply of recycled plastics from waste steams [14]. Much research has focused on plastic waste recovery with one plastic or plastic mixture. Converting plastic waste into a high energy content liquid fuel is gaining importance. Rational Energy is setting up chemical plants to convert plastic wastes, mainly PE and PP, into synthetic oil by using batch reactors by thermal pyrolysis in Minnesota and Florida [16].

1.4.1 Polystyrene

Polystyrene is an aromatic polymer made from the monomer, styrene, which is a liquid hydrocarbon obtained from petroleum processing. It is a thermoplastic, which is a solid at room temperature, while it flows if the temperature is higher than its glass transition temperature (Tg ~100 ^{o}C). Polystyrene is one of the most widely used plastics, with the production up to several billion kilograms per year. Polystyrene is a recyclable plastic, and increasing oil prices have increased the necessity of recycling polystyrene.

The synthesis reaction of polystyrene via free-radical polymerization is shown in Fig 1.2. Typically, a few thousand monomers comprise a chain of polystyrene, giving it a high molecular weight ranging from 100,000 - 400,000 g/mole. The carbon-carbon double bond in vinyl group of styrene is replaced by a much stronger carbon-carbon single bond, resulting in the high chemical stability of polystyrene.

1.4.2 Polymethyl Methacrylate (PMMA)

Poly(methyl methacrylate) (PMMA) is the synthetic polymer of methyl methacrylate, and the synthesis reaction takes place via radical polymerization (Fig 1.3). PMMA is a transparent thermoplastic, which is often used as a lightweight or shatter-resistant alternative to glass. PMMA is an economical alternative of polycarbonate (PC) if high strength is not required. PMMA is a popular plastic since it is easy to handle and process, as well as it has moderate physical properties and low cost.

PMMA has wide applications in transparent glass substitutes [17], medical technologies [18], plastic optical fibers, semiconductors [19], and roofing and waterproofing applications. Much research focused on recovering PMMA or PMMA blends with other plastic wastes. Kaminsky *et al*. [20] reported recovery of MMA monomer from PMMA in an indirect heated fluidized bed in a pilot plant with the highest yield of 98 wt%. Szabo *et al*. [21] reported recovery of PMMA and acrylonitrile – butadiene – styrene (ABS) with high yield by thermal decomposition for fuel admixture purpose.

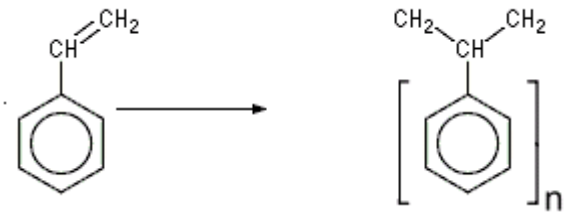

Figure1. 2 Styrene monomers undergo polymerization reaction to form polystyrene.

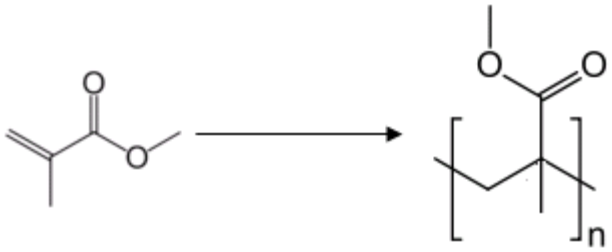

Figure 1. 3 Methyl methacrylate monomer undergoes polymerization reaction to form PMMA.

1.5 Multifunctional Reactor

Multifunctional reactors are reactors that combine at least one more function from unit operation, such as separation, heat exchange, or electrical unit operation, which conventionally would have operated in a separate piece of equipment. Many multifunctional reactors have been commercialized over the past couple of decades. For example, reactive distillation is used for separating chemicals, and reactive absorption is commercialized for removal of acid gases in the petroleum production and refining industries [22]. Multifunctional reactors are used to integrate processes in a single reactor in order to increase single-pass conversion.

The most important advantage of a multifunctional reactor is that it can enhance reaction rate, conversion, yield, or selectivity. Another significant advantage of multifunctional reactors is that they can significantly reduce the operating cost and capital investment. The multifunctional reactor may improve product quality and increase catalyst life. However, multifunctional reactors are associated with some disadvantages as well. They have complex process behaviors for relatively new technologies as they have a narrow operating window. They require more sophisticated process design and modeling, and are associated with increased development costs and higher scale-up risks [22].

The multifunctional reactors presented in this thesis integrate reaction and separation processes. More specifically, the separation processes are *in situ* condensation and adsorption for methanol synthesis reactions (chapter 2 and 3). All the experiments are carried out in a bench-scale system which requires future scale-up for higher economic profit.

1.6 Thermochemical Reforming

1.6.1 Steam Reforming

Steam reforming is a method to produce hydrogen or other useful products from fossil fuels, such as natural gas, alkanes, and oxygenates, etc. with the addition of a high temperature steam. The steam methane reformer (SMR) is widely used in industry to make hydrogen as shown in the Equation (1-1). The simplified block diagram of SMR is shown in Fig 1.4.

$$CH_4 + H_2O \rightleftharpoons CO + 3H_2 \quad \Delta H = 207kJ/mol \qquad (1-1)$$

To produce syngas (CO and H_2), the steam reformer is operated at 3-25 bar at 650-900 ^oC [23]. This reaction is highly endothermic, and hence the heat is provided by additional fossil fuel combusted externally in tubes passing through the catalyst bed. The residence time is in the range of seconds, leading to a complex transient behavior in the reactor which makes it difficult to scale down to a portable reactor, and reduce the capital cost. Current research has focused on developing small units based on similar technologies to produce H_2 as feedstock for fuels cells, including the reforming of methanol, natural gas, propane, ethanol, etc.

1.6.2 Catalytic Partial Oxidation

Catalytic partial oxidation is (CPO) a type of chemical reaction in which a fuel-oxygen mixture is partially combusted in a reactor, creating a hydrogen-rich syngas. The syngas can then be used for various applications, such as H_2 fuel cell. The general equation of CPO is shown in the Equation (1-2), (1-3). The simplified block diagram of CPO reaction is shown in Fig 1.5.

$$C_xH_y + \frac{x}{2}O_2 \rightarrow xCO + \frac{y}{2}H_2 \qquad (1-2)$$

$$C_xH_yO_z + \frac{x-z}{2}O_2 \rightarrow xCO + \frac{y}{2}H_2 \qquad (1-3)$$

For those oxygenates in which x = z, the production of syngas (CO and H_2) are from a strong endothermic decomposition reaction, and some CO_2 and H_2O are produced [23]. For alkanes in Equation 1-2 and oxygenates in Equation 1-3 with x > z, the reaction can be exothermic, and able to sustain a long operation [23]. The major advantages of carrying out a CPO reaction over steam reforming reaction is that it takes place with a residence time on the order of milliseconds rather than seconds which allows for smaller reactors. Fast kinetics and short residence time makes CPO more suitable for biomass utilization on a relatively small-scale.

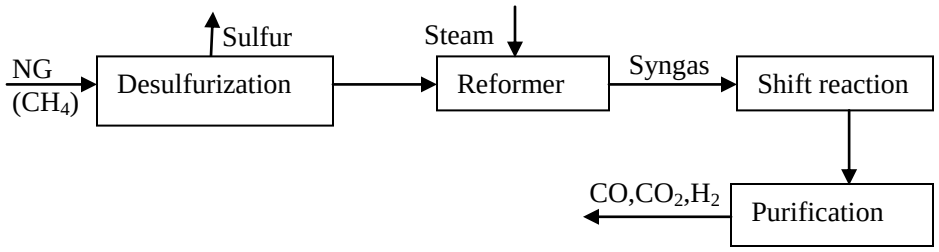

Figure 1.4 Block diagram for steam methane reforming (SMR) process: pretreatment process, reforming process, a shift reactor and the gas purification process. NG: natural gas.

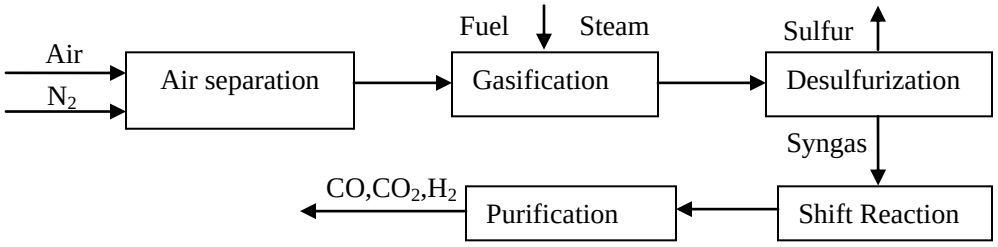

Figure 1.5 Block diagram for catalytic partial oxidation process: pretreatment process, gasification process, a shift reactor and the gas purification process. Fuel is the carbon source here.

1.6.3 Water-gas Shift (WGS) Reaction

Water-gas shift reaction is the chemical reaction in which CO reacts with water vapor to form CO_2 and H_2 (Eqn 1-4). This reaction is reversible and exothermic. Hydrogen production is favored thermodynamically at low temperatures. WGS reaction takes place at 100-120 bar and 350-370 ^oC with a residence time of less than one second. Wheeler *et al*. [24] reported that WGS reaction can occur on noble metal catalyst with CO conversion as high as 80% with the residence time on the order of tens of millisecond. WGS reaction takes place with many other reactions, such as steam reforming of methane or other hydrocarbons. This reaction is also important for the production of high purity H_2 for use in the production of ammonia and H_2 fuel cell. The starting reagent, CO, comes from the natural gas steam reforming (Eqn 1-1) or the CPO reaction of various fuels (Eqn 1-2, 1-3).

$$CO + H_2O \rightleftharpoons CO_2 + H_2 \qquad \Delta H = -41.1\ kJ/mol \qquad (1-4)$$

1.7 Millisecond Contact Time Reactor

The CPO reaction is carried out in a short contact time reactor with noble metal catalyst, typically Rh, Pt, Rh-Ce and Pt-Ce on an α-alumina support. The residence time of this reactor is within the range of milliseconds, which is 100-1000 times faster than conventional reactors. The short contact time would enable the use of smaller reactors and will reduce catalyst loading. The Schmidt group has contributed to this technique by conducting research on catalytic partial oxidation of alkanes, such as methane [25] to hexadecane [26], dehydrogenation of ethane to ethylene [27], and autothermal reforming of alkane and oxygenates [28]. Very recently, the Schmidt group has also developed a continuous process with high throughput to process biomass model compounds, such as cellulose and polyethylene [29], into syngas, as well as pyrolyze cellulose into bio-oil. Continuing research has focused on modeling the reaction kinetics and integration of this process with other unit operation for better biomass utilization.

The general millisecond reactor is composed of a quartz tube reactor with catalysts (monolith or spheres) sandwiched between two monoliths as heat shields. Heat shields on both sides of the catalyst reduce the radiative heat loss. Gaseous reactants flow through the reactor tube producing both heat and chemicals. Under reaction conditions, both heterogeous and homogenous reactions take place in the reactor with mass and heat transfer. It is generally considered to have mass transfer limitations in these conditions since the kinetics are fast enough both on the catalyst surface and in the gas phase.

1.8 Catalysts and Supports

1.8.1 Metal Catalysts

Conventional steam reformers used Ni-based catalysts supported on an α-Al_2O_3 or $MgAl_2O_4$ support with addition of peripheral components to prevent it from being deactivated by carbon or sulfur [30]. Ni-based catalysts supported by perovskite [31] or spinel crystals are relatively better in terms of stability and sulfur-resistance. However, they tend to sinter in the redox atmosphere in autothermal reformer (ATR) environments. Recent efforts have been spent on developing bimetallic catalysts to improve the performance of Ni-based catalysts [32].

Ni-based systems give reasonable syngas yields but require operation at low temperatures to reduce metal loss. Experiments involving noble metals such as Rh, Pt and Ru, show stable performances compared to other transition metals. However the disadvantage of using noble metals is their high cost. Thus exploring methods to minimize noble metal loading is crucial to make this process economically viable. The Schmidt group has reported the use of Rh, Pt, Rh-Ce and Pt-Ce catalysts to convert various fuels such C_1-C_{12} alkanes, C_1-C_3 alcohols, ethers, acids, cellulose, and polyethylene into syngas or bio-oil in the past two decades [25-28]. They have shown that the Rh catalyst is widely regarded as an excellent partial oxidation catalyst with high reforming activity downstream of the oxidation zone in the catalyst bed, while the Pt catalyst is frequently used as a combustion catalyst and has been shown to have lower

reforming activity [33]. Addition of Ce also makes the catalysts more coke resistant since it stabilizes the surface area of the catalyst and prevents the sintering of Rh particles [34]. Donazzi *et al.* [35] reported that the addition of Ce also has an active role in the CPO reaction kinetics. The role of noble metal catalysts will be explained more in chapter 6.

1.8.2 Catalyst Supports

The typical supports for catalysts in CPO reactions are α-Al_2O_3 or ɣ-Al_2O_3. Catalyst support geometry (monolith, monolith with washcoat, and spheres) also plays an important role in the CPO reactions. The monolith has the lowest surface area compared to the monolith/washcoat and sphere catalysts. The metal particle sizes are different depending on the support geometry. Metal particles (e.g. Rh-Ce) on alumina spheres are generally spherical and less than 50 nm. In contrast, these metal particles are much larger and non-uniform, when deposited over the ɣ-Al_2O_3 washcoat supported on the monolith. Previous work has demonstrated that metal particles have much better dispersion on spherical supports, as compared to that on monolithic supports [3]. This leads to better catalyst activity of metal particles on spherical supports. The morphology of catalysts was also studied by scanning electron microscopy (SEM) [33].

Degenstein *et al*. [36] studied that increasing the washcoat loading results in higher selectivity of olefins from n-hexadecane. They showed that increasing Rh loading above a few percent led to the formation of a Rh film on the catalyst support. The presence of washcoat seems to keep Rh spread out on the surface at high reaction temperatures. The high washcoat loading also decreased pore diameters.

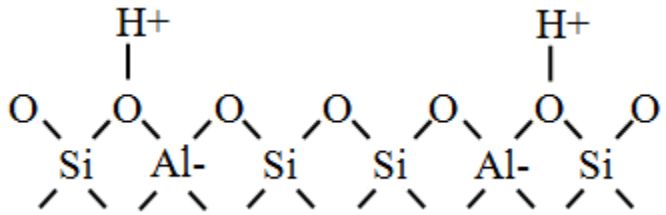

Figure 1.6 Two dimensional zeolite structure (brønsted acid site).

1.8.3 Zeolite Catalysts

Zeolites are microporous aluminosilicate materials have been commonly used as commercial adsorbents and catalysts. As of November 2010, 194 unique zeolite frameworks have been identified, and over 40 naturally occurring zeolite frameworks are known [37]. Currently, the world's annual production of natural zeolite is about 3 million tons. Zeolites are able to selectively sieve molecules based on size exclusion processes due to their regular pore structure.

Much research has focused on zeolite synthesis processes. There are several types of synthetic zeolite that come from crystallization of aluminosilicate in the presence of alkali and organic templates. The templates are later removed by calcination, leaving the microporous structures. The zeolite properties depend on reaction mixture composition, synthesis temperature, pH of the synthesis solution, temperature, reaction time, and pre-reaction "seeding time" [38-39]. Other methods, such as the microwave synthesis method, attracted much attention from both industry and academia since they were able to shorten the synthesis time [40-41].

Zeolites are widely used in industry and academic research. They can be used as catalysts for reactions or adsorbents for water purification. Their largest use is in the production of laundry detergents and as catalysts for reactions. The most commonly used zeolites are MOR (mordenite), MFI (mordenite framework inverted), FER (ferrierite), Faujasite, zeolite β, etc. Zeolites are the primary active component (15-50 wt%) in the catalyst of a fluid catalytic cracking (FCC) unit in the petrochemical industry. The proton exchanged aluminosilicate zeolites process brønsted acid sites which are used to catalyze dehydration reaction, esterification reaction and so forth.

This thesis presents the integration of CPO catalysts and zeolite catalysts in a millisecond reactor to deoxygenate biomass-derived liquid fuel (chapter 4-5).

1.9 Thesis Outline

The research for the production of sustainable liquid fuel from biomass or plastics based material has been divided into several chapters, specific to the corresponding experimental work.

1.9.1 Methanol Synthesis in a Multifunctional Reactor (*in situ* Condensation)

Methanol is emerging as a key intermediate platform for higher hydrocarbon productions. The synthesis of methanol from biomass-derived syngas in a multifunctional reactor will be discussed in chapter 2. Reaction and separation process (*in situ* condensation) are integrated in a multifunctional reactor to increase reactant single-pass conversion for small-scale applications. The conversion was increased by a factor of two due to introduction of internal condenser.

1.9.2 Methanol Synthesis in a Multifunctional Reactor (*in situ* Adsorption)

In chapter 3, the multifunctional reactors to synthesize methanol is introduced with *in situ* adsorption. $CaCl_2$, $Ca(NO_3)_2$, and LiCl are investigated as a possible absorbent in the reactor. The elevated conversion of reactant (higher than equilibrium conversion) is achieved due to *in situ* adsorption. The batch reactor reached 85% conversion in approximately 2 days which is much higher than the original equilibrium conversion (58%). This result will have important implications for methanol manufacturing.

1.9.3 Autothermal Staged Reactor

Deoxygenation of biomass molecules or biomass-derived compounds to increase their energy density is crucial for biomass utilization. Dehydration reactions are used to deoxygenate the biomass molecules or biomass-derived compounds. This operation could be located in decentralized zones without external heating sources due to highly distributed nature of biomass. Hence, the integration of exothermic CPO reaction and endothermic dehydration reaction will be suitable for biomass utilization in small-scale

operations. In chapters 4-5, the autothermal staged reactor with liquid fuel feedstocks, like methanol and butanol, is presented and discussed. This reactor achieves a high yield of dimethyl ether (80%) and of butenes (95%) with less than 100 ms residence time.

1.9.4 Fast Pyrolysis Polystyrene in an Autothermal Fixed-bed Reactor

The recovery of styrene monomers from polystyrene is studied using an autothermal fixed-bed reactor with noble metal catalyst in chapter 6. High yield of monomer (~75%) is obtained from polystyrene without the use of external heating in a short contact time. The effect of co-feeding CPO products, such as CO, CO_2, H_2 and steam is also studied. The monomer yield reaches 85% with the addition of H_2 as sacrificial fuel. This demonstrates an effective, continuous process with low operating cost and high throughput process to recover styrene monomers from polystyrene.

CHAPTER
TWO

SMALL-SCALE SYNTHESIS OF METHANOL IN A MULTIFUNCTIONAL REACTOR

SUMMARY

This chapter focuses on high pressure methanol synthesis in a multifunctional reactor with an *in situ* condenser to increase the single-pass conversion. Methanol is emerging as an important platform for production of higher molecular weight hydrocarbon. Methanol can also be used as a fuel additives or a solvent. In this chapter, three feedstock of methanol synthesis is studied and compared. The methanol synthesis process is optimized by varying the H_2 to carbon oxides (CO or CO_2) ratio and space velocity. A multifunctional methanol synthesis reactor with an *in situ* condenser provides an opportunity to remove the products during their synthesis, and shifts equilibrium in the favor of methanol production. The integration of reaction and separation process also significantly reduces the operating cost. The conversion in a multifunctional reactor is increased by a factor of two as compared to that in a conventional plug flow reactor. More multifunctional reactor designs are proposed in chapter 7 as future work.

2. 1 Introduction

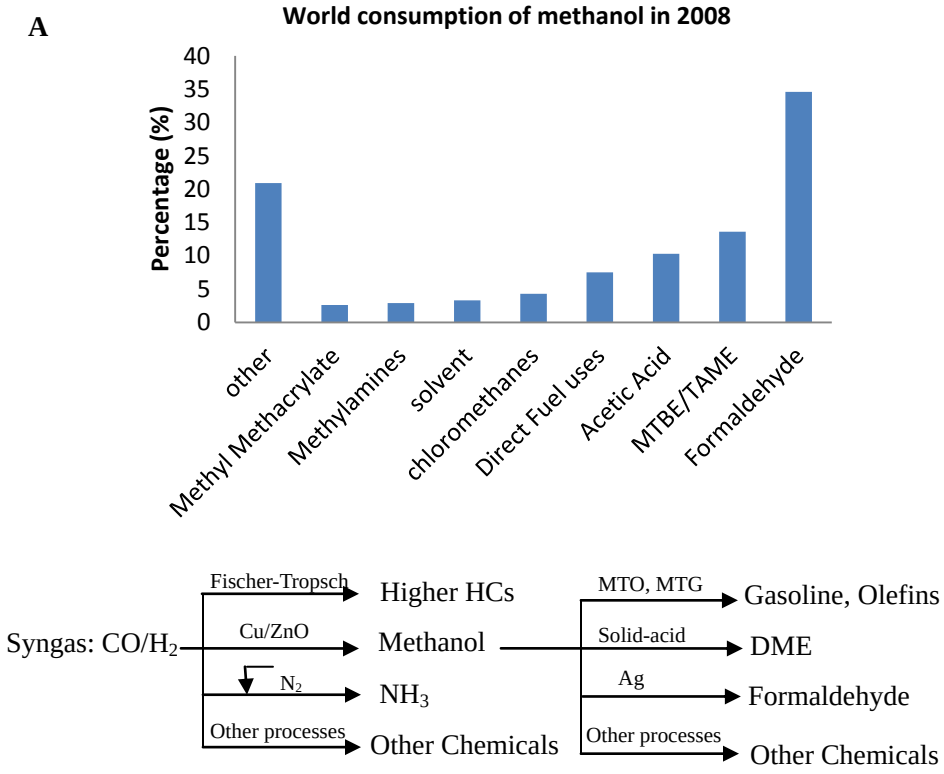

Figure 2.1 (A) World consumption of methanol in 2008 [45]. MTBE: methyl *tert*-butyl ether. TAME: *tert*-amyl methyl ether. (B) Potential syngas products [9]. MTO: methanol to olefins, MTG: methanol to gasoline.

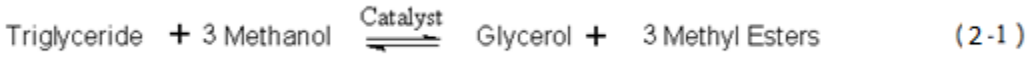

Methanol is the smallest alcohol molecule, and is a light volatile, colorless, and flammable liquid. Methanol is also called wood alcohol since it was once produced as a byproduct of the destructive distillation of wood. Methanol is also produced naturally in anaerobic metabolism of many varieties of bacteria. At room temperature, methanol can be used as antifreeze, solvent, fuel, and denaturant for ethanol. Methanol can also be used to produce biodiesel via transesterification reaction as shown in Equation (2-1). Methanol

is emerging as a platform for synthesizing larger hydrocarbons. This makes methanol attractive for transportation industry. Methanol is a good alternative fuel for automobiles and power plants, and an important feedstock for making chemicals such as formaldehyde, dimethyl ether (DME) and acetic acid [44], as shown in Fig 2.1A [45].

In terms of utilizing biomass of energy source, biomass can be successfully converted into synthesis gas (syngas) by partial oxidation in millisecond reactors [42]-[43]. As shown in Fig 2.1B [9], syngas can be used to produce olefins, gasoline, diesel, and waxes by Fischer-Tropsch reactions over Fe, Co, or Ru catalysts. Syngas could also lead to the production of mixed alcohols and aldehydes. One of the major uses of syngas is methanol production.

Methanol also finds applications in synthesis of DME by dehydration reaction and gasoline by methanol to gasoline (MTG) processes. Converting methanol into DME is attractive due to various potential uses and advantages of DME. Most importantly, DME is considered as a clean alternative fuel for diesel engines [46]-[47] and a key intermediate for the production of various chemicals including dimethyl sulfate, methyl acetate, and light olefins [48]. The physical properties of DME are similar to that of liquefied petroleum gas (LPG), making it an attractive LPG substitute [49]. Dehydration reaction (removal of oxygen atoms) in the process of producing DME from methanol is highly desirable to increase biomass energy density. In addition, synthesizing gasoline from methanol by MTG reaction is also desirable since gasoline is primarily used as fuel in internal combustion engines. Furthermore, liquid fuels, such as gasoline (34.2 MJ/L), has a higher energy density per volume than that of methanol (15.6 MJ/L).

In the 1960s, ICI Co. Ltd. laid the foundation of modern methanol production by developing Cu-based catalysts ($Cu\text{-}ZnO\text{-}Al_2O_3$) for low-pressure methanol production, decreasing the operating pressure from 200 atm at 400 ºC to 50-100 atm at 230 ºC [44]. Methanol is synthesized from CO, CO_2 and H_2 by the following three reactions:

$CO_2+3H_2 \rightleftharpoons CH_3OH+H_2O$	$\Delta H°_{rxn}$= - 49kJ/mol	CO_2 hydrogenation	(2-2)
$CO+2H_2 \rightleftharpoons CH_3OH$	$\Delta H°_{rxn}$= - 91kJ/mol	CO hydrogenation	(2-3)
$CO+H_2O \rightleftharpoons CO_2+H_2$	$\Delta H°_{rxn}$= - 41kJ/mol	Water gas shift	(2-4)

Three pathways of methanol synthesis are described in the literature: Reactions (2-2) and (2-4) will take place simultaneously for CO_2 hydrogenation, while only reaction (2-3) will occur for CO hydrogenation. In addition, reactions (2-2) to (2-4) represent parallel hydrogenation of CO and CO_2. Methanol synthesis is thermodynamically limited, and these reactions are exothermic which favor low temperature and high pressure.

Previous research has reported reaction kinetics and proposed mechanisms of methanol synthesis on Cu-based catalyst for three different pathways [50]-[51]. There is no universal kinetics for methanol synthesis reactions and some of the previous results are contradictory. Table 2.1 summarizes the important rate expressions for methanol synthesis over copper catalysts at different synthesis conditions [52]. As suggested by these kinetic expressions, methanol is an inhibitor for the reaction. It is also known from the literature that the active component of $Cu/ZnO_2/Al_2O_3$ catalyst is copper [52]. The formate and formyl species are the intermediate species for CO_2 hydrogenation and CO hydrogenation, respectively [52].

The key objective in this research is to investigate small-scale liquid fuel synthesis processes for the production of methanol with multifunctional reactors to increase the single-pass conversion. In the initial stage of this research, by comparing three methanol feedstocks, $CO/CO_2/H_2$ has been found to be the most suitable feedstock for small-scale methanol synthesis. A multifunctional reactor in which reaction and separation are integrated to increase the conversion of carbon oxides was constructed for methanol synthesis. As the part of future work (chapter 7), reactor designs, including a multifunctional reactor with baffles and rotating basket reactor would be implemented. One-step DME synthesis and one-step gasoline synthesis from syngas would also be aimed.

Table 2.1. Recent rate expressions for methanol synthesis over copper catalyst.

Reference	Catalyst	Conditions	Expression
Agny and Takoudis[53]	$Cu/ZnO/Al_2O_3$	CO/H_2 3-15 bar 250-290 °C	$r = k[p_{co}p_{H_2}^2 - \frac{p_{MeOH}}{K_{eq}}][p_{co}p_{H_2}^{0.5}]^{-1.30}$
Klier *et al*.[54]	$Cu/ZnO/Al_2O_3$	$CO_2/CO/H_2$ 75 bar 225-250 °C	$r = \frac{kA_0^3[p_{co_2}/p_{co}][p_{co}p_{H_2}^2 - \frac{p_{MeOH}}{k_{eq}}]k_{co}k_{H_2}^2k'^3}{(1+k'p_{co_2}/p_{co})^3(1+k_{H_2}p_{H_2}+k_{CO}p_{CO}+k_{CO_2}p_{CO_2})^3} + k'(p_{co_2} - \frac{p_{MeOH}p_{H_2O}}{k_{eq}p_{H_2}^3})$
Villa *et al*.[55]	$Cu/ZnO/Al_2O_3$	$CO_2/CO/H_2$ 30-94 bar 215-246 °C	$R_m = \frac{F_{CO}F_{CO_2} - F_{MeOH}/K_{eq}}{(C_1 + C_2F_{CO} + C_3F_{CO_2} + C_4F_{H_2})^3}$
Szarawarz and Reychman[56]	$Cu/ZnO/Al_2O_3$	$CO_2/CO/H_2$ 50 bar 190-260 °C	$R_1 = k_1p_{CO}^{0.5}p_{H_2}[1 - \frac{p_{CH_3OH}}{K_1p_{CO}p_{H_2}^2}]; R_2 = k_2p_{CO_2}^{0.5}p_{H_2}^{1.5}[1 - \frac{p_{CH_3OH}}{K_2p_{CO_2}p_{H_2}^3}]$
Skrzypek *et al*.[57]	$Cu/ZnO/Al_2O_3$	CO_2/H_2 50-70 bar 200-220 °C	$r_1 = k_1K_{H_2}^2K_{CO_2}[\frac{(p_{H_2}^2p_{CO_2}) - (1/K_{p1})(p_{CH_3OH}p_{H_2O}/p_{H_2})}{(1+K_{H_2}p_{H_2}+K_{CO_2}p_{CO_2}+K_{CH_2OH}p_{CH_2OH}+K_{H_2O}p_{H_2O}+K_{CO}p_{CO})^3}]$

2. 2. Experimental Setup

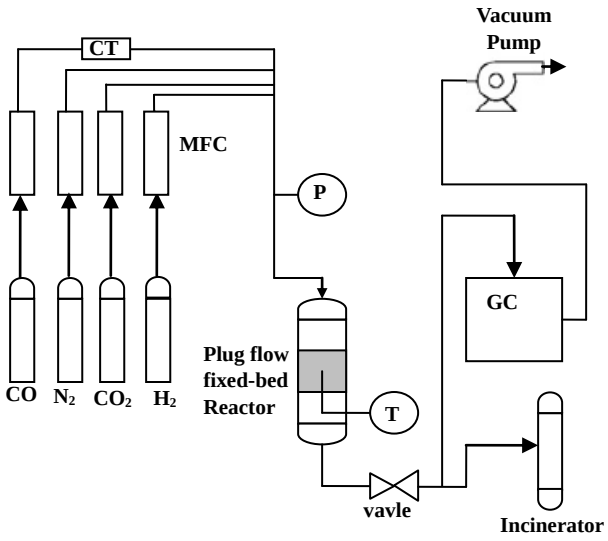

Figure 2.2 Small-scale methanol synthesis flow diagram. MFC: mass flow controller, CT: carbonyl trap, P: pressure transducer, T: temperature controller, GC: gas chromatograph.

In order to decide the best feedstock for small-scale methanol synthesis, three feeds (CO/H_2, CO_2/H_2, $CO/CO_2/H_2$) were examined in a fixed-bed plug flow reactor (Fig 2.2). Reactions were carried out at 230 °C and 50 bar unless otherwise specified. N_2 was used as an internal standard for the system. Four mass flow controllers (MFC: 5850s from Brooks Instrument) were used to control feed gases. A zeolite carbonyl trap was located downstream of the MFC to absorb carbonyls for CO [58]. Pressure was monitored by a pressure transducer, and temperature was controlled by a temperature controller. Type-k thermocouples were used to read temperatures in the catalyst bed. A valve was placed after the reactor, reducing the pressure to ambient. A 5890 HP Gas Chromatograph (GC) equipped with a Hayesep Q column was used to analyze the product stream.

Commercial catalyst $CuO\text{-}ZnO\text{-}Al_2O_3$ 51-series was purchased from KATALCO**.** The catalyst was in the pellet shape. The catalyst was grained and sieved to 300-500 μm size. The reduction procedure took place at the pressure of 8 bar with 13% of H_2 in N_2 (H_2:0.15 SLMP (standard liter per min) and N_2 = 1 SLPM) flow into the reactor. The

temperature ramp was in several steps. Temperature increased from room temperature to 130 ºC for 5 h, followed by rise from 130ºC to 180 ºC in 2 h. Finally temperature was increased from 180 ºC to 230 ºC in 5 h and maintained at 230 ºC until 24 h. Following this, temperature was lowered down to room temperature.

The total volumetric flow rate of the feed (excludingN_2) was maintained constant at 1 SLPM (standard liter/min). The feed compositions were CO_2/H_2= 1:3, CO/H_2=1:2, and $CO/CO_2/H_2$=2:1:7. The amount of N_2 fed into the reactor was 0.2 SLPM. The residence time of the reaction in the plug-flow reactor was 25.2 s. The carbon, hydrogen and oxygen atom balance was closed within typically less than 10%. The equilibrium methanol compositions and conversions were calculated from HSC software (Chemical Reaction and Equilibrium Software) at the experimental feed composition, temperature, and pressure.

2.3 Results and Discussion

2.3.1 Fundamental Studies of Methanol Synthesis

The steady state study, as shown in Fig 2.3, explores the time to reach steady state for each reaction, and the corresponding methanol composition and carbon oxide conversion. The definition of conversion is defined as shown in Equations (2-5) – (2-7). Parallel CO and CO_2 hydrogenation yielded the most methanol (13%) in the product stream with a conversion of 22%. In contrast, CO hydrogenation and CO_2 hydrogenation produced less methanol at 7.5% and 3% of the product stream with conversion of 18% and 17%, respectively. All three approaches reached steady state within 30 min. The data in this research were collected after steady state was established.

$$\text{CO}_2 \text{ conversion } = 1 - \frac{CO_{2\,flow\_rate\_out}}{CO_{2\,flow\_rate\_in}} \qquad (2\text{-}5)$$

$$\text{CO conversion } = 1 - \frac{CO_{flow\_rate\_out}}{CO_{flow\_rate\_in}} \qquad (2\text{-}6)$$

$$\text{CO, CO}_2\text{ conversion } = 1 - \frac{CO_{flow\_rate\_out} + CO_{2\ flow\_rate\_out}}{CO_{flow\_rate\_in} + CO_{2\ flow\_rate\_in}} \qquad (2\text{-}7)$$

An equilibrium study has been carried out by varying reaction temperature at a constant pressure of 50 bar (Fig 2.4). As shown in Fig 2.4, parallel hydrogenation of CO and CO_2 was relatively closer to equilibrium than the other two feedstocks (CO/H_2 and CO_2/H_2). For the reaction at different temperatures, the three feedstocks share the same trend. The methanol produced in the reaction rises to maximum and drops. An optimum methanol production took place at 230 ºC for CO_2 hydrogenation, 245 ºC for CO/CO_2 hydrogenation and 255 ºC for CO hydrogenation, respectively. As shown in this figure, for CO/CO_2 hydrogenation, methanol composition in the reaction approached equilibrium as temperature was increased. However, the catalyst ($Cu\text{-}ZnO\text{-}Al_2O_3$) deactivated near 300 ºC. In the range of suitable operating temperature (230 ºC-250 ºC), methanol composition of the reaction (12%), was far away from the equilibrium methanol composition (19 %) at 250 ºC.

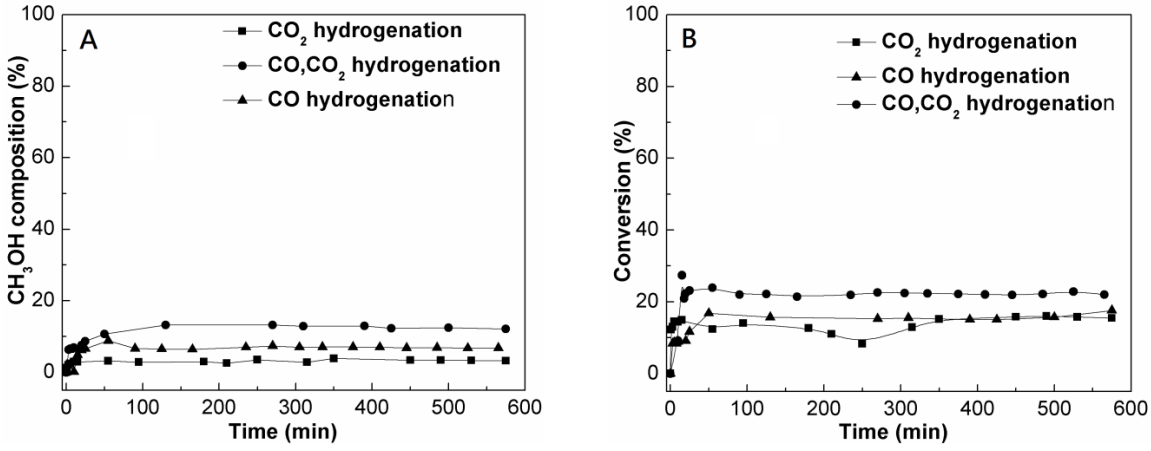

Figure 2.3 Steady state study for three methanol synthesis feedstocks. (A) CH_3OH composition vs. time; (B) Conversion vs. time. Total feed (without N_2): 1 SLMP, CO_2/H_2=1/3, CO/H_2=1/2, $CO/CO_2/H_2$=2/1/7.

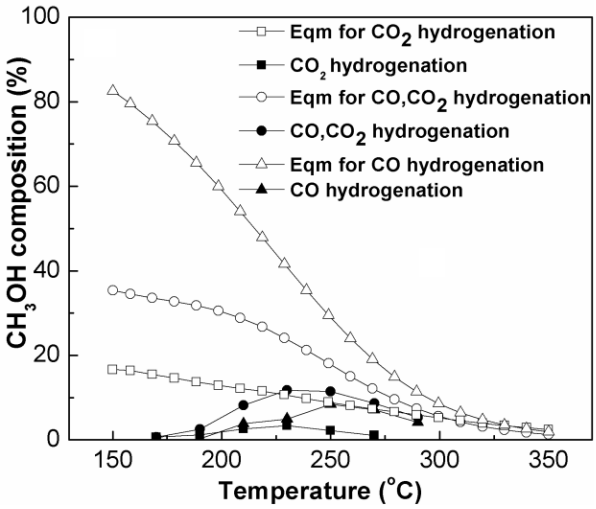

Figure 2.4 Equilibrium study for three methanol synthesis feedstocks, CH_3OH composition vs. temperature. Total feed (without N_2): 1SLMP, CO_2/H_2=1/3, CO/H_2=1/2, $CO/CO_2/H_2$=2/1/7.

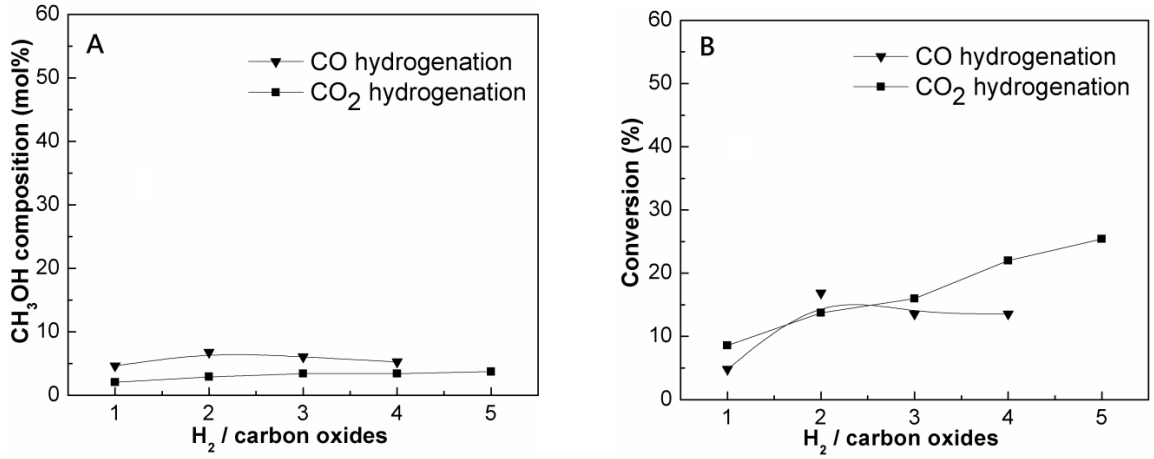

Figure 2.5 Various H_2 to carbon oxide (CO or CO_2) ratio. (A) Methanol composition vs H_2/carbon oxides ratio (B) Conversion vs. H_2/carbon oxides ratio. Total feed (without N_2): 1SLMP.

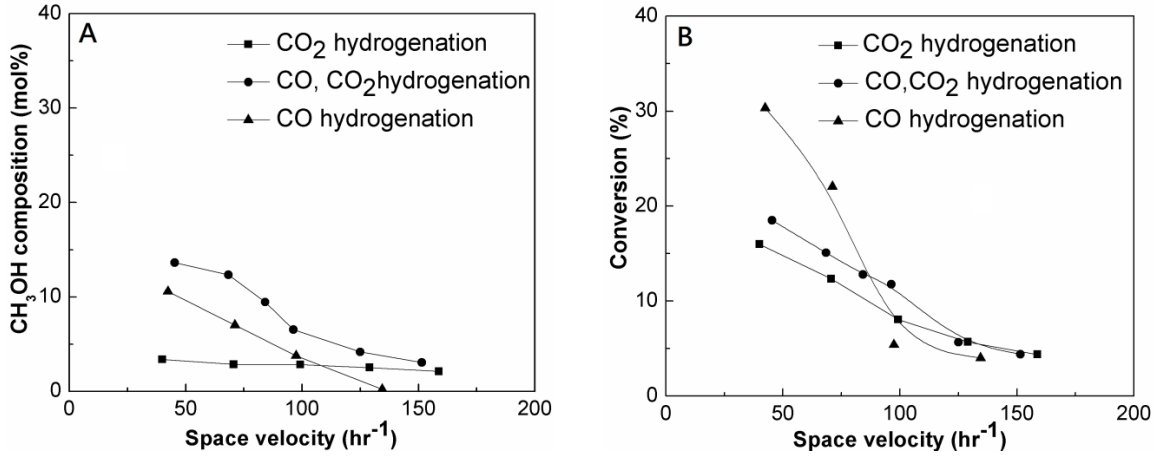

Figure 2.6 Space velocity study for three methanol synthesis feedstocks. (A) Methanol composition vs. space velocity (B) Conversion vs. space velocity. CO_2/H_2=1/3, CO/H_2=1/2, $CO/CO_2/H_2$=2/1/7.

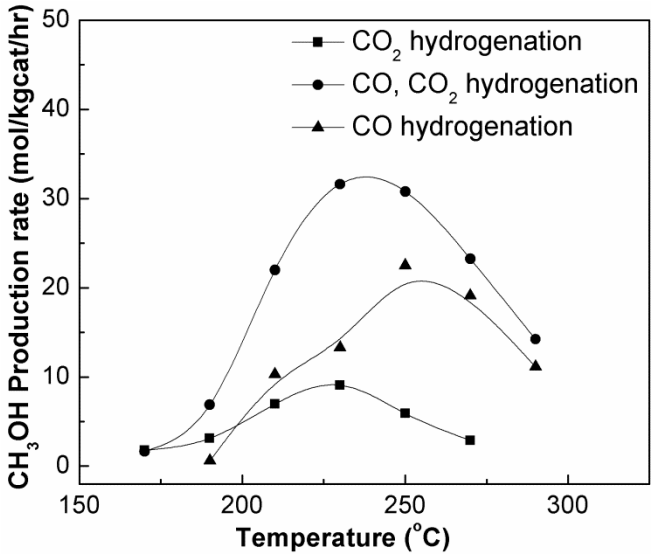

Figure 2.7 Methanol production rates for three feedstocks. Total feed (without N_2): 1SLPM; CO_2/H_2=1/3, CO/H_2=1/2, $CO/CO_2/H_2$=2/1/7.

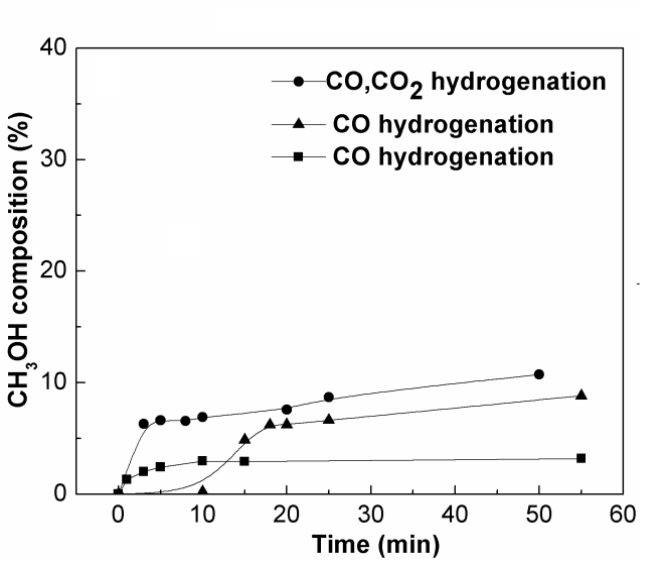

Figure 2.8 Cold start-up reaction for three methanol synthesis approaches. Methanol composition vs. time; total feed (without N_2): 1SLMP, CO_2/H_2=1/3, CO/H_2=1/2, $CO/CO_2/H_2$=2/1/7.

Various H_2/carbon oxides ratios and space velocity studies were conducted as shown in Fig 2.5 and Fig 2.6. The investigation of H_2/carbon oxides ratios is necessary since methanol is generated from syngas which may have variable H_2/CO ratio depending on the upstream processes. Fig 2.5A shows that there are no distinguishable trends outside experimental errors since the methanol composition only changes by 2.5% as H_2/CO ratio was varied from one to four, while the carbon balance closes within 5%. Study of space velocity is also important to gain better information about these reactions. Larger space velocity corresponds to smaller residence time and subsequent lower methanol production which is consistent with the data shown in Fig 2.6. The methanol composition and conversion of carbon oxides in the product stream decreases while space velocity increases.

In a small-scale methanol reactor, the amount of methanol that can be produced is a critical parameter. The methanol production rates for three feedstocks at various temperatures are compared in Fig 2.7. CO_2 hydrogenation only produced a limited amount of methanol. CO hydrogenation has a better performance in terms of methanol production, which is as high as 20 mol/kgcat-hr. Parallel hydrogenation of CO and CO_2 has the highest

methanol production rate at around 30 mol/kgcat-hr. This experimental results can be explained by hypothesized mechanisms for methanol synthesis [52],[54]-[55],[59]. The role of CO is to keep copper in a highly reduced state, which is more active than that reduced by H_2 alone. CO_2 keeps the catalyst in its intermediate oxidation state and hence a small concentration of CO_2 keeps the catalyst from excessive reduction by CO and H_2. On the other hand, large concentrations of CO_2 will block the active sites of the catalysts [52],[54]. Feeding both CO and CO_2 balances the above two effects.

Unlike large-scale industrial systems, a transient study for methanol synthesis is important in a small-scale system as small-scale system is more flexible to have more start up and shut down instances. Thus a transient study of methanol synthesis has been conducted, and the results are depicted in Fig 2.8. Temperature is increased from 25 ºC to 230 ºC within 5 min. The compositions of the product stream and carbon oxides conversion are analyzed by GC at short time intervals after the start of temperature ramp. To take the next GC measurement, reactor is cooled down to 25 ºC. In Fig 2.8, the methanol composition reaches 7% of the total products within 3 min for parallel hydrogenation of CO and CO_2, while the methanol composition is only 3% at 10 min for CO_2 hydrogenation. CO hydrogenation has a lag and only produces methanol after 5-7 min.

The catalyst for this set of experiments has been running for over 700 hrs at reaction temperature and pressure over 50 times with no significant deactivation. Based on these experiments, parallel hydrogenation of CO and CO_2 is the best feedstock for small-scale methanol synthesis, since it is closest to the equilibrium and methanol production is the fastest.

2.3.2 Multifunctional Reactor with Cold Finger

Industrial gas-phase methanol synthesis plants include pretreatment, desulfuration, steam reforming, compression, methanol synthesis, and methanol purification steps [44]. Inter-stage cooling between reactors is utilized to increase syngas conversion since the

reactions are highly exothermic and equilibrium limited. Recycling of unreacted gases is necessary as the single-pass conversion of syngas is low (10-15%) [44]. However, in small-scale systems, simpler process designs are desirable. Removing the product (methanol) *in situ* from the system by a condenser will favorably shift reaction equilibrium towards the products, and increases the syngas conversion and methanol production. Therefore, we propose integrating reaction and separation processes in a multifunctional reactor to save energy and capital cost by eliminating inter-stage cooling. In this case, the reactors in series with inter-stage cooling, and subsequent separation of methanol from other reactants (H_2O, CO, CO_2, H_2, and N_2) in the industrial-scale system will be simplified to a novel multifunctional reactor in a small-scale system.

Amor *et al*. [60] reported the performance of multifunctional reactor for methanol synthesis and benzene hydrogenation. This reactor took 20 h to reach 26% of CO conversion. This was below the equilibrium conversion which at their reaction conditions was 36%. They reached a conversion of 80% by condensing methanol out of the reactor. In this chapter, a multifunctional reactor with an internal condenser is shown in Fig 2.9. The condenser, also referred to as a cold finger, is placed in the center of the reactor. Air and water at room temperature are used as the cooling medium. Catalyst (commercial Cu-ZnO-Al_2O_3) is stored in an annulus shape inside a stainless steel mesh, and the flow pattern is shown with arrows in Fig 2.9A. Methanol and water are condensed at the surface of the cold finger. Condensed liquids drip down to the bottom of the reactor, and are periodically removed by opening two ball valves alternately. Opening valve 1 allowed liquid flow into the chamber below the reactor, while in closed position it sealed the reactor to maintain the high pressure. Valve 2 helped to withdraw the condensed liquid products out of the chamber. Three thermocouples were placed at the top, middle and bottom of the catalyst bed. The middle thermocouple was used to control the reaction temperature in the catalyst bed. The residence time in this reactor was on the order of minute. The volume of the reactor was 500 ml and the amount of the catalyst used was 30 g. The total volumetric flow rate was 1.2 SLPM, and the ratio of the feeds were $CO/CO_2/H_2/N_2$=2/1/7/2.

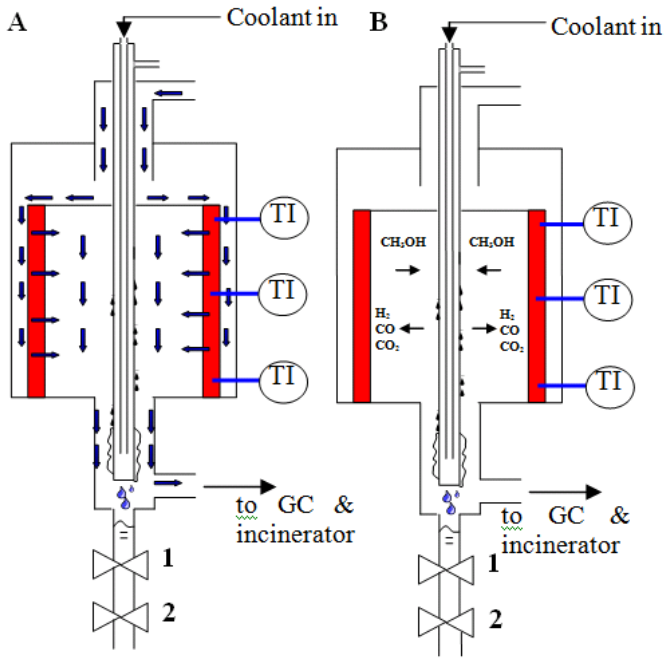

Figure 2.9 Multifunctional reactor, TI: thermocouple, shade: catalyst. (A) Arrow: expected flow pattern. (B) Arrow: diffusive flux in radial direction inside the reactor.

Table 2.3 Various reactions with and without condenser, and their corresponding carbon oxides conversions.

Reaction T	Cooling medium	Thermocouple T			Carbon oxides Conversion (%)
		Top(°C)	Middle (°C)	Bottom(°C)	
220 °C w/o condenser	–	207	220	210	15.2
220°C with condenser	water	210	220	166	35.0
230°C w/o condenser	-	220	230	222	20
230°C with condenser	Air	220	230	218	19.9
230°C with condenser	water	216	230	182	38.8
240°C with condenser	water	230	240	185	37.5
250°C with condenser	water	242	251	195	29.5
270°C with condenser	water	262	270	220	17.5

Table 2.4 Carbon oxides conversion for various cooling medium.

Reaction T	Cooling medium	Thermocouple T			Carbon oxides conversion (%)
		Top (ºC)	Middle (ºC)	Bottom (ºC)	
230ºC with Condenser	Air	220	230	218	19.9
230ºC with Condenser	Water(28ml/s)	216	230	182	38.8
230ºC with Condenser	Water(33ml/s)	220	230	176	35.9
230ºC with Condenser	water (ice bath)	222	230	173	34.9
230ºC with Condenser	water (dry ice bath)	221	230	173	33.4

The experimental results are tabulated in Tables 2.3 and 2.4. Because water was flowing in and out of the cold finger, the expected temperature of the condenser is lower than 100 °C. Before turning on the water in the condenser, the temperature gradient in the axial direction in the catalyst bed was ±10 ºC of the operating temperature. This temperature difference was within experimental error (<5%). The temperature of the catalyst bed was highest in the middle. This could be because gases are not preheated at the top. At the bottom, methanol partial pressure is high, and consequently extent of reaction and heat released by reaction is less.

It was observed that water is a much better coolant than air due to its higher heat capacity. When condenser was turned on, the temperature gradient in the axial direction in the lower half of the reactor increased to 50 ºC. It could be due to two reasons: (A) water moved through the inner layer of the tube towards the bottom where it started to remove heat. (B) Liquid methanol droplets might have evaporated into methanol vapor, absorbing heat from the catalyst bed at the bottom of the reactor. This seems plausible since the boiling temperature of methanol at 50 bar is 211 ºC, while the reaction temperature was 230 ºC.

By using a water condenser, conversion of carbon oxides at 220, 230, and 240ºC reached 35-39%, while conversion at 250 and 270ºC were lower. This multifunctional reactor indeed increased conversions before and after turning on the condenser. For

instance, at 220ºC, the conversion increased by more than factor of 2 (15% to 35%). The coldest point is identified in the reactor with the assumption that the catalyst bed layer was thin enough that the temperature gradient across the bed in the radial direction was negligible; however there were concentration gradients in the reactor that made outlet reactor conversion with equilibrium conversion hard to compare. Table 2.4 shows different conversions using various cooling media. For water as a cooling medium, no significant improvement of conversion by lowering the temperature of water was observed. It shows the inadequate heat transfer. This might result from the small heat transfer surface area since the temperature gradient in the radial direction is large enough, even with the fact that the heat conductivity of the stainless steel is sufficiently high.

The equilibrium conversion is defined at a certain temperature, pressure and composition. In order to accomplish a higher conversion, with fixed temperature and pressure, a varied composition of the reactants needs to be reacted in the catalyst bed to shift equilibrium. More precisely, shifting the equilibrium towards the product requires changing the composition of the reactants and having reactions in the catalyst bed to achieve a new, higher equilibrium value (generate more products) until 100% conversion is reached. As shown in Fig 2.9B, the methanol generated in the catalyst bed diffuses towards the condenser driven by its concentration gradient in the radial direction. The direction of the diffusion of reactants (H_2, CO, and CO_2) is the opposite. Here, once the methanol and water is condensed, higher conversion is achieved if reactants diffuse to the catalyst bed.

The increase in conversion of methanol is mainly because of the radial diffusion of the reactants from condenser to catalyst bed and subsequent reactions in the catalyst bed. We expect that the contribution from the temperature effect will be small based on following explanation. From Fig 2.4, the optimum temperature is 230 ºC, and reaction thermodynamics and kinetics are competing with each other. Therefore, a fluctuation from 230ºC is not likely to increase the conversion. The most likely reason is that the diffusive transport of reactants in the radial direction reaches the catalyst bed before exiting the reactor. The flow in the reactor is laminar based on the estimation of Reynolds

number (0.0003). Diffusion coefficient (0.00439 cm^2/s) and dispersion coefficient (0.01069 cm^2/s) at high temperature and pressure are comparable. Axial velocity (0.01495 cm/s) is also computed based on volumetric flow rate. Based on the geometry of the reactor, the time scale of radial diffusion from condenser to catalyst bed is comparable to the time scale of axial convection from top to the bottom of the reactor. The calculations are shown in Appendix A. Furthermore, the flow pattern in the reactor was non-ideal. There might be some channeling in the reactor which contributed to the increase of the conversion. Finally, the conversion of carbon oxides only reached the value listed in Tables 2.3 and 2.4. This is likely due to insufficient radial diffusion of reactants in the multifunctional reactor. Further design will put more emphasis on improving flow of the reactant in the radial direction (by mixing) to the catalyst bed, and will be discussed in section 7.1.

2.3 Conclusion

This chapter studied the feasibility of a small multifunctional reactor with *in situ* condensation to increase conversion of the biomass-derived syngas. The fundamental studies of methanol synthesis showed that parallel hydrogenation of CO and CO_2 were the reactions taking place in the multifunctional reactor. Parallel hydrogenation was closer to the equilibrium and produced highest yield of at the fastest rate. The implementation of internal condenser increased the conversion by a factor of two. Varying cooling media and the speed of cooling media was also studied. A higher single-pass conversion will be realized by a better reactor design which is proposed in chapter 7 as future work.

CHAPTER
THREE

SMALL-SCALE METHANOL SYNTHESIS WITH IN SITU SORPTION BY NANOCOMPOSITE (SALT INSIDE POROUS MATRIX)

SUMMARY

This chapter focuses on high pressure methanol synthesis in a multifunctional reactor with *in situ* adsorption of product (methanol) to increase the single-pass conversion. The absorbent is an inorganic salt, encapsulated in silica gel pores with pore size 15 nm. $CaCl_2$ in silica gel is chosen as the salt matrix to remove the methanol product and shift reaction equilibrium. By using a batch reactor, the CO conversion is improved over the original equilibrium conversion, demonstrating a successful application of the Le Chatelier's principle to increase process performance. A multifunctional reactor with mixed catalyst and absorbent bed is also constructed to shift the reaction equilibrium further. In this case, the CO conversion is higher than the initial equilibrium conversion for a period of ~20 min after which the salt matrix becomes saturated. A multifunctional reactor with *in situ* condensation and adsorption is proposed in section 3.4 in order to further increase single-pass conversion by taking advantage of the higher sorption capacity at lower sorption temperatures.

3.1 Introduction

Methanol synthesis is one of the most important processes in the chemical industry. The methanol synthesis reaction is limited by its unfavorable equilibrium. Due to unfavorable thermodynamics, methanol synthesis needs to be conducted over a catalyst at high pressures (50-100 bar), but still yields a low single pass conversion (< 20%). As a result, this process requires recycling of the reactants to increase conversion, resulting in increasing energy consumption and product cost. Shifting the equilibrium in the methanol synthesis process by removing the product is a promising way to increase the reactant conversion and consequently, to reduce the cost of methanol production.

Much research has been conducted to shift the equilibrium for the methanol synthesis reaction. Amor *et al.* [60] reported the performance of a multifunctional reactor with internal condensation to shift the reaction equilibrium. Similarly, as shown in chapter 2, we successfully increased reactant conversion by a factor of 2 by *in situ* condensation. Future more, Zhang *et al.* [61] reported a shift in the reaction equilibrium by supercritical liquid extraction. It comes to our attention that the removal of product by adsorption is generally considered a promising way to increase the conversion of reversible reactions. Kuczynski *et al.* reported [62-63] a method to adsorb the methanol product in the syngas reaction using a countercurrent gas-solid-solid trickle flow reactor (CGSSTFE) in order to increase the conversion above equilibrium. However, this reactor configuration involves a circulation of solid stream at high pressure which poses many problems when scaled up to an industrial scale. To overcome this problem, a simulated countercurrent moving-bed reactor (SCCMBR) was suggested instead of a moving bed operation [64].

Many methanol adsorbents have been investigated in the literature, such as activated carbon [65, 66], zeolites [67, 68], and alumina-based materials[69]. Very few studies showed the use of advanced materials with methanol sorption properties. Examples of these materials are mesoporous mesophase silica-based materials [70], polymers [71], pillared clays [72] and so forth. The most important parameters for the selection of a proper adsorbent for the methanol synthesis reaction are high sorption capacity under the

operating conditions and high adsorbent selectivity with respect to methanol.

$$salt + nCH_3OH \rightarrow salt \cdot nCH_3OH \quad (3\text{-}1)$$
$$CaCl_2 + 4CH_3OH \rightarrow CaCl_2 \cdot 4CH_3OH \quad (3\text{-}2)$$
$$Ca(NO_3)_2 + 2CH_3OH \rightarrow Ca(NO_3)_2 \cdot 2CH_3OH \quad (3\text{-}3)$$
$$LiCl + 3CH_3OH \rightarrow LiCl \cdot 3CH_3OH \quad (3\text{-}4)$$

It is well known that inorganic salt can absorb methanol vapor by forming crystalline solvates as shown in Equation (3-1). For example, Equations (3-2) - (3-4) show some common inorganic salts that form crystalline solvates with methanol vapor. Here, n is number of moles of methanol vapor that can be absorbed per mole of inorganic salt. The number of n ranges from 3-6 for different salts, resulting in the absorption of a large amount of methanol [73].

However, bulk salts are rarely used in the methanol sorption process due to the following reasons [73]: (1) the reaction of salt and methanol vapor forms a phase of crystalline solvate on the outer surface of the salt, hindering the methanol vapor diffusion into the salt, subsequently leading to a slow sorption process; (2) the reaction of salt and methanol vapor lead to salt recrytallization. The swelling of the salt during the formation of solvate leads to mechanical destruction of reactor wall or connections.

Godeeva *et al.* [73] introduced a concept of nanocomposites (salt inside porous matrix), and provided a design of phase composition and sorption properties for practical applications. The rationale for the design of this nanocomposite was to increase the methanol sorption ability of common porous adsorbents by confinement of inorganic salts inside their pores. This dispersion of inorganic salt inside the nano-scale ranged pores inside the matrix allows a large sorption capacity, and overcomes the drawbacks of bulk salt sorption. Godeeva *et al*. [73] found out that this encapsulation of salts inside the pores of silica gel results in a huge increase in methanol sorption capacity, which is larger than the capacity of common solid adsorbents like activated carbons or zeolites. They performed an *in situ* adsorption test and demonstrate the shift in equilibrium for the

methanol synthesis reaction by using $Ca(NO_3)_2$ with silica gel under the operating conditions P = 20 bar, T = 220 ^oC, and the reactant ratio $CO/CO_2/H_2/N_2$ = 30.0/2.0/64.8/3.2.

A more realistic operating condition (closer to industrial operating condition) for methanol synthesis is at higher pressures (50-100 bar). This requires the selection of a salt matrix that is more suitable for methanol sorption at such operating conditions (higher pressure). In this chapter, we describe how different salt are tested to choose the most suitable methanol sorption salt matrix at an operating condition of P=50 bar, T=230 ^oC, and $CO/CO_2/H_2/N_2$ = 20/2/40/20. Multiple multifunctional reactors have been built, and systematic experiments have been carried out to shift the methanol synthesis equilibrium by *in situ* adsorption.

3.2 Experimental Setup

3.2.1. Salt Matrix Preparation

Salt matrix (salt and silica gel) was prepared by dry impregnation method where the volume of impregnation solution V_{imp} was almost equal to the pore volume V_p of the silica gel. Salts ($CalCl_2$, $Ca(NO_3)_2$, and LiCl) were impregnated into the silica gel (Sigma Aldrich, pore size 150A, Gade 646, part number:236845) by a systematic method described below. Salt (30 wt% of silica gel) was dissolved in DI water, and stirred until the solution became clear indicating complete dissolution of salt in water. This clear solution was added into the salt matrix and the mixture was heated overnight in a vacuum oven at 110 ^oC. The salt mixture was taken out making sure that there was no weight change due to evaporation. The salt matrix is capable of adsorbing water produced from reaction or air moisture. Therefore, it was sealed properly when not in use or reheated in the vacuum oven at 110 ^oC prior to the conduction of any experiments.

The key step for making the salt matrix is the dry impregnation method. This method is better than wet impregnation method where $V_{imp} > V_p$. This is because in the wet impregnation method, large salt crystals can form at the external surface of the silica gel

grains instead of formation of nano-sized crystal inside silica pores. These crystals are undesirable because they reduce the methanol sorption rate.

3.2.2. Reactor System Setup

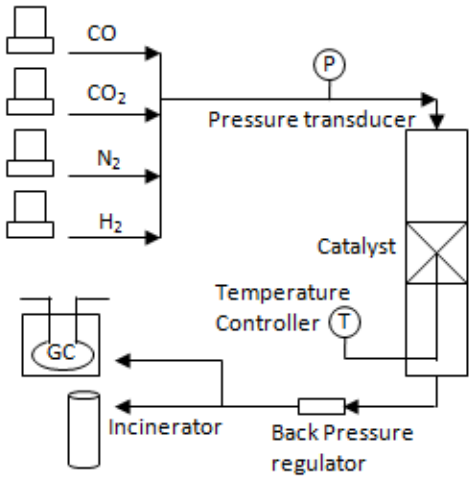

Figure 3.1 Reactor system setup for methanol synthesis with *in situ* adsorption. The salt is placed in the reactor. Amore detailed reactor design is shown in Section 3.3.

The reaction was operated at an elevated temperature (230 ^{o}C) and pressure (50 bar) as shown in Fig 3.1. The feed gases (CO, CO_2, H_2, and N_2) were fed in from gas cylinders, and passed through a high pressure mass flow controller (MFC, Brooks instrument) before mixing and entering the reactor. The detailed reactor setups are shown in the section 3.3. The catalyst used is $CuO/ZnO/Al_2O_3$ (same as in chapter 2) which was ground into powder. The temperature is controlled by a temperature controller and the pressure is controlled by a back pressure regulator. The effluents are burned in the incinerator. The catalyst reduction method is the same as stated in section 2.2.1. To preserve the reduced catalyst when not in use, a moderate pressure (~ 20 bar) is maintained so that air does not enter the reactor and oxidize the catalyst.

Data is analyzed by Agilent 6890 GC equipment with TCD and FID, and also with an Agilent Plot Q column (30 m*320 μm diameter). Nitrogen is used as internal standard

for all the other gases. The carbon, oxygen, and hydrogen atom balance is accurate within ±10%. The equilibrium concentrations are calculated by HSC software with specific reaction compositions, temperature, and pressure.

3.3 Results and Discussion

3.3.1 Test Salt Matrix Sorption Capacity

Three salt matrix candidates ($CaCl_2$, $Ca(NO_3)_2$, and LiCl) are tested for methanol sorption capability with a multifunctional reactor shown in Fig 3.2.The results of the experiments are shown in Fig 3.3. The multifunctional reactor has two reaction chambers; the top chamber contains reaction catalyst ($Cu/ZnO/Al_2O_3$), and the bottom chamber contains the salt matrix. The test is conducted by introducing $CO/CO_2/H_2/N_2$ with ratio of 20/2/40/20 to the plug flow reactor. The two chambers in the reactor are well insulated and the temperature is maintained at 230 ^oC.

Gordeeva *et al.* [73] studied the methanol sorption and desorption curves at various temperatures with LiCl/silica gel and bulk LiCl. They found out that there is a strong sorption-desorption hysteresis for bulk LiCl, while there is no hysteresis for embedded LiCl. This is an important property for the adsorbent since a strong hysteresis requires a higher temperature for regeneration of adsorbent.

Fig 3.3 shows that $CaCl_2$ and LiCl have comparable sorption capacities, while $Ca(NO_3)_2$ has relatively lower sorption capacity. $Ca(NO_3)_2$ salt matrix is saturated at around 40 min, while $CaCl_2$, and LiCl are saturated only beyond 60 min. Also, LiCl curve shows a plateau from 30 - 70 min. We hypothesize this plateau indicates the formation of a solid crystalline solvate due to the reaction (3-4). Here, n = 3 for LiCl matrix. The $CaCl_2$ curve also shows a mild plateau in the time range of 25 – 50 min which corresponds to the reaction (3-2) with n = 4. $CaCl_2/SiO_2$ is chosen as the salt matrix for the subsequent reactions since LiCl salt matrix is difficult to take out from the reactor after adsorbing methanol vapor.

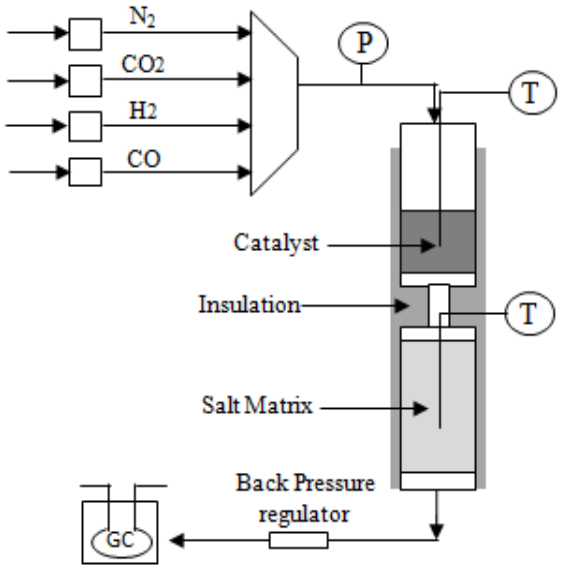

Figure 3.2 Multifunctional reactor to test sorption capacity of salt matrix. P is pressure transducer and T is temperature controller.

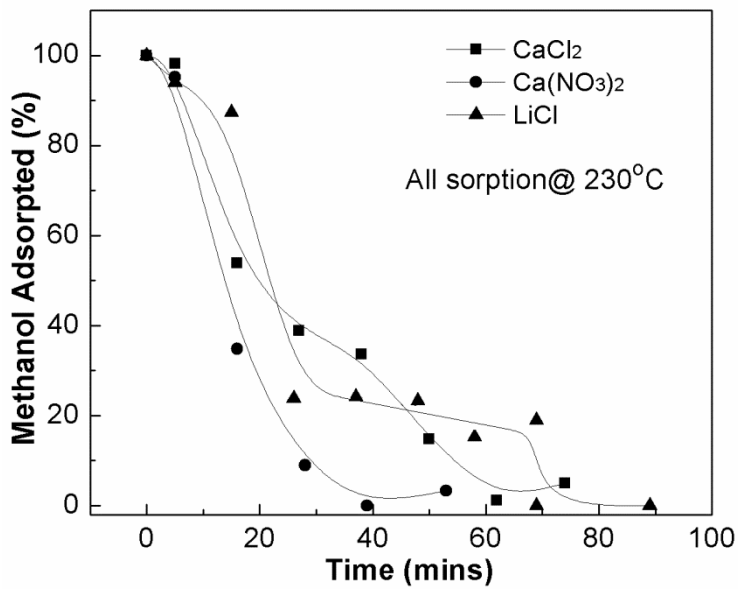

Figure 3.3 Methanol adsorption vs. time for different salt matrix ($CaCl_2$, $Ca(NO_3)_2$, and LiCl).

3.3.2 Multifunctional Reactor with *in situ* Adsorption

As mentioned in chapter 2, the equilibrium shift with *in situ* condensation of products is less likely to be clearly determined due to the presence of temperature and concentration gradients in the radial and axial directions. A multifunctional reactor with *in situ* adsorption may provide an opportunity to demonstrate Le Chatelier's principle by removing products since the reaction is at uniform temperature and compositions.

The reactor setup is shown in Fig 3.4. In the batch reactor, the catalyst and $CaCl_2$ matrix are located adjacent to each other. During the catalyst reduction period, the direction of gas flow is from the top to the bottom. Water vapor generated in the reduction period is taken out by H_2 and N_2, thus preventing water vapor being adsorbed by the salt matrix. In this batch reactor system, a small volume (<1% of total volume) of the gas is taken out through the sampling port chamber so that there is negligible effect on reactor total volume and pressure. This gives us more confidence in the accuracy of our analysis of the gas compositions. The gases (CO, CO_2, H_2, N_2) and fed into the reactor in the ratio $CO/CO_2/H_2/N_2$ = 20/2/40/2. The top and bottom on/off valve are closed once the reactor is charged with reactants at 50 bar. The pressure drop is monitored by a pressure transducer and several samples are taken to investigate the gas compositions.

The results of using a multifunctional reactor with adjacent catalyst and absorbent beds are shown in Fig 3.5. The equilibrium CO conversion (calculated by HSC software) is ~58%. Here, CO_2 hydrogenation reaction is negligible since the CO/CO_2 ratio is large (=10), which means CO_2 and water vapor generated are negligible. Reactor volume, void volume of absorbent bed, and void volume of catalyst bed are tested in order to calculate the CO conversion. The reaction reaches the original equilibrium (~58%) at around 200 min. Methanol is generated in the catalyst bed and diffuses towards the absorbent bed. The reaction rate decreases with increasing time and decreasing pressure since rate of reaction is proportional to partial pressure of reactant gases ($CO/CO_2/H_2$). After ~1600 min, CO conversion reaches 85%.

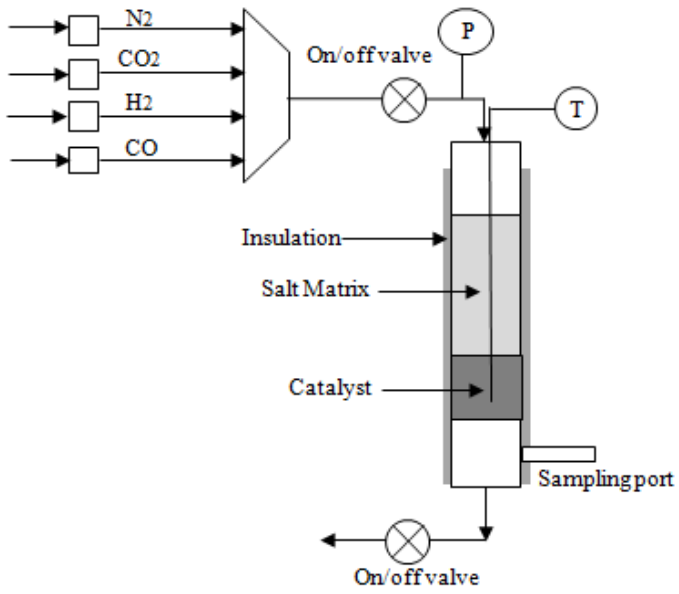

Figure 3.4 Multifunctional reactor to shift reaction equilibrium. P is pressure transducer, T is temperature controller.

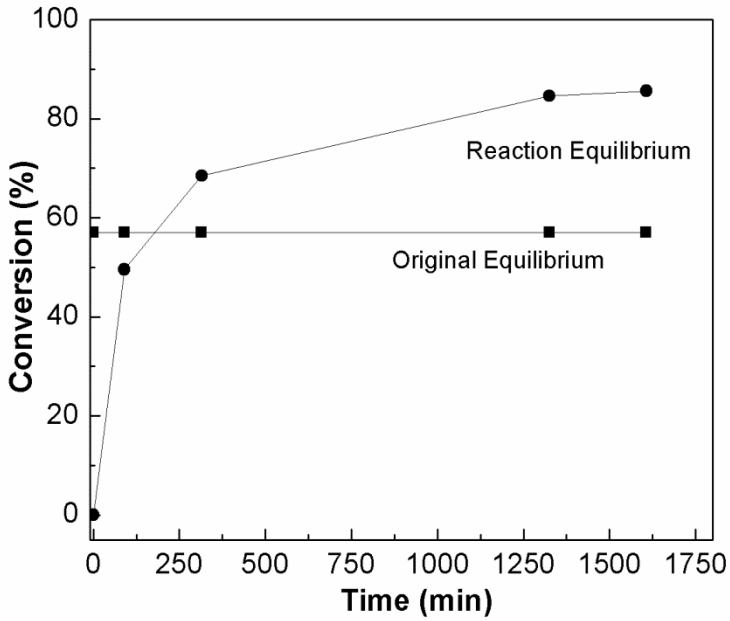

Figure 3.5 Equilibrium CO conversion and batch reactor CO conversion vs. reaction time in a multifunctional reactor. Catalyst bed and adsorbent bed ($CaCl_2$ matrix) are adjacent to each other. Equilibrium is calculated by HSC software.

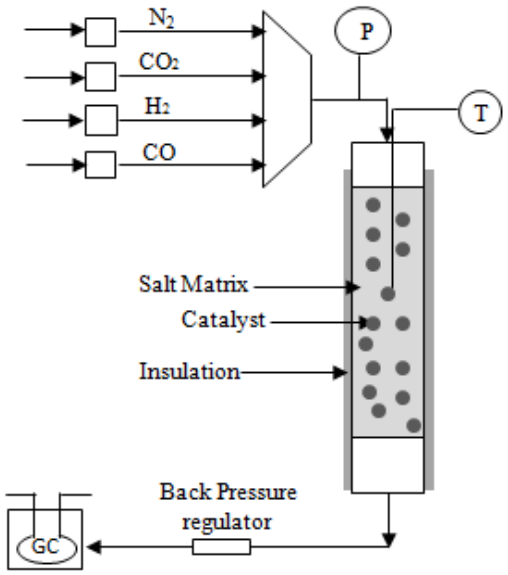

Figure 3.6 Multifunctional reactor with mixed catalyst and absorbent ($CaCl_2$ matrix). P: pressure transducer, T: Temperature controller.

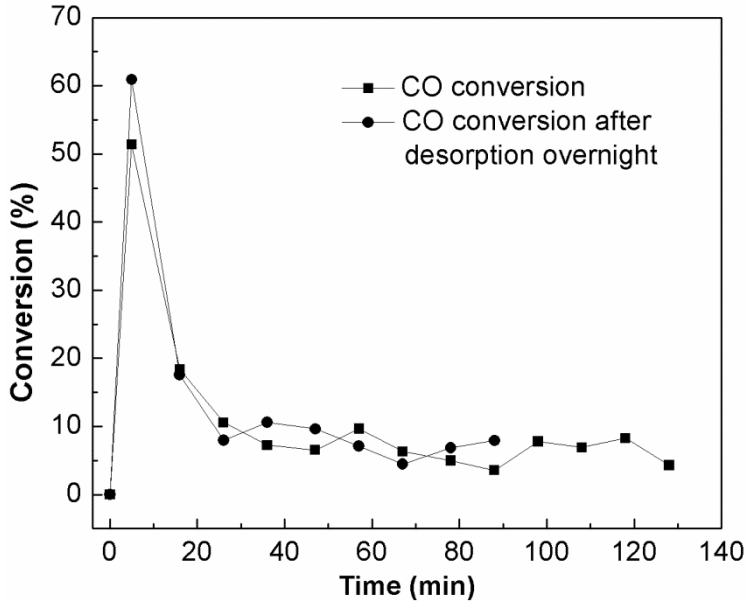

Figure 3.7 CO conversion as function of time in a multifunctional reactor in which catalyst is mixed with absorbent ($CaCl_2$ matrix) in a continuous flow system.

The methanol adsorption in adjacent beds is diffusion limited since it requires 1600 min to reach 85% CO conversion. The methanol produced needs to diffuse through the catalyst bed and into the adsorbent bed which takes a significant period of time. In order to minimize the diffusion limitation, the catalyst and absorbent should be physically mixed. Hence, a new reactor is set up and the schematic of this reactor is shown in Fig 3.6.

The reaction system in Fig 3.6 remains the same as shown in Figs 3.2 and 3.4. High pressure gases are fed in to the reactor; the temperature is controlled by a temperature controller; and the pressure is controlled by a back pressure regulator. The main difference is that the catalyst (5g) is mixed with the absorbent ($CaCl_2$ matrix, 30g) inside the reactor. The catalyst reduction procedure is the same as previously described in chapter 2. After catalyst reduction, the absorbent is saturated with water vapor which is generated in the reduction period. N_2 stream (0.2 SLPM) is passed through the reactor overnight at 110 ^oC to eliminate the water vapor and the catalyst is then ready to use. The operating $CO/CO_2/H_2/N_2$ feed ratio is 20/2/40/20 in a continuous flow system.

The results of experiments with mixed catalyst and absorbent are shown in Fig 3.7. The first attempt has a conversion peak between 0-20 min. The CO conversion reaches 52% which is comparable to the original equilibrium (~58%). The high CO conversion lasts less than 20 min as the absorbent becomes saturated quickly, this is due to significant shorting the traveling path between catalyst and adsorbent in this configuration compared to that in Fig 3.4. A desorption cycle is performed at 110 ^oC with N_2 flow (0.2 SLPM) overnight. The high CO conversion (~60%) is reproduced after overnight desorption with a conversion peak above equilibrium conversion in the time period 0 – 20 min. This shows that the catalyst maintains its activity after overnight desorption. This is also consistent with the report that the active site (Cu in $Cu/ZnO/Al_2O_3$) is deactivated by sintering at temperatures greater than 300 ^oC.

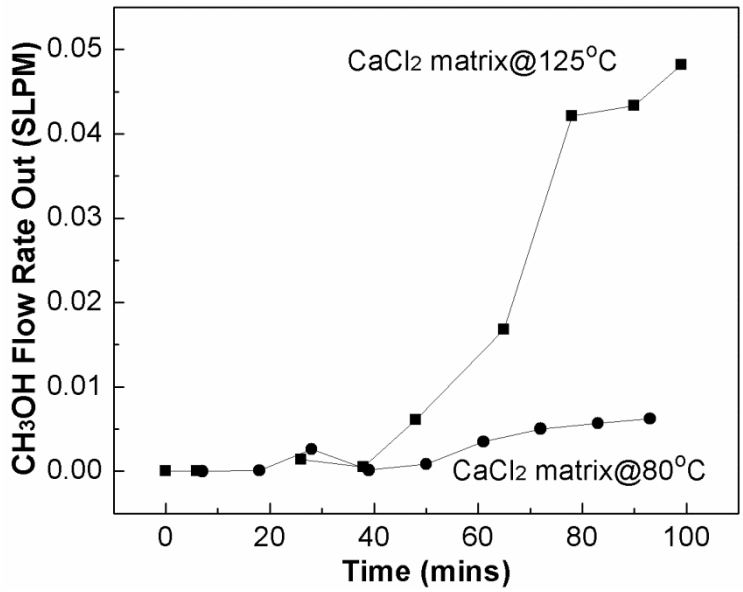

Figure 3.8 CH_3OH flow rate out (SLPM) vs. time for $CaCl_2$ matrix at lower temperature (125 ^oC and 80 ^oC) in a continuous flow reactor.

Based on the results in Fig 3.7, one can observe that the sorption capacity of $CaCl_2$ matrix is limited due to the reactor volume and the high temperature. Based on our estimation, $CaCl_2$ matrix can adsorb 0.06 g CH_3OH/g salt matrix at 230 ^oC. We are interested in increasing the sorption capacity of $CaCl_2$ matrix by lowering the sorption temperature. The results of varying the temperature are shown in Fig 3.8. Fig 3.8 shows that the CH_3OH flow rate exiting the reactor after passing through a $CaCl_2$ matrix sorption bed at a lower temperature (80 ^oC) is capable of adsorbing more methanol compared to maintaining the $CaCl_2$ matrix at a higher temperature (125 ^oC). Based on our estimation, $CaCl_2$ can adsorb 0.76 g methanol/g salt matrix at 125 ^oC, which is higher by a factor of 10 than sorption capacity of $CaCl_2$ at 230 ^oC.

3.4 Multifunctional Reactor with in situ Adsorption and Condensation

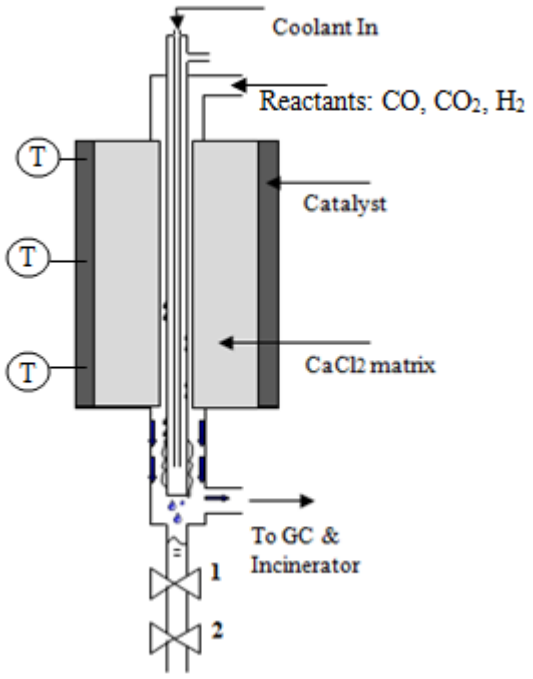

Figure 3.9 Schematic of proposed multifunctional reactor with integration of *in situ* condensation and adsorption. The internal condenser is in the middle. Methanol is condensed on the surface of the condenser. The reactor is heated by heating tape and temperature is measured by 3 thermocouples inside the catalyst bed. T: thermocouple.

Based on the results shown in Fig 3.8 and in chapter 2 (*in situ* condensation), the integration of *in situ* condensation and adsorption is proposed and the schematic of the reactor design is shown in Fig 3.9.

The catalyst ($Cu/ZnO/Al_2O_3$) is placed in an annular shape, against the reactor wall. The condenser is the same as described in chapter 2, which is a 1/4 inch diameter stainless steel tube with an inner tube (1/8 inch diameter). The coolant (water) enters the reactor and leaves the reactor from the top. The space between catalyst and the internal condenser is filled with the adsorbent, where the catalyst and the absorbent are separated

by steel mesh (McMaster). The reactants are $CO/CO_2/H_2/N_2$ with the ratio of 20/2/40/20; and the reaction temperature is 230 ^oC, and pressure is 50 bar. After reduction of the catalyst, a desorption of water vapor is necessary (110 ^oC with 0.2 SLPM N_2 flow overnight).

A continuous flow process will be investigated. Before turning on the reactor, the CO conversion vs. reaction time will be studied until absorbent is saturated. Once the absorbent is saturated, the condenser will be turned on; the CO conversion vs. reaction time will be explored again since absorbent bed increases adsorbing capacity with the help of an internal condenser. A synergic effect of *in situ* condensation and adsorption could further increase the CO conversion. Once the adsorbent bed is saturated, the desorption experiment will be performed to study desorption time and temperature. Number of adsorption-desorption cycles will also be investigated. One would expect that the adsorption capacity will be decreased after a number of adsorption-desorption cycles.

The results of this set of experiments will provide an implication for industrial applications. Two pressure swing reactors could be built, and the reactors could be operated alternatively to make sure a continuous flow process. The critical part of this set up is the time period of desorption time. This two pressure swing reactor system can only be realized if the desorption takes place on the same time scale as the adsorption process.

CHAPTER
FOUR

METHANOL DEHYDRATION TO DIMETHYL ETHER IN A STAGED AUTOTHERMAL MILLISECOND RESIDENCE TIME REACTOR*

SUMMARY

This chapter focuses on methanol dehydration to dimethyl ether (DME) in a two-stage autothermal millisecond residence time reactor using a noble metal coated catalyst in the upstream stage to generate heat and zeolite in the downstream stage to dehydrate methanol with a total residence time of less than 100 milliseconds. Two reactor configurations have been examined: (1) methanol fed from the top of the reactor with hydrogen as sacrificial fuel and (2) methanol fed between the two stages with methane as a sacrificial fuel. Methanol dehydration was also explored in a heated tube to compare with the results obtained under autothermal conditions. The DME yield of the autothermal reactor with side-entering methanol was comparable to that of methanol dehydration reaction under isothermal conditions and was much better than the methanol top-feed configuration. The highest yield of DME obtained was ~80 % at C/O ratio of 1.0 which was comparable to the non-autothermal values reported in literature (~80 %) and close to equilibrium yield (84 %). This demonstrates the ability to synthesize DME in staged autothermal reactors with short contact time, high yield and no external heating.

*Parts of this chapter appear in: Hui Sun, Lanny Schmidt, "methanol dehydration to dimethyl ether in a staged autothermal millisecond residence time reactor", *Applied Catalysis A: General*, 404, 1-2, (2011), 81-86.

4.1 Introduction

Sustainable energy sources, such as solar and wind, attract attention as potential solutions to the energy crisis because they are renewable, cost-effective and pollution free. However, these sources only generate electricity and do not meet the demand for hydrocarbon-based transportation fuels. A liquid transportation fuel is needed that can be derived from renewable sources and can be shipped and stored easily. To meet this need, alcohol fuels such as methanol and ethanol are being investigated as viable options.

Methanol is emerging as an intermediate platform for making fuels and chemicals [74]. The problem associated with methanol is that it has a low energy density (15.6 MJ/L). To overcome this problem, Mobil developed the methanol-to-hydrocarbons process in the 1970s as a way to convert methanol into high-octane gasoline. The methanol in the feed is converted to an equilibrium mixture of methanol, DME and water, which can be further processed catalytically to either gasoline (MTG) or olefins (MTO), depending on the reaction temperature and the catalyst.

The intermediate product dimethyl ether (DME) is a better option than methanol since a higher energy density is achieved by removing one oxygen atom from two methanol molecules. DME is considered as a clean diesel substitute with a high cetane number, and produces lower NOx, CO and particle concentration emissions than diesel oil [62],[75]. It has lower global warming potential compared with traditional chlorofluorocarbons and has been used as a green aerosol propellant and refrigerant [62],[76]. In addition, the physical and chemical properties of DME are similar to those of propane (LPG) [74]. Traditionally, DME has been synthesized by methanol dehydration over solid-acid catalysts, such as γ–Al_2O_3, H-ZSM-5, zeolite Y, SiO_2/Al_2O_3 or SAPOs [77]-[78]. Activities to commercialize DME are in progress in Japan, China, etc. where DME is used for vehicles and power generation [79].

Previously, the Schmidt group reported a method to convert biomass model compounds into syngas or pyrolysis oil using short contact time reactors with noble metal catalysts [56],[29]. Skinner et al. demonstrated a staged reactor for ethanol dehydration to

ethylene which achieved a 95% conversion of ethanol to deoxygenate the biomass [80]. Inspired by this, a similar reactor configuration could be used to dehydrate methanol into DME by using a staged reactor with partial oxidation in the upstream stage coupled with methanol dehydration in the downstream stage. The staged partial oxidation reactor is capable of integrating decomposition and deoxygenation to upgrade liquid fuels from low to high energy density for transportation purpose.

Here, we investigate the methanol dehydration reaction (4-1) which occurs on zeolite solid acid catalysts.

$$2CH_3OH \rightarrow CH_3OCH_3 + H_2O \qquad \Delta H_{298K} = -23.41 \text{ kJ/mol} \qquad (4\text{-}1)$$

We want to minimize the extent of methanol decomposition reaction which occurs on noble metals and has a very favorable equilibrium conversion at low pressure.

$$CH_3OH \rightarrow CO + 2H_2 \qquad \Delta H_{298K} = 90.1 \text{ kJ/mol} \qquad (4\text{-}2)$$

Because of the water gas shift (WGS) reaction, decomposition of methanol also produces CO_2 and H_2O.

$$CO + H_2O \leftrightarrow CO_2 + H_2 \qquad \Delta H_{298K} = -41.0 \text{ kJ/mol} \qquad (4\text{-}3)$$

Since DME is the product of interest, we want to minimize further dehydration of methanol to higher hydrocarbons. Methanol to gasoline (MTG) also has high equilibrium conversion and occurs readily over acid zeolite catalysts.

We show experimentally that DME production dominates over decomposition and MTG below 300 ˚C (> 95% selectivity to DME), but at 350 ˚C these side reactions become significant. Since these reactions are endothermic or mildly exothermic, the reactions would have to be run in a heated tube. We run them autothermally by adding O_2 over a noble metal decomposition catalyst. In this chapter we focus on staged catalysts and the use of sacrificial fuels (H_2 and CH_4) to minimize methanol decomposition to provide heat to drive the dehydration reaction.

This reactor uses a 1 wt% Pt/α-Al_2O_3 for catalytic partial oxidation (CPO) reactions in the first stage and zeolite H-ZSM-5 for methanol dehydration in the second stage. Two noble metals (Pt and Rh) were tested to observe the effect of the catalyst on

the first stage. Two configurations of autothermal reactors are implemented: top feed methanol with hydrogen as sacrificial fuel and side feed methanol with top feed CH_4 as sacrificial fuel. An isothermal reactor was also used to compare the results with the autothermal reactor.

4. 2 Experimental

4.2.1 Catalyst Preparation

Platinum (Pt) and rhodium (Rh) (1 wt%) were supported independently on ceramic foam monoliths (99.5% α-Al_2O_3) 18 mm in diameter and 10 mm in length with 45 pores per linear inch (ppi). Pt and Rh were coated on the monolith by the incipient wetness method [81]-[82]. Metal salts, $H_2PtCl_6 \cdot (H_2O)_6$ and $Rh(NO_3)$ were dissolved in water and deposited on the monolith as described previously [81]-[82]. Each catalyst was used for at least 10 h with no significant deactivation or coke formation observed. A commercial catalyst NH_4-ZSM-5 powder with Si/Al=25 was used. H-ZSM-5 with Si/Al=15-25 has better performance for methanol dehydration reaction in terms of catalytic activity and stability than other Si/Al ratios [83]. The proton form of the zeolite was obtained by calcining the ammonium form of ZSM-5 in a furnace with air flow. H-ZSM-5 (1.2 g) was used for all the dehydration reactions mixed with 4.8 g of quartz. H-ZSM-5 was regenerated in a furnace at 600 ˚C with a total flow of 1 SLPM of gases (20% O_2 in N_2) for 1 h.

The methanol dehydration reaction was examined in a 20-mm-ID quartz tube as shown in Fig 4.1. The CH_3OH was pumped by a syringe pump and vaporized before it entered the reactor. All experiments were carried out at atmospheric pressure. For the autothermal reactions, uncoated foams were located upstream and downstream of the catalyst-coated foam to reduce axial radiation losses from the operating catalyst. The monolith was wrapped with ceramic insulation to eliminate gas bypass. Thermocouples were placed at the center of the monolith to measure the catalyst temperatures. The reactor was insulated by fiberfrax insulation. Gas flow rates were controlled by mass flow

controllers.

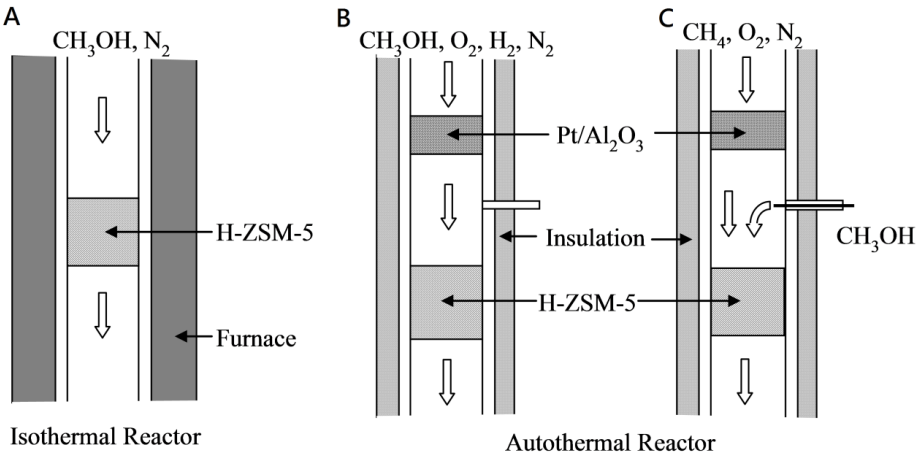

Figure 4.1 Simplified schematic of methanol dehydration reactor under (A) isothermal condition; (B) methanol top feed configuration; (C) methanol side feed configuration.

4.2.2 Reactor Design

The isothermal dehydration of methanol to DME was carried out in a vertical furnace as shown in Fig 4.1A. The catalyst (H-ZSM-5 and quartz) was supported by quartz wool. A thermocouple was placed in the middle of the catalyst bed to measure the temperature of the reaction. The total flow rate, including internal standard N_2, was maintained at 2 SLPM. The isothermal reaction temperature was controlled by a temperature controller.

The autothermal reactions for methanol dehydration were investigated in two reactor configurations. The first set of experiments explored a top feed configuration with methanol, N_2, O_2, and H_2. Here, H_2 was used as a sacrificial fuel as shown in Fig. 4.1B. The methanol/H_2/O_2 ratio was varied with balance N_2 to maintain a total flow rate of 2 SLPM. The H_2/O_2 ratio was maintained constant at 2 which is H_2 combustion stoichiometry. The C/O ratio in this reactor configuration is defined as the ratio of the number of moles of carbon in methanol to the number of moles of oxygen in O_2. The two catalyst layers were separated by a distance of 48 mm. The zeolite catalyst was supported in the reactor by quartz wool. Three thermocouples in the zeolite catalyst layer were

located at the top, middle and bottom of the catalyst layer to monitor the reaction temperatures.

The second set of autothermal experiments was performed with top feed of CH_4, N_2 and O_2. Methanol was fed from the side of the reactor as illustrated in Fig. 4.1C. CH_4 was supplied from the top of the reactor at a constant value of 0.2 SLPM. The C/O ratio here is defined as the number of moles of carbon in methane divided by the number of moles of oxygen in O_2. The total flow rate, including methanol, was maintained at 2 SLPM. An 80 ppi monolith was used on top of the zeolite in order to provide a better mixing for entering gases and methanol. A 58 mm distance was kept between two stages of the catalysts. The configuration of zeolite catalyst was the same as the first set of autothermal reactions.

4.2.3 Measurements

Gas samples of steady-state reactor products were identified and analyzed by gas chromatography and mass spectrometer (GC-MS), equipped with a thermal conductivity detector (TCD) and a flame ionization detector (FID) using a HP Plot-Q column. Column response factors and retention times were determined by calibrating known quantities of species relative to N_2. Each data point represents an average of three experimental runs.

4.3 Results and Discussion

4.3.1 Isothermal Methanol Dehydration

Methanol dehydration over zeolite H-ZSM-5 is tested isothermally to determine the temperature range and the corresponding product distribution. Methanol conversion and selectivity for isothermal methanol dehydration is plotted against the temperature as shown in Fig. 4.2A. As the catalyst temperature increases (190 to 350 ˚C), the methanol conversion increases (20-86%). The equilibrium of homogeneous methanol decomposition (to CO and H_2) and methanol dehydration (to DME only) are also plotted in Fig 4.2A. For the methanol dehydration reaction, the equilibrium methanol conversion

decreases as temperature increases since it is an exothermic reaction in which higher conversion is achieved at a lower temperature. The isothermal methanol conversion curve approaches the equilibrium curve as temperature increases because higher temperature enables higher reaction rate. This graph is consistent with the isothermal results reported that H-ZSM-5 has 100% DME selectivity and 80% DME yield at 253 ˚C [83]. The selectivity to DME remains >99% between 190 and 270 ˚C and falls at higher temperature. This shows that methanol is only converted into DME and water at lower temperatures (~270 ˚C) and is converted to secondary products at higher temperature. This is also consistent with previous findings that the reactor starts to produce unsaturated hydrocarbons over H-ZSM-5 (Si/Al=100) at about 270 ˚C[84]. The equilibrium methanol conversion (decomposition reaction without catalyst) increases (94% to 100%) as temperature increases (190 ˚C to 350 ˚C). In this temperature range, the highest production of CO and H_2 observed is < 0.1 mol% (not plotted). Significant decomposition of CH_3OH into H_2 and CO is observed at higher temperature (~400 ˚C) [85].

The product distribution of isothermal methanol dehydration at different temperatures is shown in Fig 4.2B. The methanol flow rate monotonically reduces, while DME flow rate has a peak at ~270 ˚C. At 320 ˚C and 350 ˚C, C_2 and C_3 are produced in higher amounts than C_4-C_6 species. The C_2 and C_3 are mostly light olefins (> 80%). This is consistent with the reports from many researchers that ethylene is the major primary hydrocarbon (MTO) produced and is most abundant at low temperatures; butane and especially propylene become more important at higher temperatures for the MTG process[86]. Fig. 4.2B also shows ~35% and ~30% hydrocarbons are produced over H-ZSM-5 at 350 ˚C and 320 ˚C respectively, indicating more hydrocarbons are produced at higher temperatures.

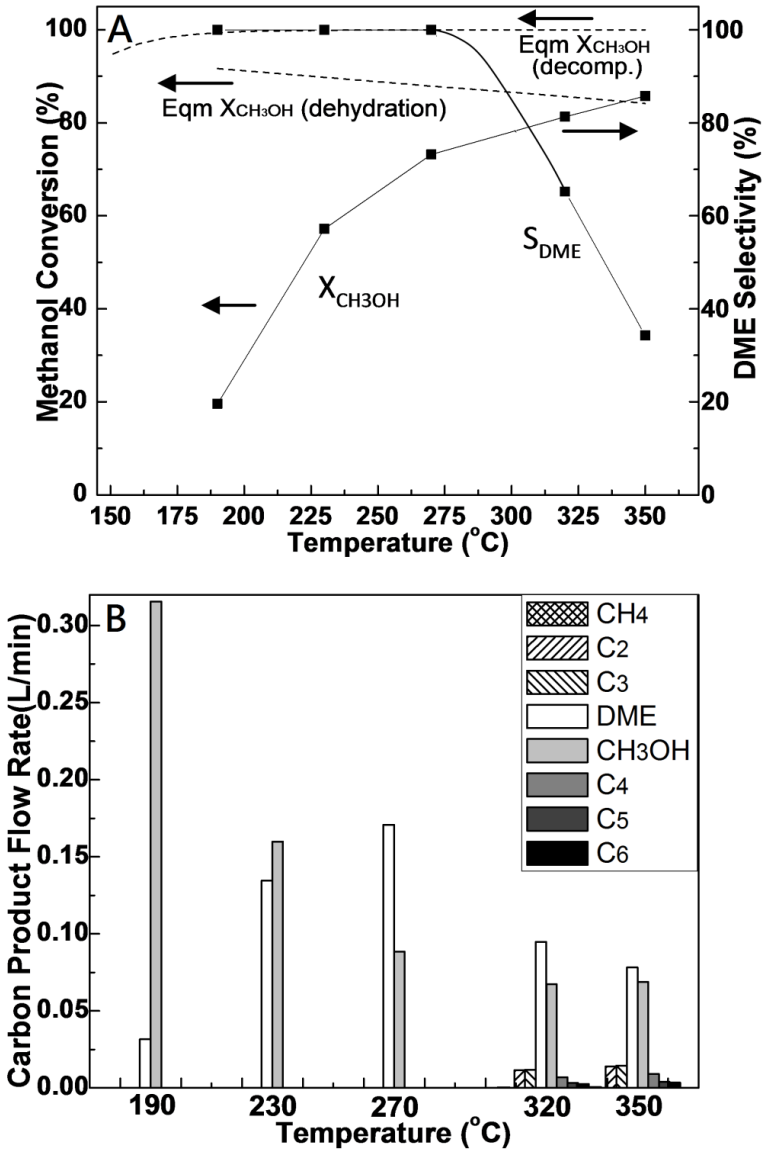

Figure 4.2 (A) (■) Methanol conversion and DME selectivity for isothermal reaction; (---) Equilibrium methanol conversion for methanol dehydration and methanol decomposition (decomp.) calculated by HSC software. (B) Carbon product flow rate of the effluent at different temperatures.

4.3.2 Autothermal Methanol Dehydration Reaction

4.3.2.1 Noble Metal Catalysts

The effect of catalyst on the first stage was studied for Pt and Rh coated monoliths since they are known to convert fuel or solid biomass model compounds into primarily syngas [36],[87]-[88]. Here, 1 wt% Pt/α-Al_2O_3 and 1 wt% Rh/α-Al_2O_3 are examined to optimize the first stage of autothermal reactor while varying C/H/O ratio from 1.62/2/1 to 2.16/2/1. At the same C/H/O ratio, Rh coated catalyst converts 8-10% more methanol and the temperature of CPO reaction is 20-40 ˚C lower than Pt coated catalyst. In terms of carbon selectivity, Rh coated monolith gives higher CO selectivity and lower CO_2 selectivity in this range of C/H/O ratio because Rh is a better steam-reforming catalyst and results in higher H_2 and CO yields [82]. For both Pt and Rh coated catalysts, as the C/O ratio increases, CO selectivity decreases and CO_2 selectivity increases, consistent with the result reported by Traxel et al. on 2-2.5 wt% Pt or Rh/α-Al_2O_3 catalyst for C/O =1.5 to 2.7 without sacrificial fuel [87]. For the following experiments, noble metal catalyst 1 wt% Pt/α-Al_2O_3 is used on the first stage for autothermal reactor since Pt converts less methanol and generates more heat.

4.3.2.2 Methanol Top Feed Configuration

The autothermal reaction with top-feeding methanol is carried out in a two-stage reactor, and the results are plotted in Fig. 4.3. H_2 here fed from the top of the reactor acts as a sacrificial fuel. The aim of H_2 addition is to preferentially oxidize H_2 and allow less methanol oxidation in the top stage and more methanol dehydration in the second stage. This is because H_2 has a higher sticking coefficient on noble metal (Pt and Rh) compare to hydrocarbons [89]-[91]. As shown in Fig. 4.3A, the first stage of the autothermal reactor converts 50% to 27% of methanol as C/H/O ratio increases from C/H/O=1.62/2/1 to 2.16/2/1. A higher ratio of methanol to oxygen results in less oxidation which generates less heat, thus lowering the operating temperatures downstream. The overall methanol conversion for the two-stage reactor varies from 91% to 78% as C/H/O ratio varies. The

methanol conversion in the zeolite layer increases as temperature decreases with varies C/H/O ratio (41% to 51%).

The DME selectivity and yield is plotted in Fig. 4.3B. At the lowest C/H/O ratio (1.62/2/1), the DME yield is only 2.9% since most of the methanol after the first stage is converted into hydrocarbons. As the C/H/O ratio increases (C/H/O=1.76/2/1), the temperature is reduced, which resulted in a 3-fold increase in the DME produced. Further increasing the fuel to oxygen ratio in the feed results in a lower temperature with more methanol available for dehydration in the second stage and hence a higher DME yield. At highest fuel to oxygen ratio, the methanol available for dehydration over zeolite is the highest (51%) and so is the DME yield (30%).

The product distributions before and after zeolite are plotted in Fig. 4.4A and B, respectively. The amount of CO, CO_2, and CH_4 produced before- and after the zeolite are the same as shown in Fig. 4.4A and B, while H_2 and H_2O are not plotted. As C/H/O ratio increases from 1.62/2/1 to 2.16/2/1, the amount of CO and CO_2 produced decreases and the H_2 production increases. This is because as the fuel to oxygen ratio in the feed increases, operating temperature decreases, resulting in a reduction of the steam reforming of CH_3OH and reserve water gas shift reaction (equation (4-3)) which produces less CO and more H_2 [92].

Fig. 4.3B shows the temperature profile on the upstream noble metal coated monolith and the downstream zeolite catalyst with varying C/H/O ratio. The zeolite catalyst stage has a temperature variation less than 20 ˚C for most cases except for the fuel lean case (C/H/O=1.62/2/1) where the temperature varies over a range of 70 ˚C. However, Skinner et al. [80] shows that ethanol dehydration in autothermal reactor having a temperature variation of 40-120 ˚C. Compared to previous results, the temperature variation in the zeolite region in our study is lower and desirable because it gives more control over the product yield and reaction temperature. The fuel lean case (C/H/O=1.62/2/1) should be avoided since we want to minimize the MTG reactions.

The operating temperature of the zeolite layer and the product distribution were also adjusted by varying the distance between two catalyst stages (58 mm to 85 mm) at a

constant C/H/O ratio (2.16/2/1). The temperature of the first stage was held constant while the average temperature of second stage varied from 297 ˚C to 265 ˚C with a temperature variation of less than 10 ˚C. The DME yield with constant C/O ratio and varying space between two stages is reduced by 10%, while the DME yield in the previous case (varying C/H/O ratio and constant distance) increases by 28%. This is because for the case of varying distance, the average temperature in the zeolite layer does not change much as distance varies from 58 to 85 mm (ΔT_{avg}=25 ˚C), resulting in small changes in DME yield. This is due to that fact that the reactor is almost adiabatic. The energy loss flux is 0.37 and 0.34 J/cm^{2}·s for top feed configuration and side feed configuration, respectively. Moving the zeolite layer down 10 mm results in the energy lost of 0.63 J/s. The calculations have been carried out in the Appendix B.

4.3.2.3 Methanol Side Feed Configuration

In the top feed experiments, a significant fraction of the methanol (27-50%) is partially oxidized in the Pt/α-Al_2O_3 layer. A part of the methanol is also decomposed into CO and H_2 without the catalyst at this relatively high temperature (> 400 ˚C). A way to increase availability of methanol for dehydration is to introduce methanol from the side of the reactor after the noble metal while CH_4 is partially oxidized in the upstream stage. In this case, the first stage can be operated at higher CH_4 to oxygen ratio (higher operating temperature) without the concern of increased methanol conversion in the Pt stage. It also reduces the methanol decomposition as it avoids the hot noble metal catalyst. In this configuration, CH_4 is used as sacrificial fuel to generate the heat for the second stage dehydration. Although CH_4 has a lower reactivity compare to methanol, CH_4 is preferred since methanol is fed from the side of the reactor and no preferential oxidation is involved. Furthermore, the price of CH_4 (nature gas) is cheaper than H_2. The temperature profile, methanol conversion, DME selectivity and product distribution for side feed configuration are plotted in Fig 4.5. The temperature of monolith and zeolite layer decreases as C/O ratio increases. The temperature variation of zeolite catalyst is ~20 ˚C except the case when C/O=0.84 where temperature variation is 90 ˚C. The C/O=0.84

is the boundary for the MTG process under this reaction condition. The highest yield of DME is ~80 % at C/O ratio of 1.01 when the average zeolite temperature is 295 ˚C. This yield is as high as others reported in literature for non-autothermal (isothermal) reactions (~80% at this temperature) [83],[93]. The product distribution is illustrated in Fig 4.5C. The large CH_4 bar is mostly (> 99%) the unconverted sacrificial fuel CH_4 coming from the first stage. The trends of the unconverted methanol after second stage and the production of hydrocarbon (C_2-C_6) are the same as the top feed configuration. The trend of DME production is different from that of the top feed configuration as DME formation shows a peak at C/O =1.01. It is desirable to have a higher methanol conversion over the zeolite catalyst. This requires lower conversion of methanol on the first stage. With methanol top-entering configuration, a lower methanol conversion on Pt stage is obtained when higher C/H/O ratio is used, leading to a higher possibility of catalyst coking. This explains the reason why the DME produces peaks in Fig. 4.5C, but not in Fig. 4.4B. For methanol side feed configuration (Fig.4.5C), after C/H/O =1.01, the temperature is low enough that DME production rate becomes slower and the production of DME falls.

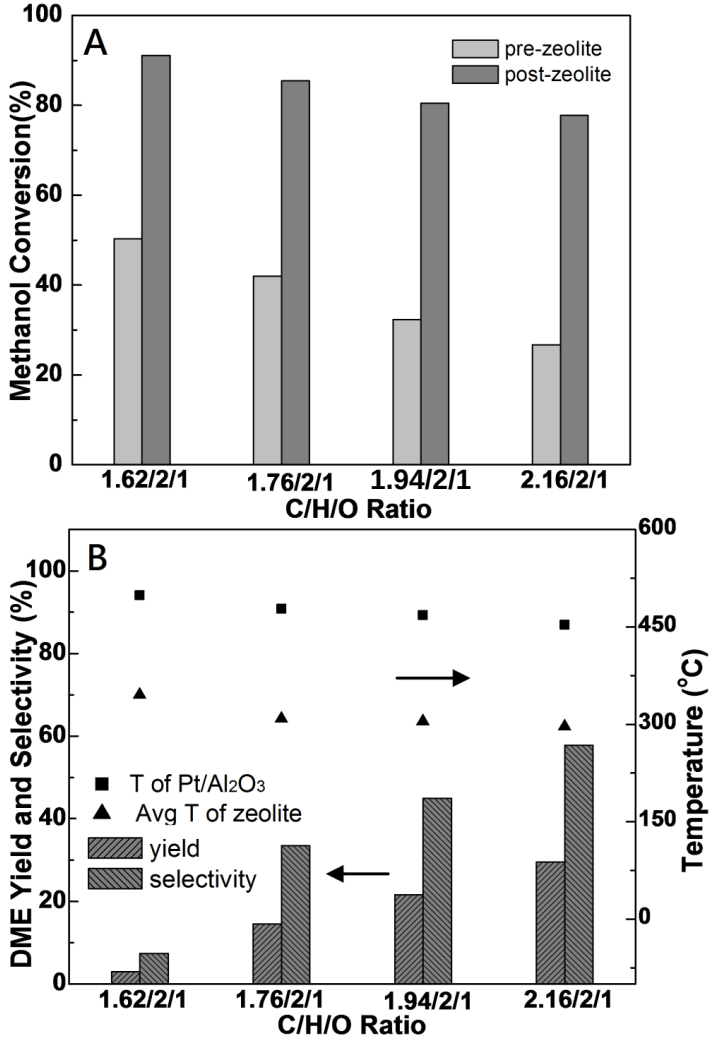

Figure 4.3 Methanol top feed configuration: (A) Methanol conversion after first stage and second stage of the reactor; (B) DME selectivity and yield and reactor temperature at two catalyst stages at varying C/H/O ratio.

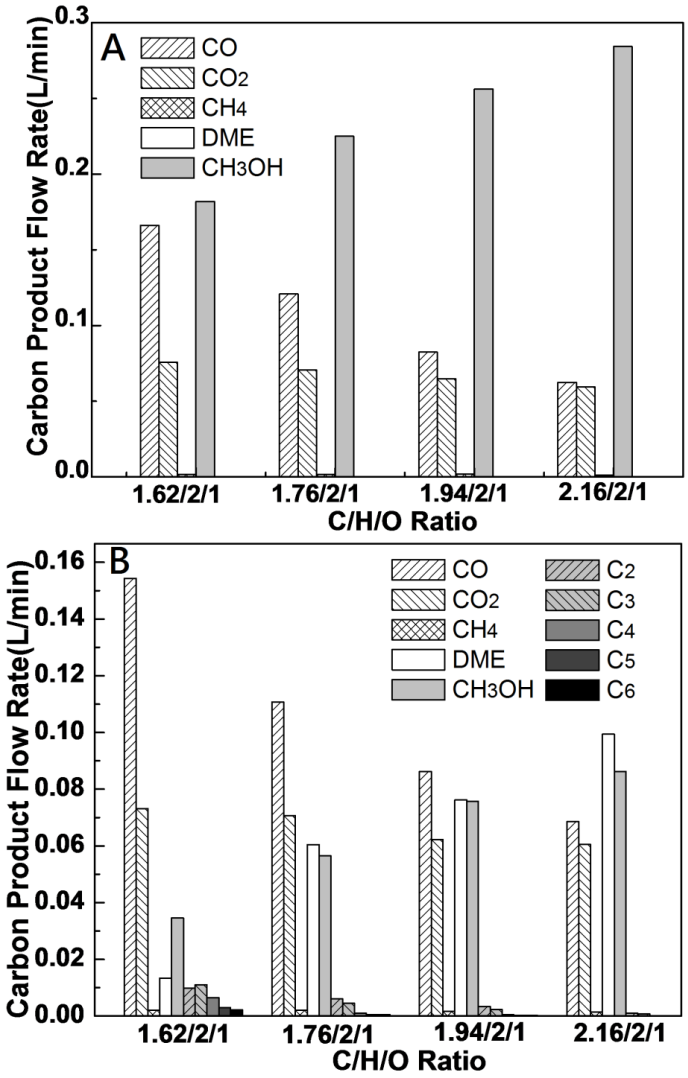

Figure 4.4 Methanol top feed configuration: product distribution of (A) pre-zeolite section and (B) post-zeolite section at different C/H/O ratio.

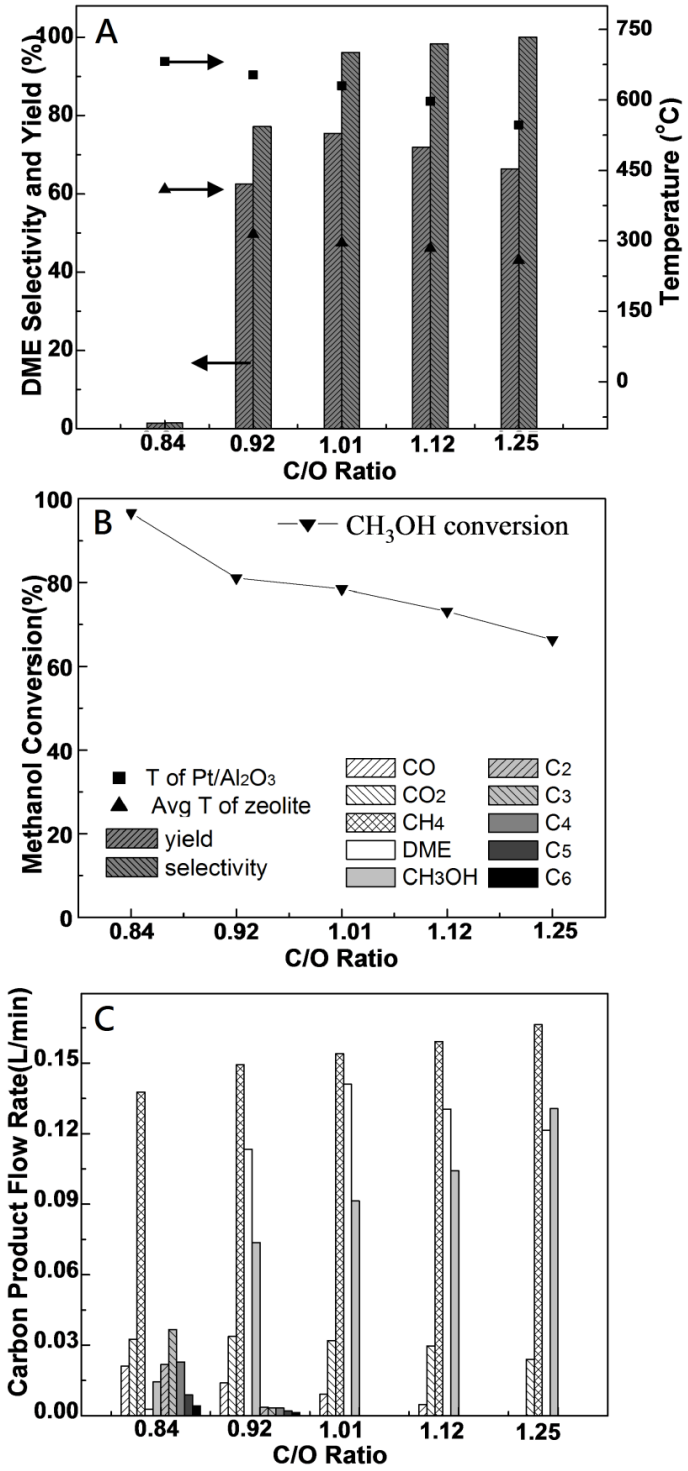

Figure 4.5 Methanol side feed configuration: (A) DME selectivity and yield and temperature profile of two catalyst stages vs. C/O ratio; the arrow pointed to the left is for the bar graph and the arrow pointed to the right is for the temperature points. (B) Methanol conversion vs. C/O ratio (C) Carbon products flow rate of the effluent at different C/O ratio.

4.3.2.4 Comparison among Three Configurations

Isothermal, top feed methanol and side feed methanol reactions are compared in terms of methanol conversion and DME selectivity in Fig. 4.6. Here, the methanol conversion corresponds to the reactions that take place in the zeolite layer, and the temperature used for plotting is the average temperature on the zeolite bed. One observes that the side feed condition has almost the same amount of methanol converted as an isothermal reaction. This is because the temperature variation across the zeolite layer is small (less than 20 ˚C) except the case corresponding to the lowest C/O ratio. In contrast, the methanol conversion is much smaller for methanol top feed, in spite of varying C/O ratio or space between the two stages (not plotted). This is because almost half of the methanol introduced is used to provide heat on the first stage. In this case, the methanol entering the second stage is at lower methanol partial pressure. Upon reducing the amount of methanol by half (i.e. at half the original partial pressure) and carrying out the reaction under the same conditions (same amount of zeolite and under the same temperature), the dehydration rate is observed to decrease by a factor of two, suggesting that the dehydration reaction rate is first order in methanol concentration. This is consistent with the findings of other researchers [94].

As shown in Fig 4.6B, the DME selectivity for top feed is lower because CO and CO_2 are generated as by-products from methanol. The DME selectivity is higher for side feed configuration because the source of CO and CO_2 is CH_4, not methanol. The DME selectivity for the isothermal reaction is comparable to the side feed configuration since CO and CO_2 are not produced. The difference in DME selectivity between the isothermal reaction and the side feed configuration is due to the temperature variation in the zeolite layer. DME selectivity for both configurations is comparable up to a temperature of about 350 ˚C (difference <12%). Beyond this temperature, the apparent difference in selectivity is not of interest because the reaction chemistry changes producing hydrocarbons from methanol.

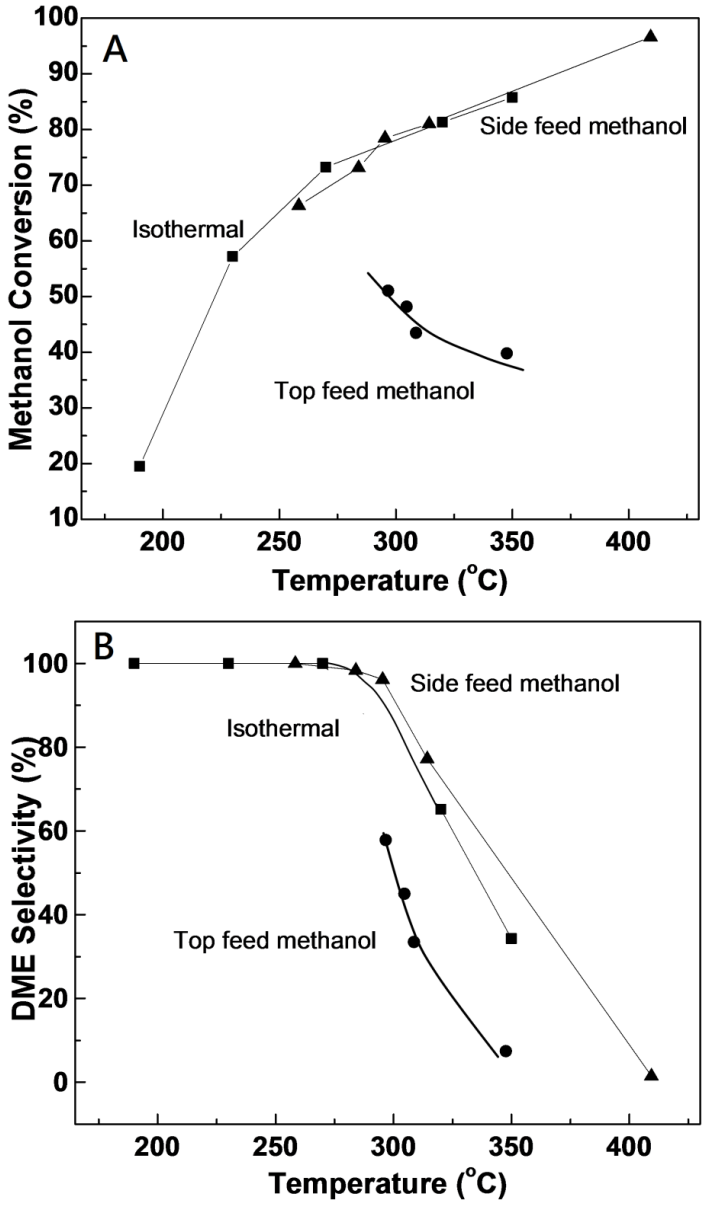

Figure 4.6 (A) Methanol conversion for three different conditions vs. temperature; (B) DME selectivity of three different conditions vs. temperature.

4.4 Conclusion

Methanol was dehydrated to DME using a two-stage autothermal short contact time reactor with up to 100% DME selectivity and ~80% DME yield. A platinum catalyst was found to give less methanol conversion and generate more heat in the upstream stage than Rh. We show experimentally that DME production dominates over decomposition and MTG below 300 ˚C (> 95% selectivity to DME), but at 350 ˚C these side reactions become significant. Higher operating temperature and larger conversion of methanol in noble metal layer and zeolite layer could be adjusted by decreasing methanol to oxygen ratio or the distance between stages. Isothermal experiments using H-ZSM-5 catalyst achieved 75% DME yield while the highest yield of DME was 30% for methanol top feed configuration. The highest yield of DME was obtained using side feed configuration (~ 80%) which is comparable to the value reported in literature (~ 80%). In conclusion, the autothermal reactor discussed here achieves methanol upgradation by removal of one oxygen atom through a dehydration reaction, resulting in a higher energy density yet clean liquid fuel, DME. This reaction can be designed to give high DME selectivity and yield by pairing a noble metal catalyst with a zeolite layer.

CHAPTER
FIVE

AUTOTHERMAL REFORMING OF BUTANOL TO BUTENES IN A STAGED MILLISECOND REACTOR: EFFECT OF CATALYSTS AND ISOMERS*

SUMMARY

Dehydration and isomerization of butanol is studied in an autothermal short contact-time reactor containing a 1 wt% Pt stage followed by a zeolite or ɣ-Al_2O_3 stage downstream to convert butanol into butenes with up to 95% yield at residence times on the order of 100 milliseconds. CH_4 is fed as a sacrificial fuel to the Pt stage and butanol is fed between the stages to avoid undesired oxidation and reforming reactions of butanol over Pt. The energy released by CH_4 catalytic partial oxidation drives downstream butanol dehydration and isomerization.

The effect of catalyst is studied by comparing the performance of HZSM-5, HFER, and ɣ-Al_2O_3 catalysts. Higher yields (20%) of butenes were obtained with ɣ-Al_2O_3 and HFER than with HZSM-5. The absence of Brønsted acid sites in ɣ-Al_2O_3 and the small pore structure of HFER lead to reduced yields of large side products such as higher hydrocarbons that promote oligomerization reactions. A 95 % butene yield is obtained with HFER at temperatures ranging from 280-350 ^oC and a 95 % yield with ɣ-Al_2O_3 at temperatures between 320-350 ^oC. Only a 75% butene yield was obtained with HZSM-5 at 230 ^oC.

The effect of hydrocarbon structure on product formation is studied by comparing conversions of each butanol isomer using a heated tube reactor at temperatures between 200-400 ^{o}C. The reactivity of butanol follows as: t-butanol > 2-butanol > iso-butanol > 1-butanol. *trans*-2-butene and *cis*-2-butene are primarily formed from linear butanol isomers, while isobutene forms from branched butanol isomers. Conversions and product distributions of butanol isomers formed over HZSM-5 in a staged reactor are comparable (<10% difference across all species) with data using a heated tube reactor at similar temperatures.

We successfully demonstrate an alternative pathway to dehydrate butanol into butenes with an autothermal staged reactor compared to conventional methods for applications in small-scale biomass utilization. The largest advantage of this reactor is the integration of highly exothermic autothermal stage and endothermic alcohol dehydration stage which provides an alternative processing technique to maintain the bed temperature.

[*]Parts of this chapter appear in: Hui Sun, Samuel Blass, Edward Michor, and Lanny Schmidt, "Autothermal reforming of butanol to butenes in a staged millisecond reactor: effect of catalysts and isomers", accepted by *Applied Catalysis A: Genreal* (2012). DOI: 10.1016/j.apcata.2012.07.039

5.1 Introduction

Significant research has focused on the development of processes to convert biomass to fuels and chemicals with the goal of decreasing dependence on fossil fuels. The production of butanol from biomass has recently attracted both industrial and academic interest [95]-[96]. Various processes for producing butanol isomers from biomass are described in the literature. 1-butanol can be produced by traditional ABE fermentation process with a production ratio of 3:6:1 of acetone: butanol: ethanol. Recently, Liao et al. [97] demonstrated that iso-butanol can be produced by yeast or micro-organism from sugar, such as glucose or cellulose. A biosynthetic pathway reported by Atsumi et al. [98] achieved a high yield, high-selectivity production of iso-butanol from glucose.

Deoxygenation of butanol is investigated as a means of increasing the energy density of butanol. On the other hand, dehydration of butanol into butenes has a potential application on improving market acceptance of alcohols. In spite of a lot of efforts, alcohols have rarely gained acceptance beyond their inclusion as blending components in the fuel. The conversion of butanol into butenes overcomes this obstacle and results in the production of material that is valuable as fuel intermediate and as petrochemical intermediate.

Previous studies have focused on the mechanisms of butanol dehydration over solid-acid catalysts [99]-[101], and skeletal isomerization of linear butene into branched butenes [102]-[105]. Butene can play a prominent role in the fuel production. The butene isomers obtained from butanol dehydration can be oligomerized to liquid fuels for transportation purposes [106]-[108]. In the alkylation process, one mole of C_4 olefins reacts with one mole of isobutane to form an isoparaffin which is 4 carbon number heavier [109]. In addition, Isobutene is also widely used as a precursor for polymers and octane-enhancing additives for gasoline [101]. Traditionally, isobutene is produced via isomerization in a heated tube from linear butene with a 40% yield with residence times up to ~10 seconds [102]-[104]. Linear butene is obtained by catalytic cracking of petroleum products [101].

Autothermal staged reactors have been studied as a means of deoxygenating biomass using ethanol as model systems. Our previous results demonstrated methanol dehydration to dimethyl ether (DME) with high yield (~80%) and ethanol dehydration to ethylene with a 95% yield in a staged reactor at a residence time of 100 milliseconds [10],[110]. In this work we extend this analysis to butanol because the feedstock contains a greater number of C-C bonds than methanol or ethanol thus enabling it to undergo both dehydration and isomerization reactions. Concurrent dehydration and isomerization reactions of butanol isomers to butenes are rarely reported in the literature. The novelty of the staged reactor lies in the combination of two catalytic functions in a single tube. The upstream Pt stage functions as an internal heat source by catalyzing partial oxidation reactions of CH_4. The energy released heats the downstream zeolite stage which catalyzes dehydration and isomerization reactions. The autothermal staged reactor is a departure from conventional methods of producing butene from butanol, because heat is generated internally rather than being provided externally. The largest advantage of this reactor is that it pairs exothermic and endothermic dehydration chemistry which provides an alternative processing technique to maintain an adequate bed temperature [111].

Dehydration and isomerization in a staged reactor occurs at residence times of approximately 100 milliseconds which is faster than conventional processes (residence time is ~100 times larger [102],[104]). Small scale butanol processing in an autothermal staged reactor is a high throughput process and is a good candidate for replacing conventional fuel and chemical platforms in a biofuel-driven economy.

In this work, 1 wt% Pt/α-Al_2O_3 was used for catalytic partial oxidation (CPO) reactions on the first stage and HZSM-5, HFER, or ɣ-Al_2O_3 for butanol dehydration/isomerization on the second stage. The axial temperature gradient along the downstream stage was resolved to help explain reactor performance. The effect of hydrocarbon structure was investigated by reacting four different butanol isomers into the heated tube reactor. The product selectivities and yields obtained from experiments with a heated tube reactor and autothermal reactor containing HZSM-5 catalyst are compared. Finally, the results lead to the development of an autothermal steady state operating

configuration that permits integration of CPO of CH_4 and deoxygenation of biomass derived butanol chemistry at high process feed rates.

5.2 Experimental

A schematic of the staged reactor is shown in Fig 5.1 (right). Platinum (1 wt% Pt) was coated on ceramic foam monoliths (99.5% α-Al_2O_3) 18 mm diameter and 10 mm length with 45 pores per linear inch (ppi) using the incipient wetness method [29],[56],[112]. Uncoated foams were placed at the front- and back-faces of the catalyst to reduce axial heat loss. All monoliths were wrapped with ceramic insulation to eliminate gas bypass. K-type thermocouples were placed at the center of the monolith to measure catalyst temperatures and the reactor was insulated with fiberfrax insulation. Each catalyst was used for at least 20 h with no significant deactivation or observed coke formation. All experiments were carried out at atmospheric pressure.

Commercial catalysts (Zeolyst) NH_4-ZSM-5 powder with Si/Al=25 and NH_4-FER powder with Si/Al= 28 were used. The proton form of the zeolite was obtained by calcining the ammonium form in a furnace from room temperature to 500 ^oC with 1 ^oC/min temperature ramp and 5 hour soak in air. Either HZSM-5, HFER, or γ-Al_2O_3 (0.6g) were mixed with 2.4 g of quartz and situated between two 80 ppi monoliths in the reactor. The zeolite was regenerated in a furnace at 600 ˚C with a total flow of 1 standard liter per min (SLPM) of air for 1 h. The upstream and downstream stages were separated by 80 mm. A fused silica capillary (Agilent, 0.53mm ID) was placed in the center of the reactor through a bottom port which was then sealed with a septum as a guide for a thermocouple. The axial temperature profile was measured by motion of the thermocouple inside the quartz capillary tube [113]-[114].

CH_4 was fed as a sacrificial fuel to the Pt stage at 0.2 SLPM. The C/O ratio, defined as the molar feed rate of methane over the twice the molar feed rate of O_2, was changed by varying oxygen flow. Butanol isomers were introduced to the reactor at 0.18 ml/min. Butanol was vaporized using a syringe pump and a resistive heating element and

introduced into the reactor halfway between the two stages through a 1/8 inch stainless steel tube containing 8 holes (0.016" ID) and welded shut at one end as shown in Fig 5.1 (right). The holes allowed for more uniform dispersion of butanol vapor in the reactor. The total flow rate to the reactor was held constant at 1.7 SLPM.

Gas samples of products at steady-state were identified and analyzed by a gas chromatograph equipped with thermal conductivity and flame ionization detectors. Response factors and retention times were determined by calibrating known quantities of species relative to N_2 which was used as an internal standard. Gas flow rates were controlled by mass flow controllers (Brooks Instrument).

The configuration of the heated tube reactor is similar to the staged reactor but without the Pt stage. A quartz tube (19 mm ID) placed inside a clamshell furnace as shown in Fig 5.1(left). The total flow rate was maintained at 1.7 SLPM with the same amount of butanol introduced (0.18 ml/min). Reaction temperature was controlled by a temperature controller (Omega, CSC32). For all the experiments, the carbon selectivity (S_c) is defined in equation (5-1) where v_j is the number of carbon atoms in molecule j, and F_j is the molar flow of species j.

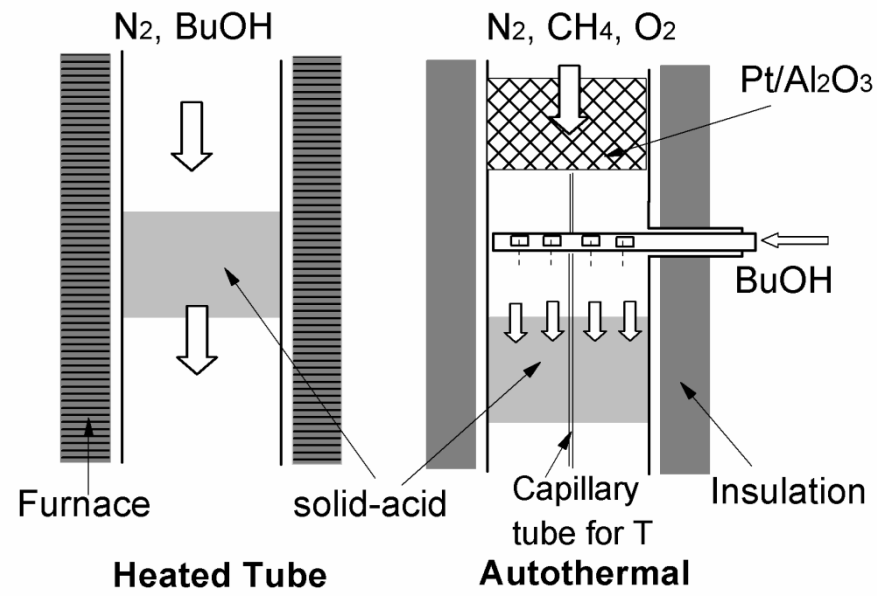

Figure 5.1 Simplified schematic of the heated tube reactor (left) and autothermal staged reactor (right) for butanol dehydration and isomerization reactions. The arrow direction indicates the direction of the flow. The dotted lines represent the flow pattern of butanol vapor.

$$S_c = \frac{v_j F_j}{\sum_j v_j F_j}; \quad j \neq \text{fuel} \qquad (5\text{-}1)$$

5.3 Results and Discussion

5.3.1 Autothermal Staged Reactor: Top Stage

The hydrogen selectivity (S_H) and CO selectivity (S_{CO}) of the top stage is plotted in Fig 5.2A. Fig 5.2A also depicts the upstream and downstream stage temperatures (right y-axis). The reaction temperature of the downstream zeolite stage is controlled by adjusting the C/O ratio on the upstream Pt stage. Higher temperatures are obtained by feeding more oxygen into the reactor to increase the amount of combustion. The kinetics of catalytic partial oxidation on Pt is too slow to enable the CPO reaction to reach equilibrium [87]. The temperature regime on the Pt stage ranges from 500 ^{o}C to 825 ^{o}C as C/O is varied from 0.53 to 1.67. This results in zeolite temperatures ranging from 200 to 355 ^{o}C. The vertical bar in Figure 2A indicates that the difference in top and bottom temperature on the second stage is ~50^{o}C with HZSM-5 catalyst. Despite the 300 ^{o}C variation in temperature of the Pt stage, the zeolite stage temperature gradient is consistently -3.3 ^{o}C per mm because the reactor is well insulated with ~0.4 J/cm^2-s heat lost as reported in previous results [110] .

The axial temperature profile in the reactor shown in Fig 5.2B with isobutanol feed is plotted at various C/O ratios. A noticeable temperature drop (up to 65 ^{o}C) is apparent at a 55 mm distance from the Pt stage which is where butanol is introduced into the reactor. This temperature drop is attributed to heat transfer between the Pt stage exhaust at 500-700 ^{o}C to the butanol vapor at 150 ^{o}C. A steeper drop in temperature is observed at low C/O ratios where the back shield monolith temperature can reach up to 700 ^{o}C. At the C/O = 1.40-1.67, the temperature gradient is constant between the two stages while at the C/O = 0.53-1.11, the temperature gradient increases at 80 mm. At higher temperatures, a

greater rate of heat transfer to the butanol vapor occurs. Butanol has to travel farther before radial heat loss becomes significant again. At 80 mm, the temperature gradient returns to its original value. The temperature gradient is approximately linear in the zeolite region, suggesting radial heat loss might be dominant and any thermal contribution from dehydration/isomerization reaction may be negligible.

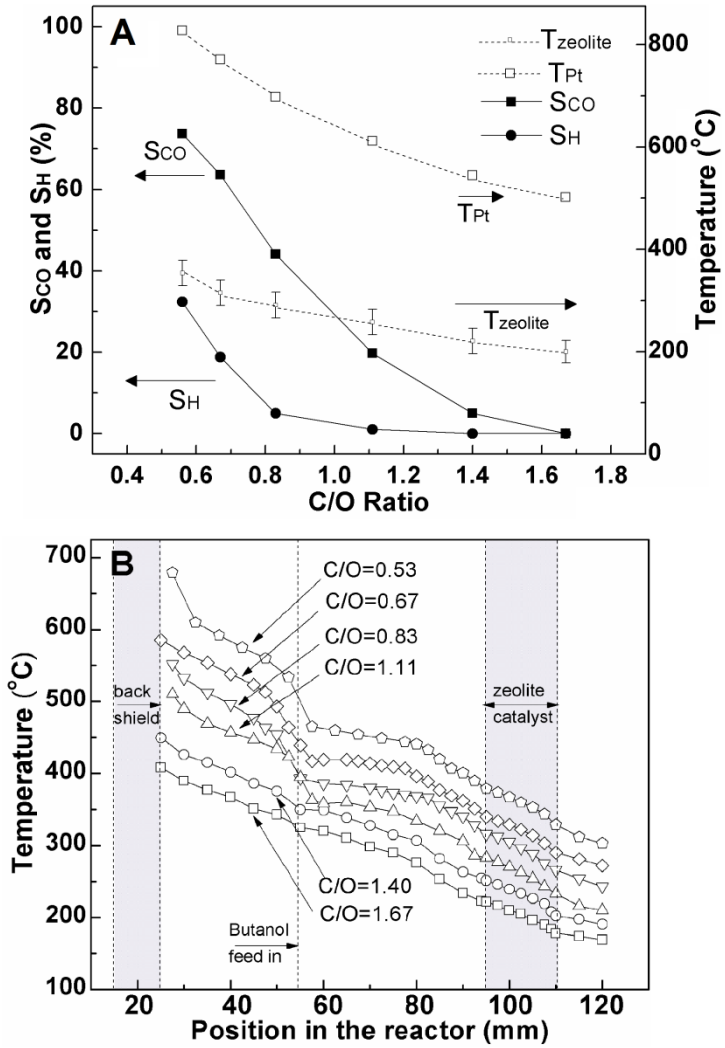

Figure 5.2 (A) Hydrogen selectivity (S_H) and CO selectivity (S_{CO}) and temperature profiles at various C/O ratio in the autothermal reactor. (B) Axial temperature profile at different C/O ratio vs. position in the autothermal reactor. Figure (A)-(B), catalyst is HZSM-5 and feed is iso-butanol.

5.3.2 Autothermal Staged Reactor: Effect of Catalysts

Figs 5.3 and 5.4 depict C_4 olefin yield and butanol conversion over ɣ-Al_2O_3, HFER and HZSM-5 catalysts in the autothermal staged reactor. The axial downstream stage temperature is averaged (T_{avg}). The corresponding C/O ratio is shown on the top axis. As shown in Fig 5.3, the total C_4 olefin yield over HFER and ɣ-Al_2O_3 increases with T_{avg} and reaches a maximum of 90-95% between 280 and 350 ^oC. Over HZSM-5, the C_4 olefin yield goes through a maximum of 75% at 230 ^oC after which it decreases with increasing temperature. The temperature at which a maximum C_4 olefin yield is obtained over HFER is 40 ^oC lower than yields over ɣ-Al_2O_3. Over all three catalysts studied, the C_4 olefin yield from 1-butanol follows the same trends as those from isobutanol but requires an additional 20 ^oC to reach same yields.

Fig 5.4 shows 1-butanol and isobutanol conversion and the selectivities of all observed C_4 species over each catalyst studied as a function of T_{avg}. As seen in Fig 5.4A-D, conversion of isobutanol over ɣ-Al_2O_3 reaches 100 % at 320^oC and over HFER at 280 ^oC, while the total C_4 selectivity remains constant at 90-95%. On ɣ-Al_2O_3 and HFER, no isobutene is formed from 1-butanol feed, while 50-60% selectivity of isobutene is formed from isobutanol over ɣ-Al_2O_3 (Fig 5.4A) and 40-50% over HFER (Fig 5.4C). HZSM-5 has the highest activity compared to HFER and ɣ-Al_2O_3 since the conversion reached 100 % at 250 ^oC which is lower than 280 ^oC for HFER and 320 ^oC for ɣ-Al_2O_3. However, the total C_4 selectivity decreases by 50% over HZSM-5 with increasing temperatures as larger compounds are formed. The selectivity of isobutene increases by 15% over HZSM-5 (Fig 5.4F), indicating the occurrence of isomerization reactions.

As evidenced by the conversion of butanol, the presence of Brønsted acid sites in the catalysts make zeolites more active than ɣ-Al_2O_3 which primarily contains Lewis acid sites. The high activity of HZSM-5 limits the range of temperatures over which a high C_4 selectivity can be obtained. A high C_4 selectivity is only obtained over HZSM-5 between 200-250 ^oC but it can be reached over the entire range of T_{avg} studied with HFER and

ɣ-Al_2O_3. The 10-membered ring (MR) HZSM-5 has larger cavities exist in place of intersection of channels make it more active than HFER which has only 10x8 MR pores [102]. ɣ-Al_2O_3 primarily has Lewis acid which are too weak to catalyze oligomerization and isomerization reactions. Therefore C_4 olefin yields are higher over HFER and ɣ-Al_2O_3 because C_4 olefins are not consumed in oligomerization and isomerization reactions. In addition, HFER is suggested to be optimal for isomerization of linear butenes to isobutene due to shape selectivity effects [104],[115]-[116]. HFER has a pore size enabling isobutene diffusion but suppressing dimer and oligomer formation which are byproducts and cause catalyst deactivation.

While there is precedence for isomerization reactions of C_4 hydrocarbons over HFER, the conditions used previously are significantly different than ours. Ménorval et al. reported isomerization of n-butene *to* isobutene on HFER with residence times ranging from 1 min to 4.7 min, and achieving conversions of 15.3% to 43.8% at 350 ^oC, respectively [117]. In Fig 5.4C, the C_4 selectivity over HFER remained relatively constant indicating the lack of isomerization reactions, however, this might simply be due to the short residence times used (100 milliseconds compared with 1 minute used by Ménorval et al.). In Fig 5.4D *trans*- or *cis*-isomers shows a slight changing in selectivity (~13%), indicating the presence of double bond isomerization between *trans*- and *cis*-isomers, but with no isobutene formation. Comparing the performance of HFER and HZSM-5, which have the same Si/Al ratio, the extent of isomerization over HZSM-5 catalyst is more apparent than on HFER and may be attributed to the larger pore size of HZSM-5.

The deactivation test carried out for three catalysts shows that the conversion of isobutanol at 400 ^oC over HZSM-5 decreases by ~20% over 2 h, due to pore blockage by carbonaceous deposits formed over Brønsted acid sites. The conversion of isobutanol over HFER decreased by 10% after 4 h and remained constant over ɣ-Al_2O_3 for 8 h. The small pore size of HFER and the lack of strong acid sites on ɣ-Al_2O_3 minimize the production of side products such as higher hydrocarbons which deactivate the catalysts. This also demonstrates that HFER and ɣ-Al_2O_3 are more suitable catalysts for autothermal staged reactors than HZSM-5. These catalysts have a slow rate of

deactivation and require temperatures between 280-350 ^{o}C to achieve a high C_4 yield. High temperatures are not an issue for autothermal staged reactors due to an internal heat source which enables high temperatures to be easily reached.

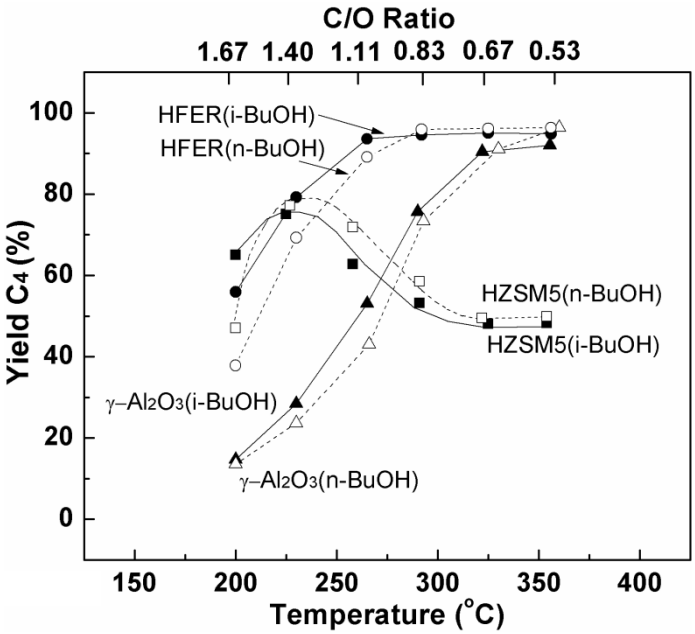

Figure 5.3 $C_4^=$ yield in autothermal staged reactor at various C/O ratios for three catalysts. Open symbols are C_4 yield with n-butanol feed, while closed symbols are those with iso-butanol feed. We take the average temperature of the top and bottom temperature to represent the average temperature (T_{avg}) of the second stage. Here, the temperature of every data point is the average temperature, and it has a corresponding C/O ratio shown on the top axis.

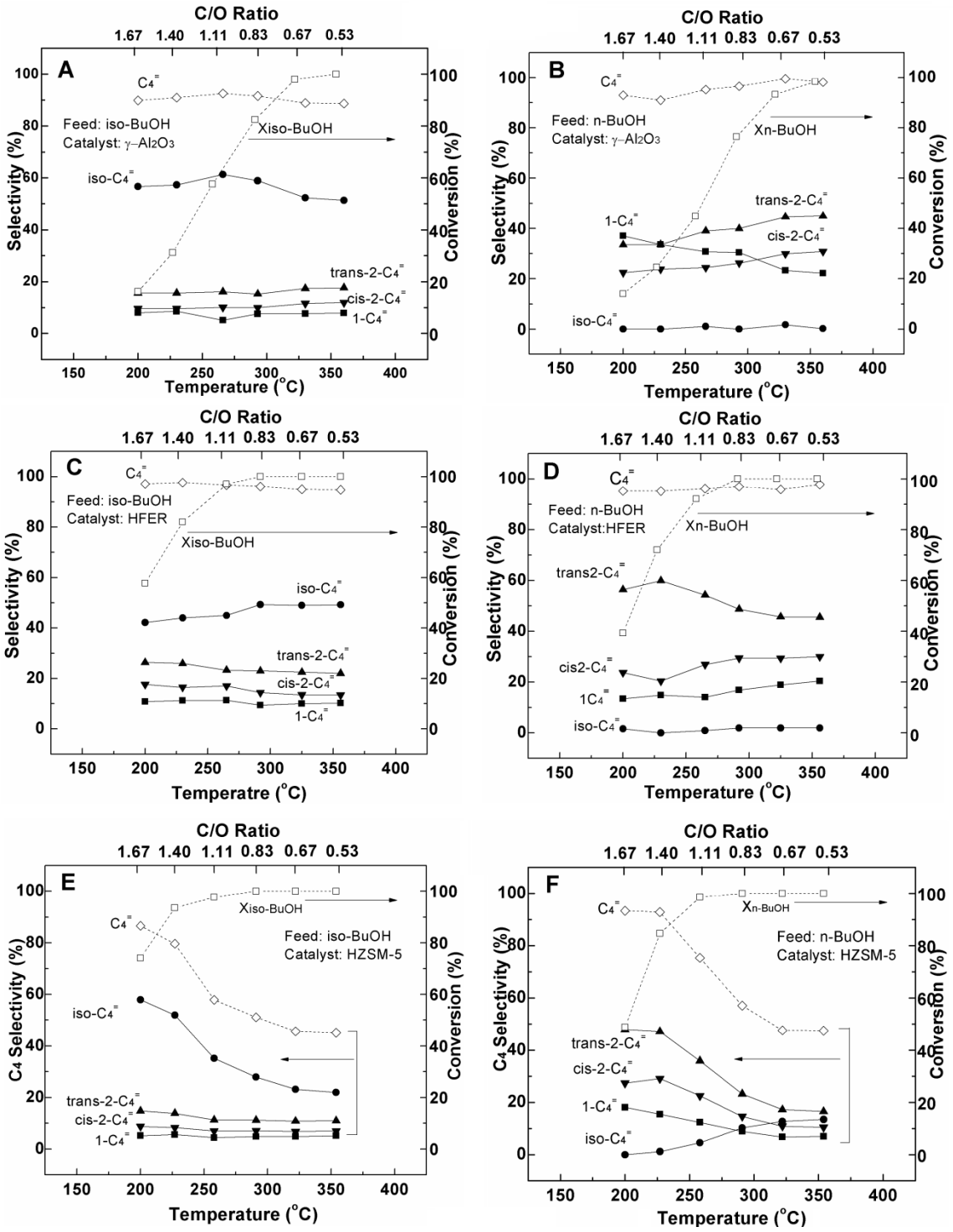

Figure 5.4 $C4^{=}$ selectivity, conversions for autothermal reforming of iso-butanol(left panel) and n-butanol (right-panel) with three catalysts. (A)-(B) show C_4 selectivity and conversion with catalyst ɣ-Al_2O_3, (C)-(D) is with catalyst HFER and (E)-(F) is with catalyst HZSM-5. X represents conversion here.

5.3.3 Heated Tube Reactor: Effect of Isomers

HZSM-5 is chosen as the catalyst to study the effect of isomers since it catalyzes the formation of a greater range of products than HFER or ɣ-Al_2O_3 enabling us to probe a larger number of reactions. In Fig 5.5A, t-butanol has the highest reactivity since the temperature at which it reaches 98% conversion (200 ^oC) is lower than temperatures for other isomers. At 200 ^oC, 2-butanol, isobutanol, and 1-butanol react with 88%, 72%, and 39% conversion respectively. This result is also consistent with the higher activation energies of 1-butanol, 2-butanol and isobutanol dehydration over NaHZSM-5 catalyst ~135-160 kJ/mol, compared to 80 kJ/mol for t-butanol dehydration at 60-185 ^oC [99],[118]-[121]. A lower activation barrier for t-butanol means a lower temperature is needed to reach 100% conversion.

In Fig 5.5B, it can be observed that 1-butanol is mainly transformed into linear butenes between 250-300 ^oC, while butenes are transformed into higher olefins and paraffins above 300 ^oC. The yield of C_5 and C_{6+} go through a maximum at 300^oC, while the concentration of propylene and ethylene continually increase with temperature. This suggests that C_{5+} products are intermediates while C_2 and C_3 species are final products. The amount of linear butenes, which are primary products in the dehydration reaction, initially decreases due to oligomerization to higher olefins. The butene yield becomes constant at temperatures greater than 300 ^oC. Product distributions from 2-butanol, t-butanol and isobutanol share the same trends as 1-butanol except below 250^oC where the total C_4 yields are different according to butanol isomer reactivity. Dehydration reportedly takes place at temperature less than 150^oC while skeletal isomerization occurs at temperatures between 300-500^oC one [101] with primarily dimerization mechanism over HZSM-5 [116]. In our studies, the selectivity of C_3 is larger than that of C_5 at 300-400 ^oC. We postulate that C_5 is the intermediate product which will be further cracked into C_3 and C_2.

In Fig 5.5C-D, the selectivities of C_4 olefins with 2-butanol and t-butanol feed are plotted, while those with iso-butanol and 1-butanol feed are plotted in Fig 5.6C-D (closed

symbol). In Fig 5.6D, *trans*-isomer which has a ΔH_f = -10.8 kJ/mol is thermodynamically preferred over the *cis*-isomer which has a ΔH_f = -7.7 kJ/mol even though the *cis*-isomer is more structurally favored on a catalyst surface due to reduced steric hindrance [105]. In addition, the selectivity of isobutene increases from 0 to 15% (T = 200-400 ^oC) indicating the occurrence of isomerization. Fig 5.5C shows that the C_4 olefin selectivities from 2-butanol dehydration are similar to 1-butanol dehydration (Fig 5.6D). In Fig 5.6C, the selectivity of isobutene decreased from 64% to 20% (T = 200 – 400 ^oC) with iso-butanol feed. t-butanol converts to isobutene with greater ease than other butanols, resulting in a high isobutene selectivity (90% selectivity at 200 ^oC in Fig 5.5D).

The literature suggests that a carbenium-ion transition state forms over the Brønsted acid site in the dehydration/isomerization process [102],[122]-[124]. Willams et al. [99] suggest the presence of an alkoxide intermediate for butanol dehydration at temperatures less than 150 ^oC. In our experiments, dibutyl ether is not observed in the product stream due to its instability at high temperature (>200 ^oC). The differences in products formed from each butanol isomer are attributed to the different intermediate structures that form. We postulate that butanol forms an alkoxide intermediate by eliminating water. The alkoxide structure then isomerizes to another alkoxide structure via a carbenium-ion-like transition state. The lack of isobutanol formation from 1-butanol reactions over all catalysts is evidence of a series reaction in which dehydration to an alkoxide is followed by isomerization. Branched products (isobutene) form from branched butanol isomers such as t- and iso-butanol while linear products (1-butene, 2-butene) form from linear butanol isomers such as 1- and 2-butanol. We postulate that linear alkoxide intermediates (structure I in Fig 5.6D and II in Fig 5.5C) are isomerized into branched products (structure III in Fig 5.6C and IV in Fig 5.5D) via a methyl-cyclopropyl carbenium-ion-like transition state before desorbing as olefins [122],[123]. Branched alkoxides are more stable than linear alkoxides so they barely isomerize to linear products.

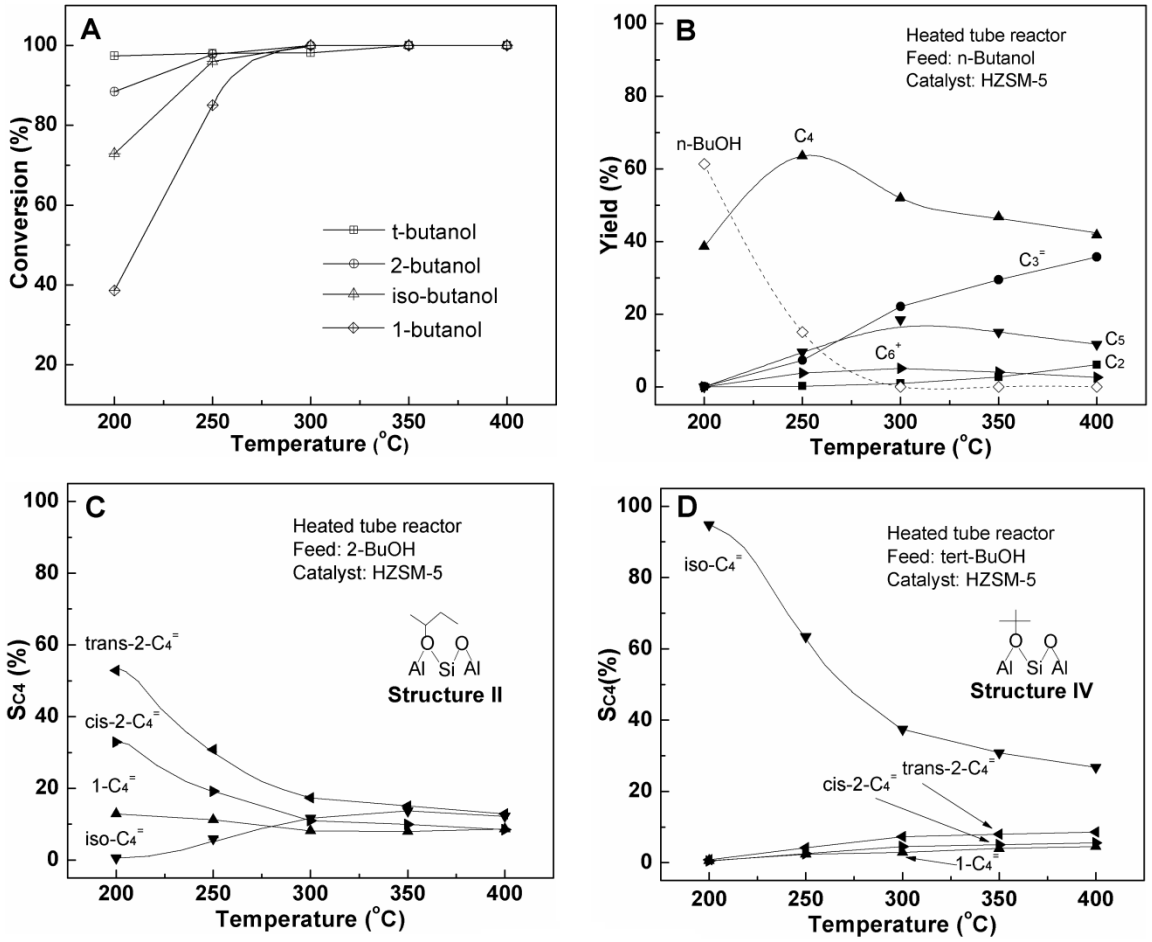

Figure 5.5 (A) Conversion of 4 butanol isomers in a heated tube reactor over HZSM-5 at various temperatures. (B) Product yield of heated tube reactor over HZSM-5 catalyst with n-butanol feed at various temperatures, (C) C_4 species selectivity for 2-butanol in a heated tube reactor over HZSM-5 catalyst. The C_2-C_3 and C_5-C_{6+} are not shown here for simplicity. (D) C_4 species selectivity for t-butanol in a heated tube reactor over HZSM-5 catalyst. Structure II and IV are corresponding alkoxide structures formed in isomerization process.

5.3.4 Autothermal Reactor vs. Heated Tube Reactor and its Implication

Product selectivities from the autothermal staged reactor experiments are plotted against those from the heated tube experiments in Fig 6. With an iso-butanol feed (Fig 5.6A and 5.6C), the selectivities of all products (C_3-C_{6+}, *trans*- and *cis*-isomers, iso-$C_4^=$ and 1-$C_4^=$) from the autothermal experiments are comparable to those from the heated tube experiments. With 1-butanol feed (Fig 5.6B), the selectivities of total C_4 and C_5 are comparable, while the C_3 selectivity is lower in the heated tube experiments by about 8% and the C_{6+} selectivity is higher by the same amount. In Fig 5.6D, the selectivity of *trans*- and *cis*-isomers is ~8% higher in the autothermal experiments, while 1-butene is lower by the same amount.

The differences in product selectivities between the heated tube and autothermal reactors may be due to the temperature gradients found in the autothermal reactor. The temperatures previously reported here are representative of all temperatures in the zeolite stage. The product selectivity between the autothermal and heated tube reactors with isobutanol and 1-butanol feed are comparable to each other (<10% difference). The differences can primarily be attributed to the similarity in the dehydration activation energy of isobutanol and 1-butanol. Zamaraev et al. reported that the activation energy ($\Delta H^{\neq}$) of isobutanol to isobutene is 138.1±8.4 kJ/mol[99], while activation energy of 1-butanol to n-butene is 133.9±8.4 kJ/mol at 105-185 ^oC with NaHZSM-5 catalysts [119]. This shows that the dehydration reaction rate of isobutanol and 1-butanol have similar sensitivity to temperature. Therefore, the deviation from heated tube reactor to autothermal staged reactor is comparable with both iso-butanol and 1-butanol feed. Additionally, linear butanol isomers undergo isomerization reactions while branched isomers do not. These isomerization reactions may be more sensitive to temperature changes than alcohol dehydration. This increased sensitivity would result in linear butanol isomers displaying a greater difference in product selectivities when comparing products formed on a zeolite with a temperature gradient as in the autothermal reactor or without a gradient as with the heated tube reactor.

The ability to sufficiently preheat the butanol by direct contact with hot exhaust gases implies that it is not necessary to employ a fired heater or a combustion chamber to preheat butanol. This could potentially reduce the capital cost of the process.

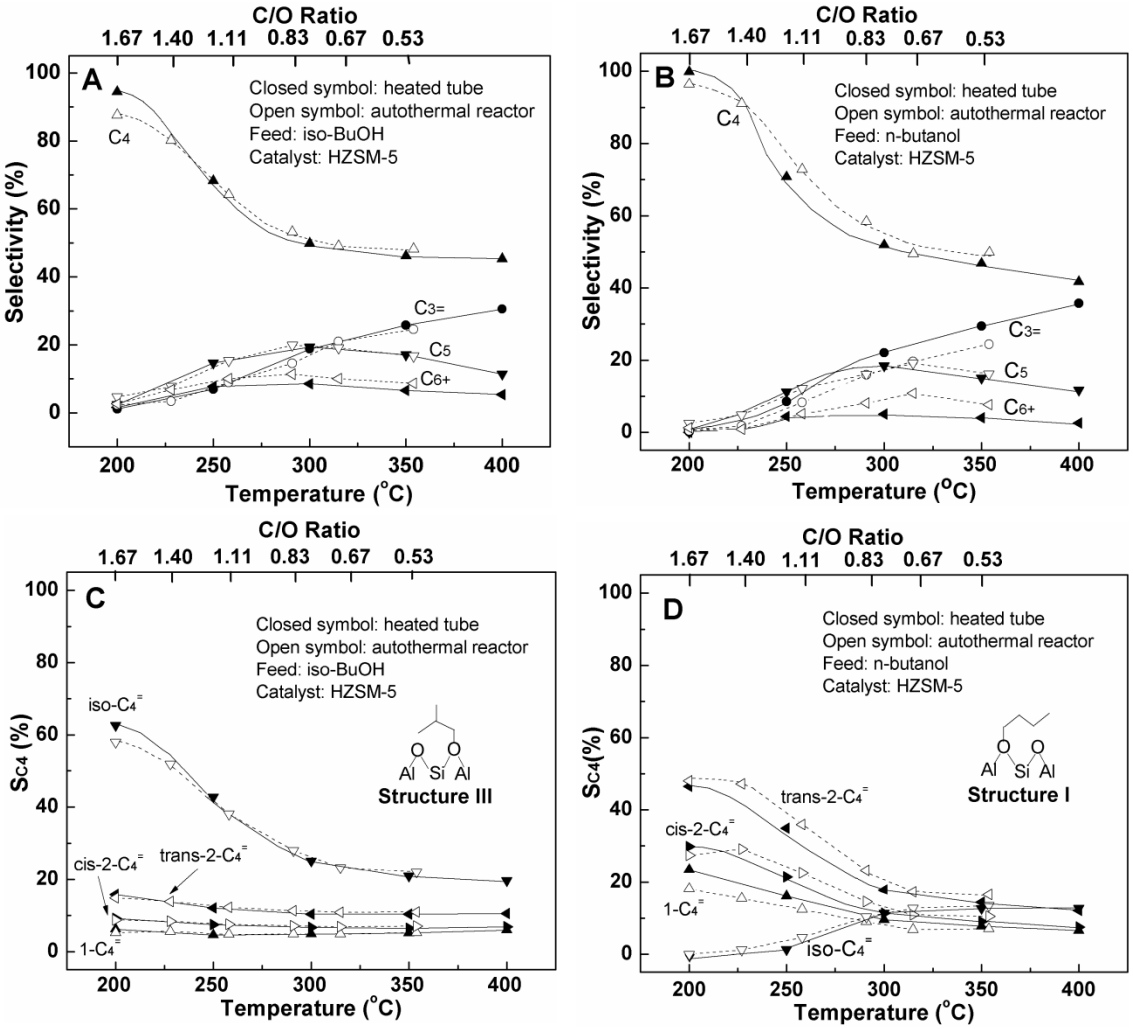

Figure 5.6 Comparison between autothermal staged reactor (open symbol) and heated tube reactor (closed symbol) in terms of product distribution (Fig. 6A-B) and $C_4^=$ selectivity (Fig. 6C-D). Autothermal reaction product selectivity is plotted vs. T_{avg} (bottom x-axis) and C/O ratio (top x-axis). (C)-(D): The C_2-C_3 and C_5-C_{6+} are not shown here for simplicity. Structure III and I are corresponding alkoxide structures formed in isomerization process.

5.4 Conclusion

Autothermal reforming of butanol isomers were investigated in a staged reactor with an upstream stage consisting of 1wt% Pt catalyst on α-Al_2O_3 and a downstream stage consisting of either ɣ-Al_2O_3, HFER, or HZSM-5 catalysts. The reactivity of the butanol isomers was studied by comparing their conversions over a range of temperatures. HFER and ɣ-Al_2O_3 have a 90-95% C_4 yield while the maximum C_4 yield over HZSM-5 is 75% due to its pore structure and acid strength effects. In the heated tube reactor, the reactivity of the butanol isomers is as follows: t-butanol > 2-butanol > isobutanol > 1-butanol. *trans*- and *cis*-isomers are obtained from linear butanol isomers, while isobutene is formed from branched butanol isomers. With HZSM-5, the product selectivities in the autothermal staged reactor were comparable to those from a heated tube reactor with a difference of <10 %. The autothermal staged reactor demonstrates the integration of exothermic and endothermic chemistry. The direct contact between butanol and hot exhaust gas has the potential applications to replace the fire heater or the combustion chamber, reducing the capital cost of the process.

CHAPTER
SIX

OXIDATIVE PYROLYSIS OF POLYSTYRENE INTO STYRENE MONOMERS IN AN AUTOTHERMAL FIXED-BED CATALYTIC REACTOR*

SUMMARY

This chapter focuses on oxidative pyrolysis of polystyrene into styrene monomers in an autothermal fixed-bed reactor. A continuous, no external heating, high throughput process has been developed by integration of several processes: depolymerization of polystyrene, catalytic partial oxidation of styrene monomers, steam reforming of styrene and water-gas-shift reaction. The highest styrene selectivity is ~75% at high C/O ratio (C/O>2.0). The effect of cofeeding CPO products (CO, CO_2, H_2 and H_2O) was also investigated. The addition of CO, H_2O has no significant effect on styrene selectivity, while the addition of H_2 (sacrificial fuel), increases the styrene selectivity to ~85%. Co-feed CO_2 increases steam reforming activity, resulting in less styrene selectivity. Steam reforming polystyrene in this system is also investigated by adding steam at low C/O ratio (0.8-1.1). The largest H_2 selectivity is ~70% showing that aromatics are H deficient and is not a good candidate for H_2 production.

---

*Parts of this chapter appear in : Hui Sun, Corey Rosenthal, and Lanny D. Schmidt, "Oxidative Pyrolysis of Polystyrene into Styrene Monomers in an Autothermal Fixed-Bed Catalytic Reactor", accepted by *ChemSusChem*, 2012, DOI number: 10.1002/cssc.201200412.

6.1 Introduction

Previously, our laboratory developed an autothermal reactor configuration with a noble metal catalyst to process solid biomass, such as cellulose and polyethylene (PE), for production of sustainable fuels. Inspired by this continuous, efficient, and char-free process, we used an autothermal fixed-bed reactor to fast pyrolyze polystyrene (PS) in an attempt to maximize the yield of styrene monomers. We obtained up to 85% styrene monomers yield with negligible lower polymers in a very stable process. The integration of autothermal fixed-bed reactors in the pyrolysis of polystyrene is found to efficiently recover monomers from waste plastics.

The disposal of plastic wastes is recognized as a major environmental issue as plastics are non-biodegradable. In 2005, the total amount of US Municipal Solid Wastes (MSW) was 28.9 million tons and 20-30% by volume are plastic wastes [125]. The conventional solutions, such as landfilling and incineration, are expansive and problematic to the environment. An ideal solution would be recycling and recovery, in which waste plastic is converted into economically valuable hydrocarbons. One such possible method is the pyrolysis of plastic wastes, which has attracted much attention from both academia and industry.

Due to its good processing properties, polystyrene (PS) is one of the most widely used plastics for various purposes. Numerous studies have examined pyrolysis of PS, both isolated and in mixtures with other main plastics wastes found in MSW. Scott *et al.* performed an atmospheric-pressure fluidized-bed pyrolysis of polystyrene[126]. Darivakis et al. reported that the total volatile yield from PS approaches 100% at temperature approaches to 800 ^{o}C but the condensable fraction is only 30% mainly consisting of styrene [127]. Other experiments pyrolyzed PS in the temperature range of 360-520 ^{o}C and found the product to be comprised mainly of styrene with minor amounts of dimers and trimers [128]-[129]. PS is mixed with other plastics (e.g. high-density polyethylene (HDPE), low-density polyethylene (LDPE), polypropylene (PP), and poly(vinl chloride) (PVC)) to examine the interaction of plastics in mixed-plastics

pyrolysis[130].

These examples of PS or PS mixture pyrolysis have mostly required batch reactors under high pressure [127]-[130]. The long processing time and large equipment requirements associated with this approach lead to high maintenance costs and make the reactors difficult to scale up. Therefore, an effective, continuous process with low operating cost and high process feed rates is highly desirable. Previously, our group developed an autothermal reactor with a noble metal catalyst to process biomass model compounds, such as cellulose into syngas or liquid products [29],[56],[33]. Inspired by this continuous, efficient, and char-free process, we utilized an autothermal fixed-bed reactor to fast pyrolyze PS in an attempt to maximize the yield of styrene monomers. In addition, the effect of introducing catalytic partial oxidation products, such as CO, CO_2, H_2 and steam, on product selectivity is investigated. The integration of autothermal fixed-bed reactors in the pyrolysis of polystyrene is found to efficiently recover monomers from waste polystyrene.

6. 2 Experimental

A schematic of the autothermal fixed-bed reactor is shown in Fig 6.1. An auger/hopper system (Schenck AccuRate) was used to feed polystyrene particles (600-850 μm, 35g/hr) to the reactor. Gas flow rates were controlled by mass flow controllers (Brooks Instrument). The catalyst supports were 1.3 mm diameter α-Al_2O_3 spheres (4g, 1cm bed). Metals were impregnated onto the supports by the incipient wetness techniques as reported previously [110],[131]. Al_2O_3 sphere is chosen as catalyst support because it is reported to have consistently high front face temperature due to higher conductive heat transfer rates as compared to monolith [132]-[133].

Two types of catalysts were used in polystyrene pyrolysis experiments: Rh-Ce catalysts and Pt-Ce catalysts with 2 wt% of each metal on each catalyst. Uncoated monolith (99.5% α-Al_2O_3) was placed at the back-face of the catalyst to reduce axial heat loss. The monolith was wrapped with ceramic insulation to eliminate gas bypass. K-type

thermocouples were placed at the back of the catalyst to measure the back-face catalyst temperatures and the reactor was insulated with fiberfrax insulation. The reactor was heated after the catalyst region to avoid any condensation of products.

For all experiments, polystyrene was completely pyrolzed at the front face of the catalyst to give 100% conversion of the solid feed. All experiments were carried out at atmospheric pressure. Gas samples of products at steady-state were identified and analyzed by a gas chromatograph equipped with thermal conductivity and flame ionization detectors. All the product species were analyzed by GC-MS in a separate run. Selectivities to product species were calculated on an atomic carbon basis (S_C) and an atomic hydrogen basis (S_H). The product selectivity was defined as (atoms in the product species)/ (atoms in the converted fuel). Carbon, hydrogen and oxygen balances typically closed with ±10%. In the steam reforming experiments, co-fed steam was not counted as fuel. Equilibrium calculations were performed with HSC 7.1 software by minimizing Gibbs free energy.

6.3 Results and Discussion

$(C_8H_8)_n \rightarrow nC_8H_8$	(6-1)	Depolymerization
$(C_8H_8)_n \rightarrow m(C_8H_8)_n + n(1-m)C_8H_8$	(6–2)	Polymer/monomer production
$(C_8H_8)n \rightarrow nC_8 + 4nH_2$	(6-3)	Coke formation
$C_8H_8 + 4O_2 \rightarrow 4H_2 + 8CO$	(6-4)	Oxidation
$C_8H_8 + 8H_2O \rightarrow 8CO + 12H_2$	(6-5)	Steam reforming
$H_2O + CO \leftrightarrow H_2 + CO_2$	(6-6)	Water-gas shift reaction

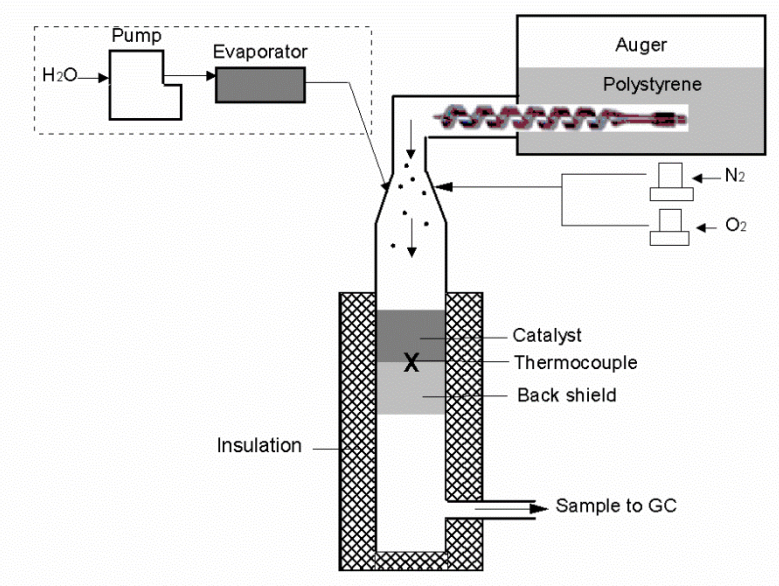

Figure 6.1 Experimental schematic for the production of polystyrene monomer or syngas from polystyrene feedstock. Pump and Evaporator in the dashed box are added for experiment with steam addition to the system.

6.3.1 Oxidative Pryolysis of Polystyrene

All possible reactions which take place in this autothermal reactor are shown in equations (6-1)-(6-6). Polystyrene particles directly contact a hot surface at temperature within a range of 600-900 ^{o}C. We postulate polystyrene particles first undergo a depolymerization reaction (Eqn 6-1), thereafter the styrene monomers mix with oxygen to undergo a surface oxidation reaction within the front part of the catalyst bed (Eqn 6-4) in the oxidation zone [92]. The steam reforming of styrene monomer into syngas (Eqn 6-5) and water-gas shift reaction (Eqn 6-6) occur in the later part of the catalyst bed (in the reforming zone). The undesired products coke and PS polymers could be formed as shown in Eqn (6-2)-(6-3). Here we want to maximize Eqn (6-1) while minimizing Eqn (6-2)-(6-5) in order to increase the amount of styrene.

Temperature and product selectivity (S_C and S_H) are plotted against C/O ratio, which is the ratio of carbon atoms in the solid feed to the atoms of oxygen in the O_2 feed (Fig 6.2). Higher temperatures are obtained by feeding more oxygen (lower C/O ratio) into the reactor to increase the amount of combustion. It was found that the Pt-based catalyst has

a higher catalyst temperature compared to Rh-based catalyst at all C/O ratios investigated (Fig 6.2A), suggesting more reforming activity occurs with Rh-Ce catalyst than Pt-Ce catalyst, especially at low C/O ratios (1.0-1.4).

Pyrolysis produces syngas at all C/O ratios. Both S_H and S_{CO} decreases with increasing C/O ratio, while S_{CO2} remains at a relatively constant value (10-20%) at various C/O ratios (Fig 6.2A, C-D). Equilibrium H_2, CO and CO_2 selectivity are also plotted in Fig 6.2A, 6.2C (dotted lines). The H_2 selectivity approaches ~50% of the equilibrium H_2 at lower C/O ratio (1.0 -1.2) with the Rh-Ce catalyst, indicating that catalytic partial oxidation (CPO) reaction is away from equilibrium.

All the hydrocarbon products are classified as other products. Selectivity of other products (S_{other}) increases with increasing C/O ratio (Fig 6.2C-D). The styrene monomer is the major product in S_{others} with minor amount of benzene, toluene, ethylbenzene and α-methylbenzene (Fig 6.2E-F). CH_4, ethylene and propylene are also detected with less than 0.5% selectivity; hence they are not explained in the following analysis. Styrene dimers and trimers are not observed throughout our experiment due to relatively high reaction temperature (600-900 ^oC). This is consistent with the observation reported from D. S. Scott *et al.* [126]. The styrene selectivity reaches a maximum ($S_{styrene}$=75%) at C/O=2.0 and maintains this selectivity in the range of C/O=2.0-2.4 with both catalysts. Furthermore, at low C/O ratio (C/O=1.0), the selectivity of styrene monomers is 20-40% over Rh- or Pt-based catalysts, demonstrating the high stability of gas phase styrene. Balonek *et al.* [81]showed that styrene has lower conversion (80-44%) in the C/O ratio range of 1.0-2.0 over Rh-Ce/ɣ-Al_2O_3 compared to other aromatics, such as benzene, toluene, and ethylbenzene. It is suspected that the lower conversion results from the higher bond energy associated with the carbon double bond of the ethenyl group. We surmise this high gas phase stability is also due to the conjugate structure between ethenyl group and benzene ring. All the minor products maintain constant selectivity (less than 6%) at all C/O ratios investigated as shown in Fig 6.2E-F. In addition, Rh-Ce catalyst has been shown to be stable for long periods of time at high operating temperature without signs of catalyst deactivation. A deactivation test was carried out at

C/O=2.0 over Rh-Ce/α-Al_2O_3 catalyst for 8 h (Fig 6.2B). Temperature increased by 20 ^oC, while styrene yield remained at 72±4%. CO, CO_2 and H_2 selectivities remained constant as well.

Noble metal (Rh or Pt) also plays an important role in product selectivity of polystyrene pyrolysis. The Rh-Ce catalyst lead to higher S_H than Pt-Ce catalyst at all C/O ratio, with the highest S_H approaching 50% at C/O=1.2. The Rh-Ce catalyst also produced more CO compared to the Pt-Ce catalyst with a peak selectivity of 55% at C/O=1.0. In addition, Rh-Ce coated spheres were observed to give lower selectivity to styrene, most notably at low C/O ratios, with the difference in selectivity between catalysts decreasing as the C/O ratio increased. At C/O = 1.0-1.2, $S_{styrene}$ using the Pt-Ce catalyst is twice as large as $S_{styrene}$ using the Rh-Ce catalyst, yet at C/O=2.0, Rh- and Pt-coated catalyst produced the same styrene selectivity (~75%). Those differences can be explained as Rh catalyst is widely regarded as an excellent partial oxidation catalyst with high reforming activity downstream of the oxidation zone in the catalyst bed, while Pt catalyst is frequently used as a combustion catalyst and has been shown to have lower reforming activity [114],[134]-[136].

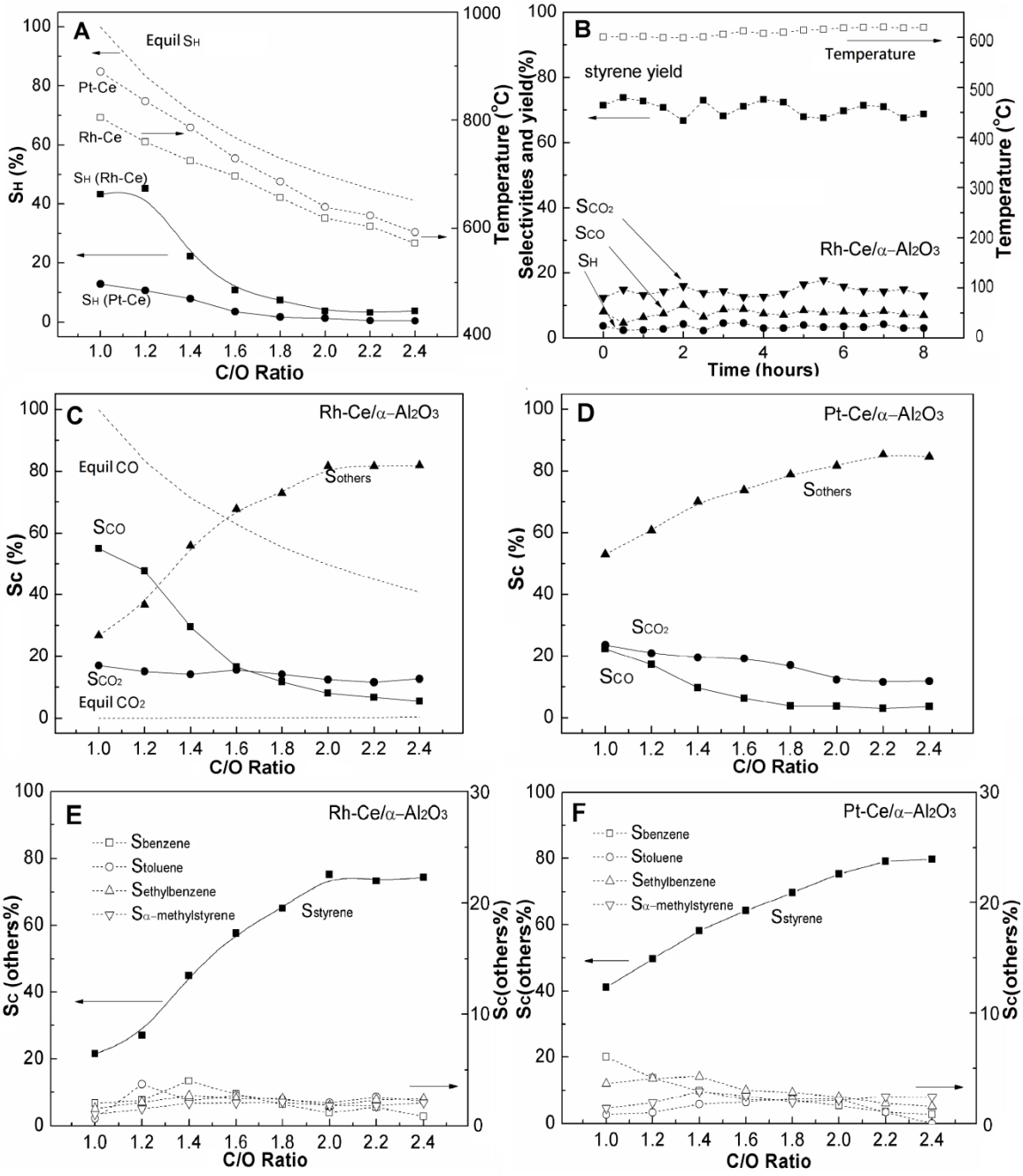

Figure 6.2 Pryolysis of polystyrene in an autothermal reactor (A) H_2 selectivity (S_H) and reaction temperatures; dotted line is the equilibrium H_2 selectivity at various C/O ratio with Rh-Ce catalyst; (B) deactivation test at C/O = 2.0 with Rh-Ce/α-Al_2O_3 catalyst; carbon selectivity (S_C) over Rh-Ce/α-Al_2O_3 catalyst are shown in (C) and (E); carbon selectivity over Pt-Ce/α-Al_2O_3 are shown in (D)and (F). In (C), dotted lines are equilibrium CO, CO_2 selectivity within investigated C/O range.

6.3.2 Effect of CPO Products (H_2, CO, CO_2 and H_2O) Addition

Effect of adding the CPO products are studied and the results are shown in Figure 6.3-6.5. H_2 was added to the feed gases and the results are depicted in Fig 6.3. Experiment was conducted with a constant polystyrene flow rate and H_2 flow rate with increased N_2 flow (2.0 SLPM) as a safety precaution for lab-scale operation. The O_2 flow rate is varied to obtain desired C/O ratio. Using Rh-Ce/α-Al_2O_3 catalyst, the styrene selectivity is 44-70% at C/O= 1.4-2.2 without the addition of H_2. Addition of H_2 consistently increases styrene selectivity by 10-15%. A similar trend can be observed for H_2 addition using Pt-Ce/α-Al_2O_3 catalyst. A larger increase (15-20%) in styrene selectivity is observed at C/O=1.4-1.8 with Pt-based catalyst. Peak styrene selectivity reaches 85% for both catalysts at high C/O ratio (2.2). The fast reaction between O_2 and H_2 limits the O_2 available to partially oxidize styrene monomers [33]. Previous work by Bodke *et al*. reported that the addition of H_2 which acts as a sacrificial fuel in a catalytic partial oxidation system is able to increase the yield of ethylene from ethane [137]. This is due to the higher sticking coefficient of H_2 on noble metal catalysts and also the high diffusion coefficient of H_2 in a mass transfer limited system [110].

Effects of cofeeding CO and CO_2 are shown in Fig 6.4. The temperature of the reactor with CO addition is 20-50 ^oC higher than without CO addition, most notably at lower C/O ratios as the temperature discrepancy decreases with increasing C/O ratio. In terms of H_2 selectivity, there is a significant decrease upon adding CO at low C/O ratios (1.4-1.8), while H_2 selectivity is comparable at higher C/O ratios. In Fig 6.4B, the styrene selectivity with and without CO addition are comparable at all C/O ratios investigated. These findings demonstrate that cofeeding CO to the system does not have significant effect on product selectivity with Rh-Ce catalysts. This results is consistent with previous work which has shown that CO coverage is negligible on Rh catalyst at operating temperature above 600 ^oC [138].

As seen in Fig 6.4A, temperature decreases after cofeeding CO_2. The reactor is quenched due to low temperatures (<570 ^oC) at C/O ratios greater than 2.0. H_2 selectivity

with CO_2 addition is lower than no CO_2 addition at lower C/O ratios (1.4-1.8), but greater at higher C/O ratios. Similar to the temperature profile, styrene selectivity decreases with CO_2 addition by 5-15%. The CO selectivity (not plotted) increases by 12-15% with CO_2 addition. It is generally agreed that CO_2 has a strong positive influence on reforming activity and should theoretically increase the CO and H_2 selectivity [139]. The decrease H_2 selectivity observed here might be due to another effect from increasing reverse WGS.

Effect of steam addition is also studied and the results are shown in Fig 6.5. The reactor is quenched at high C/O ratio (C/O>1.1 and S/C=1.0). The temperature decreased with both increasing C/O and S/C ratios (Fig 6.5A). Backface temperatures within the catalyst bed ranged from 700 to 955 ^{o}C. The H_2 selectivities for different C/O and S/C ratios are shown in Figure 6.5B. With steam addition (S/C=0.5-1.0), the H_2 selectivity passes through a maximum. This is because at lower C/O ratios, combustion reactions dominate which reduces H_2 selectivity, while at high C/O ratios, reforming activity is suppressed by lower temperature, which also reduces the H_2 selectivity. H_2 selectivity increases from S/C=0 to S/C=1 due to increased WGS activity. The highest H_2 selectivity is ~70% at C/O=0.9 and S/C=1.0. The CO selectivity decreases with increasing C/O and increasing S/C ratios (Fig 6.5C). At the same C/O ratio, CO selectivity decreases with increasing S/C ratio due to increasing WGS activity. The addition of steam does not have a significant effect on styrene selectivity as shown in Fig 6.5D. The highest H_2 selectivity at S/C=1.0 is only ~70% , showing that aromatics are not a good feedstock to generate syngas since its structure is H_2 deficient, e.g. styrene only has H/C~1.

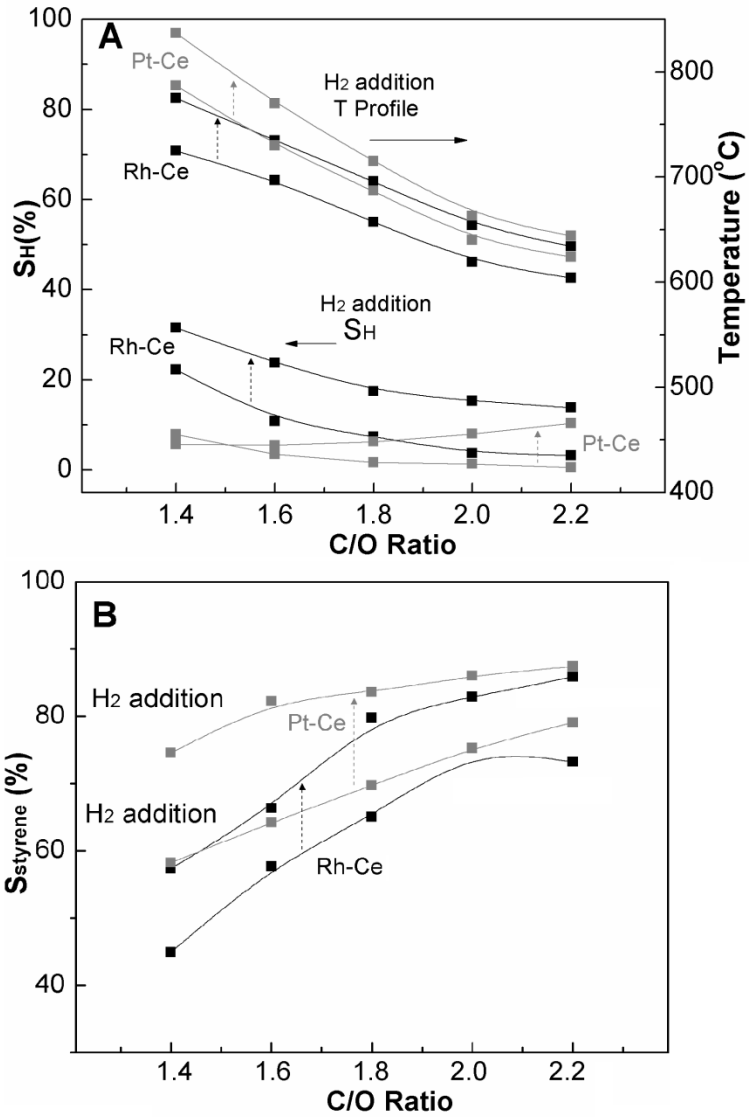

Figure 6.3 (A) H_2 selectivity and temperature profile before and after H_2 addition vs. C/O ratio on Rh-Ce/α-Al_2O_3 and Pt-Ce/α-Al_2O_3 catalysts (B) Styrene selectivity before and after H_2 addition vs. C/O ratio on Rh-Ce/α-Al_2O_3 and Pt-Ce/α-Al_2O_3 catalysts. Arrow appoints to the experimental results with H_2 addition.

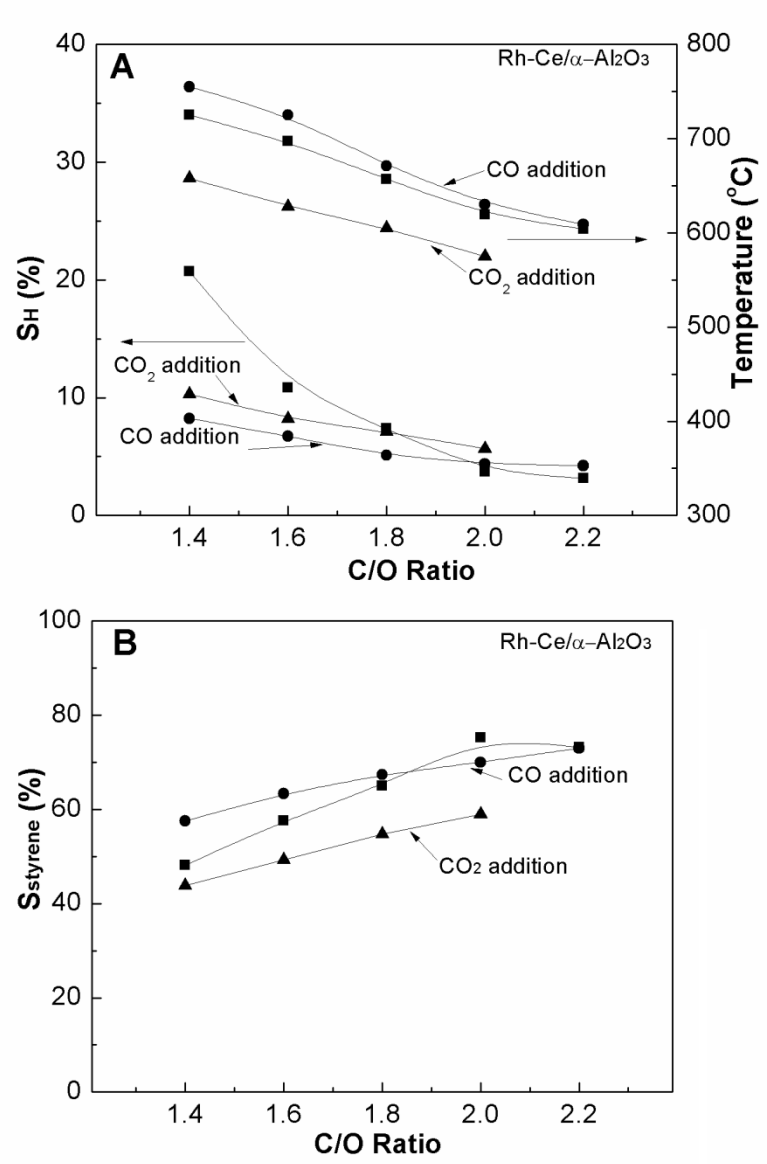

Figure 6.4 (A) H_2 selectivity and temperature profile vs. C/O ratio on Rh-Ce/α-Al_2O_3 with CO and CO_2 addition. Here, 0.4 SLPM CO or 0.4SLPM CO_2 premixed with N_2, O_2 and polystyrene particle at various C/O ratios. (B) Styrene selectivity vs. C/O ratio on Rh-Ce/α-Al_2O_3 with CO and CO_2 addition. Sphere symbol: CO addition, triangle symbol: CO_2 addition.

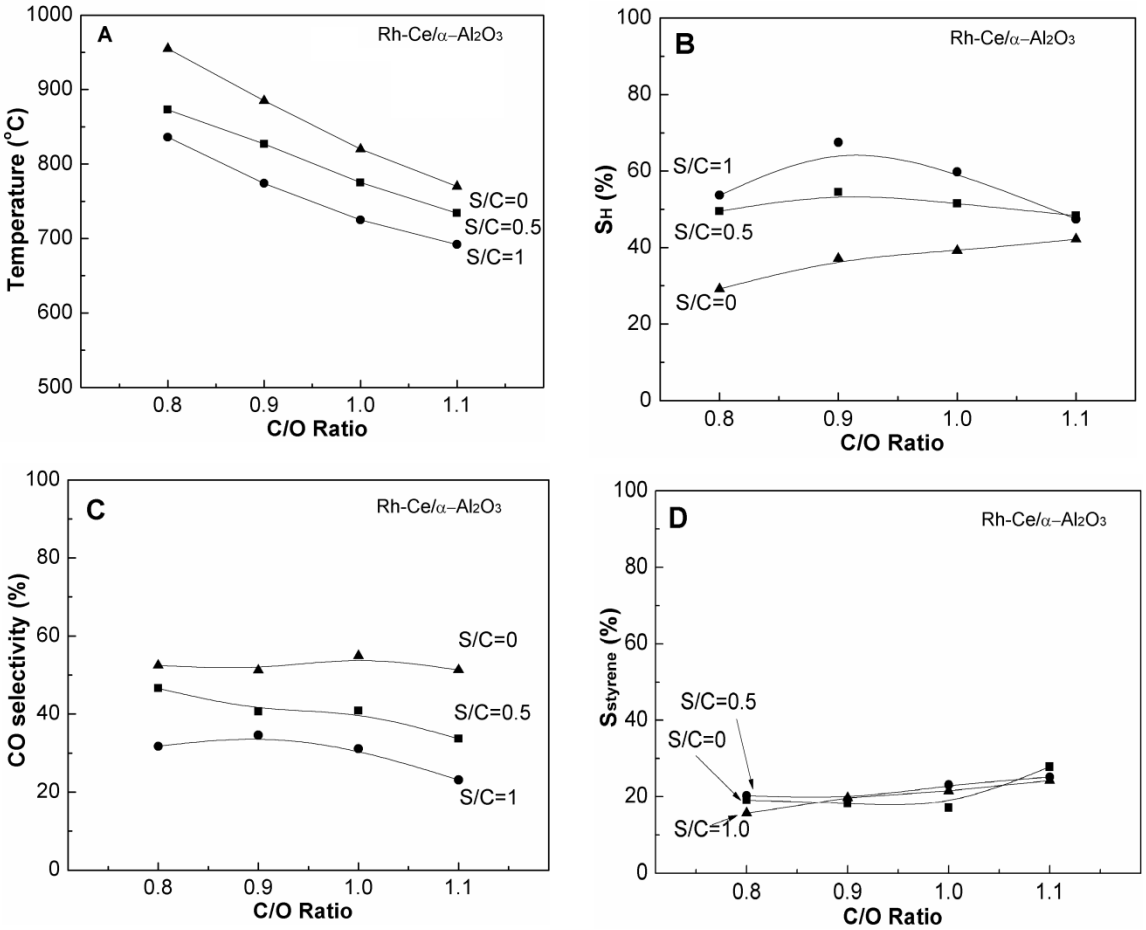

Figure 6.5 (A) Temperature; (B) hydrogen selectivity (S_H); (C) CO selectivity and (D) styrene selectivity results with Rh-Ce catalyst for steam addition at C/O = 0.8 - 1.1 and S/C = 0.0 – 1.0.

6.4 Conclusion

These experiments demonstrate that a fixed-bed catalytic reactor can be operated autothermally to produce high yields of styrene monomers (~80%) from polystyrene with ~20 ms resident time for long periods of time without deactivation. This enables continuous operation with high feed rates without the need for external heating. Autothermal pyrolysis of polystyrene provides an efficient method to recover monomers from waste polystyrene. Multiple processes including depolymerization of polystyrene, pyrolysis of styrene, steam reforming of styrene, and water-gas-shift of gaseous effluents, have been integrated into a single process. The highest styrene selectivity achieved was ~75% at C/O = 2.0 - 2.4 with Rh-Ce or Pt-Ce catalysts. With H_2 addition as a sacrificial fuel, styrene selectivity can reach 85% at C/O=2.2 with both catalysts.

CHAPTER
SEVEN

FUTURE WORK

SUMMARY

This chapter is focused on possible avenues for advancing the performance of existing technologies that convert biomass or plastics into higher value liquid fuels or chemicals. Future methods for methanol synthesis in a multifunctional reactor such as different reactor configurations are proposed. For instance, a multifunctional reactor with baffles or a spinning catalyst bed is proposed. One-step DME synthesis from syngas in a multifunctional reactor and one-step synthesis of gasoline from syngas are also proposed. Additionally, potential opportunities for reactor technology with a focus on staged reactors are discussed. The idea of reacting syngas with hydroxymethyl furfural (HMF) over a bifunctional catalyst to elongate the carbon chain in a staged reactor is discussed. A CPO reaction on the top stage with the Guerbet reaction on the second stage to synthesize butanol from ethanol is also worth investigating. In addition, plastic wastes, e.g. PE, PP, and PMMA, are analyzed for their feasibility to be fast pyrolyzed into monomers or liquid fuels.

7.1 Methanol Synthesis in Multifunctional Reactors

7.1.1 Methanol Synthesis in a Multifunctionl Reactor with Baffles

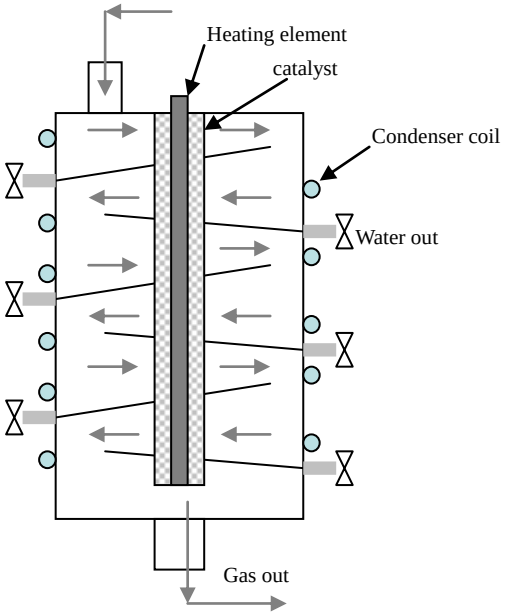

Figure 7.1 Methanol synthesis in a multifunctional reactor with baffles. Condenser is coiled outside the reactor (2D, shown as dots here). The reactor is heated in the center by a heating element. The catalyst is located in the center of the reactor. Water is periodically withdrawn from the side of the reactor.

In order to increase the carbon oxides conversion, a better reactor design with inclined baffles is proposed, and the reactor design is shown in Fig 7.1. The external condenser is coiled outside the reactor, and the catalyst is heated from the center of the reactor by a heating element. The gaseous reactants enter the reactor from the top and leave the reactor from the bottom. Water accumulates near the reactor wall due to gravity since the baffle is inclined. Water is periodically withdrawn as shown in chapter 2, and the small volume purged per withdraw (< 1% of the total volume) will not affect the reactions taking place in the reactor. The gas flow pattern is shown by gray arrows inside the reactor. The existence of baffles forces the gaseous reactants to travel a much longer distance inside the reactor resulting in an increased residence time.

The first set of experiments will include running the reaction in a continuous flow system (Fig 7.1). The condenser will be turned on when the reactor reaches steady state. After turning on the condenser, methanol vapor in the reactor near the condenser is condensed and withdrawn periodically. The concentration of methanol vapor is lower near the reactor wall than near the catalysts resulting in a net concentration flux traveling from the catalyst to the reactor wall. The concentration gradient and net concentration flux of CO and CO_2 is opposite to that of methanol. Hence, more carbon oxides generate methanol in the catalyst bed, resulting in increased conversion. The total flow rate ($CO/CO_2/N_2/H_2$) will be varied to investigate the optimal residence time for higher conversion.

The second set of experiments needed is semi-batch. A small amount of $CO/CO_2/H_2/N_2$ mixture is fed to the reactor to maintain the pressure and fast kinetics. Reaction equilibrium is reached before the condenser is turned on. After methanol is condensed near the reactor wall/condenser, the reactants will reach higher carbon oxides conversion, reaching a in a new equilibrium. The continuous flow system will be compared to a semi-batch system. The conversion of the semi-batch system is expected to reach almost 100%.

7.1.2 Rotating Basket Multifunctional Reactor

The rotating basket is a design that enhances gaseous flow in the radial direction. The rotating basket was discovered by Carberry in 1966 [140]. Pereira *et al*. calculated the particle Reynolds number and mass transfer coefficient in packed beds and found a match with their experimental results [140]. Chang *et al*. used a high gravity rotating packed bed (HGRPB) reactor to study adsorption removal of methanol from solution [141]. A rotating basket enables the reaction to reach equilibrium faster than the static system, however, conversion would not exceed the value predicted by equilibrium. The integration of a rotating basket and *in situ* condensation is expected to shift the equilibrium and achieve almost 100% conversion in a multifunctional reactor.

As the catalyst rotates, the methanol produced is condensed at the surface of the condenser (cooling coil) in the reactor. The reactants (CO, CO_2, and H_2) in the gas phase are forced to pass through the catalyst and reach a new equilibrium with a higher conversion of carbon oxides. The advantage of the rotating basket reactor is that it can force convection through the catalyst bed and avoid the use of a recycle pump which would increase energy consumption.

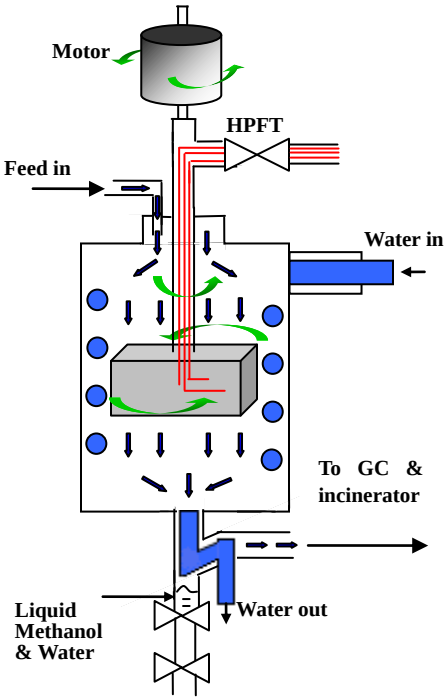

Figure 7.2 Rotating basket design for multifunctional reactor. Condenser is coiled inside the reactor (dots 2D view) HPFT: high pressure thermocouple feed through.

The proposed apparatus is shown in Fig. 7.2. A stirred autoclave reactor (300 ml, max P: 100bar, max T: 300ºC) will be used, and the propeller will be replaced by a catalyst basket. The catalyst $Cu/ZnO/Al_2O_3$ (30 g) will be contained inside a stainless steel mesh connected to a motor, and the rotation speed of motor will be adjusted by voltage. Thermocouples, connected to the center of the rod fixed to the motor and the spinning basket, will be placed in the three positions on the right hand side of the catalyst bed (temperature profiles will be symmetric for both sides) and pass through a high

pressure port. The reactants will be preheated to 230ºC and fed from the top, then purged from the bottom of the reactor. The catalyst is heated by a heating tape placed around the top of the rod (same as the thermocouples, but not shown in Fig 7.2). The condenser will be 1/4 inch ID (inner diameter) stainless steel tubing coiled inside the reactor. The operating temperature and pressure will be maintained at 230 ºC and 50 bar.

The methanol is synthesized from $CO/CO_2/H_2/N_2$ feeds in a rotating basket reactor by a continuous process. The reactions will be allowed to reach steady state before the coolant (water) is fed to the condenser. After the condenser is turned on, liquid methanol and water will be periodically withdrawn from the reactor by a two valve mechanism (chapter 2). The conversion of carbon oxides before and after turning on the condenser will be analyzed. Water flow rate will be varied (18-33 ml/s) to investigate the changes in carbon oxide conversion. The rotation speed will also be varied to probe the changes in the conversion. It is expected that as the rotation speed increases, the conversion will increase due to forced convective flow and reduced external mass transfer limitations. A maximum conversion might exist when reaction kinetics, not external mass transfer, is the limiting step.

Methanol synthesis in a batch reactor with a rotating catalyst basket will take place in a second set of experiments. In this case, the reactor, initially with reactants at 50 bar, is closed from both reactor ends and only a small amount of sample (< 1 vol%) is withdrawn periodically to analyze the compositions in the reactor by GC. Excess N_2 will be fed to avoid large changes in pressure as the reaction proceeds to completion. The water flow rate and the rotation speed will be varied to test the conversion of the carbon oxides after the condenser is turned on, and the conversion vs. time will be evaluated. The continuous flow process and batch reactor will be compared in terms of performance. In the latter case, a conversion approaching 100% is expected.

7.1.3 One-step DME Synthesis from Syngas in a Multifunctional Reactor

$CO+2H_2 \rightleftharpoons CH_3OH$	ΔH^o_{rxn}= -90.4kJ/mol	CO hydrogenation	(7-1)
$CO_2+3H_2 \rightleftharpoons CH_3OH+H_2O$	ΔH^o_{rxn}= - 49.4kJ/mol	CO_2 hydrogenation	(7-2)
$2CH_3OH \rightarrow CH_3OCH_3+H_2O$	ΔH^o_{rxn} = - 23.0 kJ/mol	CH_3OH dehydration	(7-3)
$CO+H_2O \rightleftharpoons CO_2+H_2$	ΔH^o_{rxn} = - 41.0kJ/mol	water gas shift	(7-4)
$3CO+3H_2 \rightleftharpoons CH_3OCH_3+CO_2$	ΔH^o_{rxn} = - 258 kJ/mol	Overall reaction	(7-5)

As discussed in the chapter 2, DME is a clean diesel substitute with properties like LPG, and a key intermediate for other important chemicals. The DME synthesis reaction involves four reactions as shown in (7-1) to (7-4) with the overall reaction (7-5).

DME is commonly synthesized by two methods. The first is a two-step method, consisting of methanol synthesis over a metallic catalyst, such as Cu/ZnO, and the subsequent dehydration of methanol to DME over a solid-acid catalyst, such as γ–Al_2O_3, HZSM-5, zeolite Y, SiO_2/Al_2O_3 or SAPOs [77]-[78]. The second method is a synthesis gas to dimethyl ether (STD) method which was developed for the direct synthesis of DME from syngas in a single reactor over a bifunctional catalyst composed of metallic and acidic components [62],[142]-[143]. The advantage of the STD process is that the methanol produced from reaction (7-1) and (7-2) is immediately consumed by reaction (7-3), and water generated is continually removed by reaction (7-4) to produce CO_2 and H_2 which are the reactants for methanol synthesis. These reactions suppress the reverse reaction of the methanol synthesis equilibrium allowing syngas conversion to be higher than permitted by thermodynamics in the methanol synthesis reactions[59]. The bifunctional catalyst performs methanol synthesis and methanol dehydration functions. Hybrid catalysts, where two catalysts are physically mixed, show better performance than composite catalysts prepared by a co-precipitation method [144]. The major byproducts are long-chain hydrocarbons that block active sites and deactivate the catalyst as coke. It

is known that surface acidity, which is governed by Si/Al ratio in solid-acid catalysts, determines the product distribution [145]-[146]. The higher acidity corresponds to a lower Si/Al ratio, and weak acid sites catalyze the methanol dehydration process [145].

JFE Co. constructed a 5 ton/day (5TPD) pilot plant for direct DME synthesis from natural gas in a slurry reactor in 2001 [62]. JEF subsequently built a 100TPD DME demo-plant in Hokkaido Japan in 2004 [62]. A recirculation of unreacted gases was involved and the total conversion exceeded 95% with a 1.8 recycling ratio. The pilot-plant was composed of three parts: an autothermal reformer (natural gas to syngas), DME synthesis, and DME separation. Another one-step DME pilot plant of 0.28 ton/day (100 ton/year) from biomass in a fixed-bed reactor was developed very recently in China [147]-[148]. The overall CO conversion is 73% with recycling. A pressure swing adsorption (PSA) unit with propylene carbonate was used to partially remove CO_2 in the syngas stream obtained from biomass gasification. Synthesized DME was adsorbed by pure water and purified in the rectification tower [148].

In this proposed experiments, direct DME synthesis should initially be carried out in a plug flow reactor with a bifunctional catalyst [149]-[150]. Methanol synthesis catalyst, $Cu/ZnO/Al_2O_3$, and methanol dehydration catalyst (HZMS-5 or γ-Al_2O_3) should be mechanically ground and mixed with a 1:1 ratio (total 5g) [151]. Methanol dehydration catalyst HZSM-5 is more active than many other catalysts (e.g. γ-Al_2O_3, TiO_2/Al_2O_3) [77], but also favors light olefins production. DME selectivity is only 20% at direct DME synthesis temperatures (280ºC) while γ-Al_2O_3 performs better under similar conditions. The performance (reaction conversion and selectivity) of two catalysts (HZSM-5 and γ-Al_2O_3) should be compared.

As shown in the multifunctional reactor with baffles (Fig 7.1) and a rotating basket (Fig 7.2), complete conversion of carbon oxides could be expected. With the successful integration of reaction and separation, these novel reactor designs are able to apply to direct exothermic DME synthesis reactions which are equilibrium-limited. By using a multifunctional reactor, DME reaction equilibrium could be shifted toward products and a higher conversion to DME could be achieved by condensing out the product DME. One

significant advantage of using a multifunctional reactor containing baffles or a spinning catalyst basket is that it can avoid using an energy consuming recycle pump. As mentioned previously, there are few pilot-plants for direct DME synthesis in the world, but all of them incorporate recycle streams to exceed 90% conversion.

The dew point of DME in the gas mixture under reaction conditions will be estimated based on plug flow reactor results (temperature, pressure, and gas compositions). DME reactions occur at higher temperature (250-290°C) than that of methanol (230°C) [152],[145]. The multifunctional reactor with a condenser (room temperature water as coolant) might not be sufficient to condense DME out of the system. There are two proposed ways to solve this problem: (a) the pressure of DME reactions should be increased to 80-100 bar, leading to a higher dew point making condensation of DME more likely to occur in the reactor, and (b) a refrigerated circulator (Sigma-Aldrich, product No.Z617202) will be used to cool and circulate the water (1°C) inside the reactor.

The multifunctional reactor with baffles and spinning catalyst basket will be implemented for direct DME synthesis with a bifunctional catalyst. The catalysts are 30 g of physically mixed Cu-ZnO-Al_2O_3 and silica modified γ-Al_2O_3. The operating conditions will be based on results obtained from experiments as described in Section 7.1.1 and 7.1.2. After reaching steady state, the condenser will be turned on. The amount of DME that is not condensed is analyzed by GC at different pressures (50, 80 and 100 bar). The condensed sample (DME, methanol, and water) will be analyzed in a separate GC run. For a multifunctional reactor with baffles, both the batch reaction and the continuous flow reaction schemes will be investigated to maximize conversion. Rotation speed will be varied for the rotating basket reactor. Most importantly, the conversion of carbon oxides vs. time will be measured, analyzed and compared for both reactors.

7.1.4 One-step Syngas to Gasoline Ranged Hydrocarbon

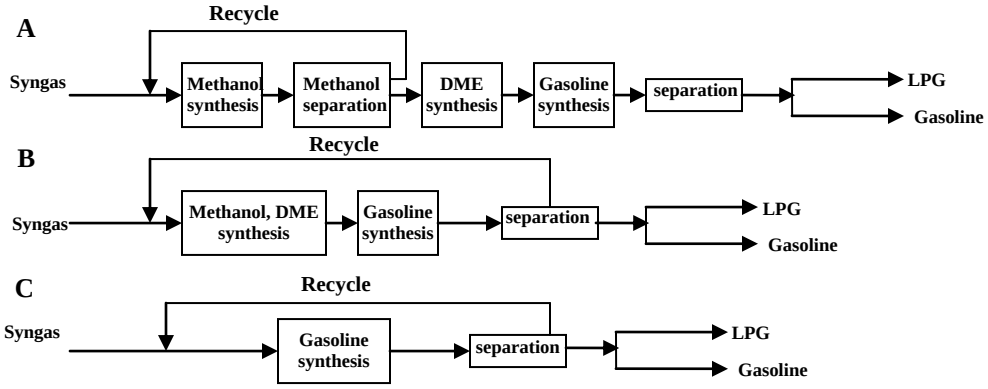

Figure 7.3 Different types of gasoline synthesis processes. (A) Mobil process (B) Topsoe's integrated gasoline synthesis process (TIGAS) process (C) Bifunctional catalysis process[153],[155].

Synthetic gasoline from biomass-derived syngas is highly desirable after successful synthesis of methanol and DME in a multifunctional reactor. Traditionally, gasoline-range higher hydrocarbons are obtained by the Fisher-Tropsch process which faces many limitations [154]. The methanol-to-gasoline (MTG) process was discovered by Exoon Mobil in the 1970s and commercialized in New Zealand ten years later. Three simplified industrial processes that convert syngas to gasoline are shown in Fig 7.3 [155]. Process C (Fig 7.3C,one-step syngas to gasoline) is highly appealing since it would significantly reduce the capital cost and energy consumed by this all-in-one reactor. The bifunctional catalyst makes this MTG process possible because the metallic part of the catalyst catalyzes methanol synthesis and zeolite part catalyzes MTG reactions. The desirable products are the long-chain hydrocarbons (C_5-C_{11} gasoline fraction). The short-chain hydrocarbons (C_1-C_4), considered as LPGs [155]-[156], are in the vapor phase at ambient temperature and pressure. Researchers reported the optimum formulation of the catalyst, the effect of operating condition (CO/H_2 feed only), kinetic modeling and catalyst deactivation for direct gasoline synthesis over CrO_3-ZnO/HZSM-5, Cu-ZnO/HZSM-5, and Cu-Zn-Cr oxide/zeolite catalysts [154],[156]- [159]. The purpose of this part of the research is to synthesize gasoline from syngas with greater C_5+ selectivity by using

improved bifunctional catalysts for small-scale systems.

Table 7.1 Catalyst for direct synthesis of gasoline from syngas. The catalyst synthesis method is shown in Appendix C.

No.	Metalic part	Solid-acid Part Catalyst	Si/Al ratio
Catalyst 1	Cr_2O_3-ZnO	HZSM-5	46
Catalyst 2	Cr_2O_3-ZnO	HZSM-5	154
Catalyst 3	Cr_2O_3-ZnO	HZSM-5(NaOH treated)	46
Catalyst 4	Cr_2O_3-ZnO	HZSM-5(NaOH treated)	154
Catalyst 5	Cr_2O_3-ZnO	ZnO_{doped}/HZSM-5	46
Catalyst 6	Cr_2O_3-ZnO	ZnO_{doped}/HZSM-5	154

A plug flow fixed-bed reactor will be used with a bifunctional catalyst. De Lasa *et al.*[156] found Cr_2O_3-ZnO to be the most suitable for direct gasoline synthesis. Cr_2O_3-ZnO together with post-synthetic modification of HZSM-5 will be used in this proposed study. The synthesis method is included in the Appendix C. The mechanically mixed bifunctional catalyst will be loaded inside the fixed-bed reactor in a 1:1 ratio. The reaction will be run at 400ºC and 50 atm.

7.1.4.1 Cr_2O_3-ZnO/HZSM-5

The operating conditions of CO_2 hydrogenation and CO/CO_2 hydrogenation converting syngas into gasoline will be investigated in this proposed research. CO_2 hydrogenation will be studied since it is a greenhouse gas, leading to global warming. This is also because an operating condition for CO_2/H_2 feeds, which is important for a small system, has not been conducted. The rationale for studying $CO/CO_2/H_2$ feeds is that CO_2 is present in the syngas after the gasifier if biomass is the primary carbon source[148], and $CO/CO_2/H_2$ feeds in direct gasoline synthesis have not been previously reported. For both sets of experiments, all the operating parameters, such as space velocity, temperature, pressure and H_2/carbon oxides ratio will be explored and optimized. It is expected that more methanol would be produced and subsequently converted to gasoline

for $CO/CO_2/H_2$ feeds compared to CO_2/H_2 feeds, especially when methanol synthesis is the rate limiting process [157].

7.1.4.2 Cr_2O_3-ZnO/ NaOH treated HZSM-5

Research has been extensively carried out for post-synthetic or direct synthesis to modify zeolite to improve catalytic performance of MTG process [160]. Recently, a post-synthetic treatment of H-ZSM-5 (Si/Al=46) by 0.2M NaOH improves catalyst stability and C_5+ selectivity which increased by a factor of 1.7 for MTG process at 370ºC and 1 atm [160]. This modification of zeolite has not been incorporated into direct gasoline synthesis. We propose mixing a NaOH-treated HZSM-5 with Cr_2O_3-ZnO to directly synthesize gasoline and obtain higher catalyst stability and higher C_5+ selectivity. HZSM-5 with Si/Al=46 and 154 will be treated with 0.2M NaOH and physically mixed with Cr_2O_3-ZnO [156]. Due to larger pore volumes, faster H_2 transfer, and the presence of Lewis acidity, the selectivity towards the gasoline fraction (C_5+) of catalyst 3 (Table 7.1) will be higher than that of catalyst 1 [160]. The trend will be the same for catalyst 4 and 2. Furthermore, catalyst 4 will have a higher selectivity of C_5+ and produce a larger portion of C_8, C_9 than catalyst 3 [156]. Characterization techniques such as nitrogen physisorption (BET), X-ray diffraction (XRD), and scanning electron microscopy (SEM) will be used to analyze the catalyst properties and the morphologies before and after reaction.

7.1.4.3 Cr_2O_3-ZnO/metal oxide doped HZSM-5

Another post-synthetic modification of zeolites is to dope metal oxides (CuO, CuO/ZnO, ZnO) into the HZSM-5 (Si/Al=46) framework resulting in additional acidic sites, increasing the conversion of methanol to gasoline for the MTG process at 400ºC and 1 bar [161]. ZnO/HZSM-5 has double the conversion and more C_5+ product distribution than from HZSM-5 alone. We propose incorporating a metal oxide doped HZSM-5 into direct gasoline synthesis. ZnO will be doped into the HZSM-5 (Si/Al=46 and 154) framework (Table 7.1). CuO will not be doped since it will be reduced to Cu during

reduction period, which can catalyze methanol synthesis and lose its activity when the temperature exceeds 300 ºC. The catalytic performance in terms of higher selectivity of C_5+ of the doped catalyst (catalyst 5) will be better than that of the catalyst without doping (catalyst 1) and the same trend will hold for catalyst 6 and catalyst 2 [156]. Catalyst 6 should produce a larger portion of C_8 and C_9 than catalyst 5. It will be interesting to compare the performance of catalyst 4 and 6. In addition, XRD will be used to verify the structure of the catalyst with doping.

7.2 Staged Reactor

7.2.1 One-step Synthesis of (Hemi)acetal from Syngas and HMF

5-hydroxymethyl furfural (HMF), a furanic compound that can be obtained by the dehydration of sugars, may be used as a fuel precursor. HMF has been recognized as a "key substance between carbohydrate chemistry and mineral oil based chemistry" [162].

Kuster [163] and Lewkowski [164] *et al.* reviewed the chemistry, catalysts, reaction temperature, and solvents for the production of HMF from sugars. HMF is synthesized by dehydration of hexoses. The cheapest hexose is glucose, while most literature suggestes HMF is more favorably produced from fructose. One hypothesis is that the formation of HMF from hexose proceeds via an open chain mechanism which lowers the HMF formation, while the production from fructose is through a straight chain resulting in higher conversion [163]-[164]. Another explanation states that glucose must first isomerize to fructose to convert to HMF [165]. The mechanisms and kinetics of HMF synthesis reaction from fructose in an aqueous media has been extensively studied. Torres *et al*. [166] reported a design case study to continuously produce HMF from fructose to minimize the cost per mole of HMF, and study the effect of different solvents, fructose prices, capital investment, and kinetics on the cost.

We integrated CPO and alcohol dehydration reactions in chapters 4 and 5. Methanol synthesis with thermodynamic limitation was also investigated in chapter 2 and

3. Higher chain length liquid fuel could be produced by chain elongation reactions such as esterifications or aldol condensation, etc. Based on these results, a hemiacetal or acetal should be produced from methanol and HMF (reaction (7-6) and (7-7)), which is one or two carbons longer than HMF. Further, this integration is able to overcome the thermodynamic limitation of methanol synthesis.

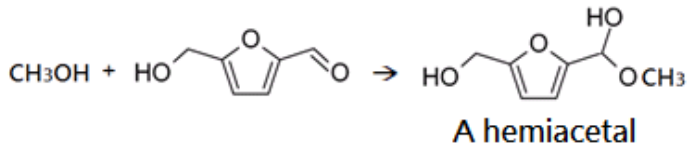

(7-6)

A hemiacetal

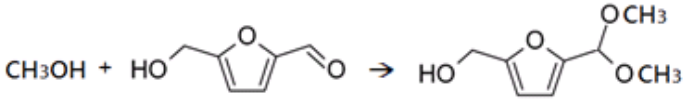

(7-7)

An acetal

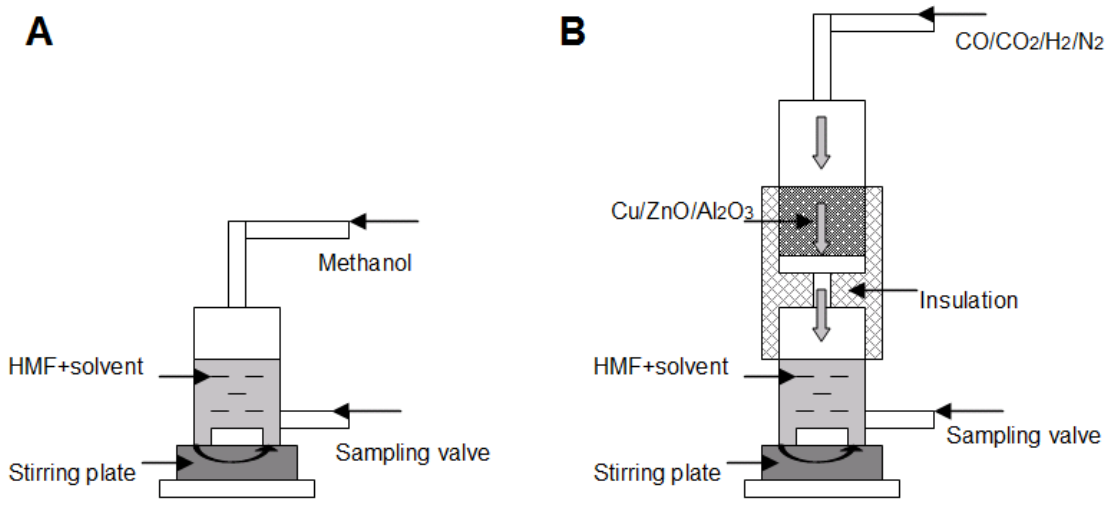

Figure 7.4 Proposed reaction setup for methanol reaction with HMF. The solution is mixed by a magnetic stirring plate. In (A), the reaction is under atmospheric pressure; In (B), reaction is at 50 bar.

Reactions (7-6) and (7-7) normally take place in an aqueous medium with water or other solvents at moderate temperatures. A systematic study of these two reactions will be carried out. The optimal reaction conditions of reaction (7-6) and (7-7) will be investigated in the first set of experiments. The proposed reaction setup is shown in Fig 7.4A. A stainless steel reactor tube will be placed on top of a stirring plate. HMF and solvent will be added in the reactor vessel which is stirred and heated by the stirring plate. Methanol will be introduced from the top of the reactor to react with HMF in the liquid phase at atmospheric pressure. Liquid samples will be withdrawn from the sampling valve and analyzed by high-performance liquid chromatography (HPLC). Water, ethanol, propanol, and butanol will be tested to determine the optimal solvent. The catalyst will also be studied by adding acids or solid-acids (HCl or zeolite), and their corresponding product distributions will be measured.

The one-step methanol synthesis and reacting with HMF will be carried out, once the reactions (7-6) and (7-7) are optimized. The methanol synthesis reaction occurs at high pressure (50 bar) and higher temperature (230 ^{o}C). The reaction setup is shown in Fig 7.4B. The solvent vessel will be similar to a methanol synthesis reactor vessel (stainless steel) on top. Total flow rate of the gaseous feed $CO/CO_2/H_2/N_2$ will be 1.0-1.5 SLPM with the flow ratio of 25/5/50/20. The space between the top catalyst bed ($Cu/ZnO/Al_2O_3$) and liquid solvent will be short (< 2 cm) in an attempt to overcome methanol equilibrium. The methanol produced in the top stage will instantly react with the HMF solvent in the second stage. The gas flow rate will be varied to optimize the hemiacetal and acetal production. The sample will be withdrawn from the sample valve and analyzed by HPLC.

7.2.2 Butanol Synthesis from Ethanol by Guerbet Reaction

The integration of CPO and alcohol dehydration has been examined in chapter 4 and 5. The integration will be implemented in such a way that the products of the first stage are the reactants of the second stage.

As mentioned in chapter 4 and 5, higher carbon number alcohols are highly useful as

solvents, chemical intermediates or fuel oxygenate additives. In the commercial multistep process, olefins derived from crude oil are used to generate alcohol, such as 1-propanol, 1-butanol, 2-methyl-1-propanol and 2-methyl-1-butanol [167]. The market for higher alcohols is currently large and highly depends on the crude oil prices. Low-cost process for the production of long chain carbon alcohol is highly desirable from renewable CO_2-neutral ethanol.

The Guerbet reaction is a multistep reaction with a multifunctional catalyst at temperatures higher than 300 ^{o}C [168]-[169]. The reactions involve dehydrogenation of short-chain alcohols to aldehyde intermediates followed by condensation to long-chain aldehydes and catalytic reduction to the larger alcohols [167]. The proposed mechanism of butanol production from ethanol is shown in Fig 7.5 [112].

The Guerbet catalyst comprises of two parts: a solid condensation catalyst and a hydrogenation catalyst. Ueda *et al*. reported a low-pressure Guerbet reaction over MgO catalyst with 1-propanol and 2-methylpropan-1-ol as products [170]. Very recently, Tsuchida *et al*. developed a nonstoichiometric hydroxyapatite (HAP), a highly active calcium phosphate compound and found that it catalyzed selective conversion of ethanol to n-butanol via the Guerbet reaction [171]-[172]. This catalyst contains both acidic and basic sites, depending on synthesis conditions. The authors found that the yield of 1-butanol is a function of the probability of ethanol activation (α) on the catalyst surface [171]-[172].

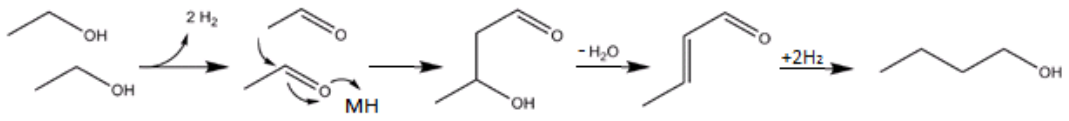

Figure 7.5 Proposed mechanism of Guerbet reaction for ethanol. M is heterogeneous metal oxide such as MgO or CaO[112].

Kruger *et al.* [131] measured the ethanol conversation and acetaldehyde selectivity of ethanol CPO on Rh and Pt catalysts at various C/O ratios and temperatures. The ethanol conversion decreases with increasing C/O ratio. Following the opposite trend, the acetaldehyde selectivity increases with increasing C/O ratio. In this study, acetaldehyde is the aldehyde intermediate in Guerbet reactions from ethanol feed. A staged reactor with CPO reaction of ethanol on the top stage and a HAP catalyst on the second stage to upgrade unreacted ethanol is proposed for higher alcohol production (butanol). Furthermore, Guerbet reaction requires moderately elevated temperature and benefits from the addition of H_2. The effect of co-feed intermediate species (acetaldehyde) on the product distribution will be investigated by this two stage reactor configuration. Investigation of this reaction as a function of H_2 and CO partial pressure, temperature, pressure should lead to optimization of this process.

7.3 Oxidative Fast Pyrolysis of Plastic Wastes

The effective conversion of waste plastics into high-value liquid fuels and chemicals would provide another method of recycling waste plastics. Current plastic-recycling technologies are energy intensive, create large amount of solid carbon, and are difficult to scale up.

Autothermal catalytic oxidative pyrolysis of waste plastic may be an efficient and continuous process to produce liquid fuels and chemicals. As shown in chapter 6, polystyrene is pyrolyzed into styrene monomers with up to 85% yield. Here, more plastic wastes are proposed to be oxidatively pyrolyzed in an autothermal reactor.

The most common thermoplastics are PE, PP, PS, PVC, PET, and PMMA. Based on our previous results of PE and PS, plastic PE, PP and PMMA will be chosen to model conversion of plastic waste to liquid products for future utilization. Furthermore, experiments involving PE, PP, and PMMA may provide insight for future experiments involving PET and PVC.

7.3.1 Experimental Methods

The proposed experimental setup is shown in Fig 7.6, which is similar to that in Fig 6.1. A custom hopper/auger will be used to control the flow of the solid plastic particles (PE, PP, and PMMA) into the quartz tube and onto the catalyst front surface, which will then enter the catalyst bed and react. Make up gas (N_2 ad O_2) will also be premixed and preheated from the top of the reactor. The reactor will be insulated to prevent any condensation. The thermocouple will be placed at the back-face of the catalyst bed. The back-face heat shield monolith will be used to prevent axial radiative heat lost from the catalyst.

The previous results on oxidative pyrolysis of PS may provide insight to pyrolysis of PE, PP, and PMMA. Operating the proposed catalytic system at high C/O ratios would encourage the cracking of polymers to monomers while preventing complete decomposition into CO (as in syngas). A Rh-Ce (2 wt % each) on α-Al_2O_3 spheres would be a good catalyst to use at high C/O ratios due high catalyst stability and coke resistance.

The oxidative pyrolysis products will be sampled from a sampling port located below the back shield monolith and analyzed by GC or liquid chromatography (LC). A separate GC-MS run will be required to identify all the species produced. As shown in Fig 7.6B, a second catalytic bed will decompose the volatile effluents from the first catalyst bed into small and easily quantifiable species for more accurate calculation of carbon and other atomic balances. Two sample methods (gas phase and liquid phase measurement) will be compared: (1) the sample line will be heated to 400 ^oC to avoid any condensation. The gas sample will be analyzed by GC; (2) the effluent will be passed through a condenser in which the heavy products are condensed. In the latter case, the gas sample will be analyzed by GC, while the condensed sample will be analyzed by LC. Effluents exiting the reactor after the catalytic bed are incinerated to prevent the release of toxic chemicals in the environment.

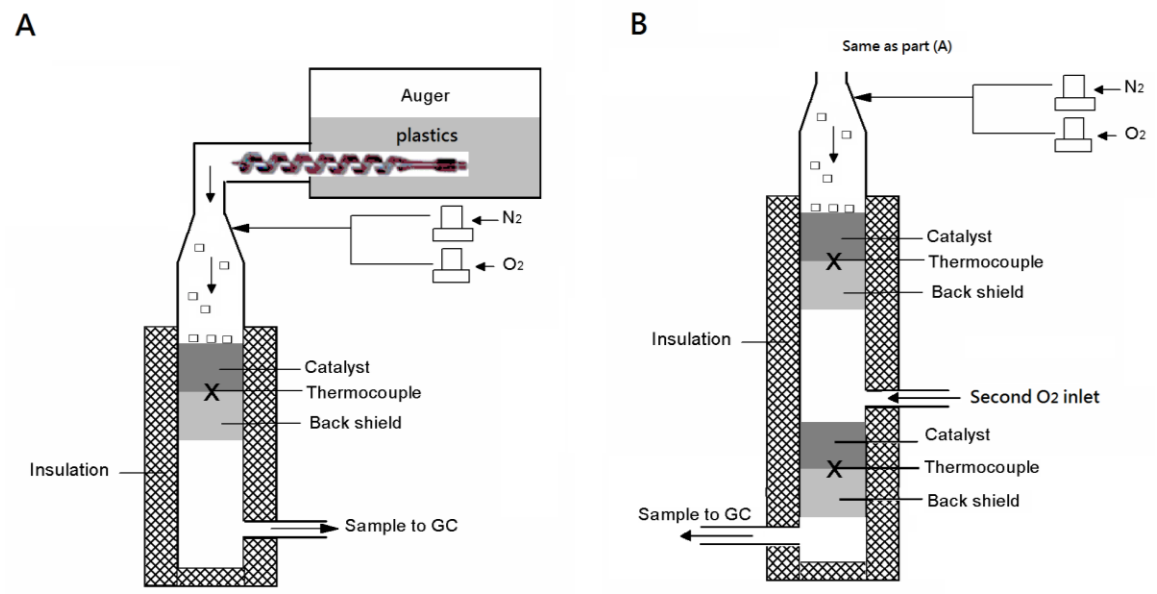

Figure 7.6 Schematic of reactor setup for oxidative pyrolysis of waste plastics (PE, PP, and PMMA); (A) Reactor setup with one catalyst bed; (B) Reactor setup with two catalyst beds.

7.3.2 Fast Pyrolysis of Polyethylene (Polypropylene)

Our group has studied fast pyrolysis of solid biomass compounds, such as cellulose or polyethylene, into syngas at low C/O ratio with Rh-Ce/α-Al_2O_3 catalyst at temperature up to 1000 ^oC [29]. In this study, liquid fuels (C_5-C_{20}), but not gas products (C_1-C_4), nor wax products (C_{21} above), are desirable products from waste plastics for transportation purpose. Unlike PS pyrolysis, in which the monomer styrene is the main product, PE pyrolysis produces a large variety of products ranging from C_1-C_{50} species. In addition to gas and liquid products, traditional PE pyrolysis also produces solid coke residues. Miskolczi *et al.* reported the formation of undesirable aromatics and coke by thermal degradation of PE above 450-460 ^oC which resulted in higher rates of cyclization reactions [173]. Furthermore, Lee *et al*. obtained PE pyrolysis liquid yields of 71-81 wt% with consistently 1.5 wt % coke over zeolite Y catalyst [174].

The reactions will be carried out as shown in Fig 7.6 by adjusting C/O ratio as well as inlet feed concentrations to analyze product distributions. Balonek *et al*. [175]

demonstrated pyrolysis products (C_{2+}) increases and temperature decreases with increasing C/O ratio in autothermal PE pyrolysis. High C/O ratios enable decreased extent of polyethylene oxidation leading to lower temperature and lower syngas production (CO/H_2). Balonek *et al.* [175] demonstrated that pyroslysis of PE reaches a carbon selectivity of 90% to pyrolysis products (products other than CO, CO_2 or CH_4) at a C/O ratio of 3.4. The PE pyrolysis products were generally brown soft waxes after condensation. Balonek *et al*. [175] also showed a sample chromatograph where a sample is dissolved in heptane and analyzed by GC-MS. C_{12}-C_{30} are easily identified by the GC-MS with straight chain monomers being the most abundant and dienes and alkanes being less abundant.

PE pyrolysis in an autothermal reactor will be optimized by investigation of C/O ratio, temperature, feed concentration, and product distributions. In order to prevent the wax formation, the effluent gas without condensation will go through a second catalyst bed as shown in Fig 7.6B, where long carbon chains will be further cracked into smaller carbon chains.

According to the literature, pyrolysis of PE and PP have similar product selectivities. Jung *et al*. [176] showed PE and PP pyrolysis produces similar gas, liquid, and solid product selectivities between 500-800 ^{o}C. William *et al.* [177] reported that PE and PP yield very similar molecular weight distribution of aliphatic products, including alkanes, alkenes, and alkadienes in fluidized bed pyrolysis experiments. Pyrolysis of PP will be carried out in the next step with an autothermal fixed-bed reactor. PP generally produces a larger variety of products than PE since it has more methyl side chains. The reactor setup and product analysis methods will be similar to those in PE pyrolysis.

7.3.3 Fast Pyrolysis of PMMA

Previous studies have investigated conversion of PMMA to MMA monomers for waste plastic recovery. Pyrolysis is one of the most common technologies in the literature. Kaminsky et al. reported pyrolysis of highly filled PMMA in an indirect heated fluidized bed for monomer recovery. They were able to recover 98 wt % of methylmethacrylate

(MMA) at 450 ^{o}C with throughputs of ~1 kg/h in laboratory plants and with throughput of 30 kg/h in mini pilot plant [20]. They also found out that the yield depends on the pyrolysis temperature [178]. Arisawa et al. reported the kinetics and mechanism of flash pyrolysis of PMMA with 600-1000 ^{o}C/s within the temperature range of 380-600 ^{o}C controlled by T-jump/FTIR spectroscopy [179].

Fast pyrolysis of PMMA in an autothermal fixed-bed reactor will be investigated and the experimental setup will be the same as shown in Fig 7.6. The C/O ratio will be varied to optimize the monomer yield since MMA recovery requires moderate temperatures (400-500 ^{o}C). Products will be identified and analyzed by GC-MS. Noble metals (Pt, Rh, and Ce) on α-Al_2O_3 will be examined to maximize the monomer yield. A second stage of catalyst bed will be added if the polymer products are present in the effluent in large amounts (Fig 7.6B).

Fast pyrolysis of PMMA in an autothermal reactor will provide a small-scale, efficient and economical alternative to the traditional processing methods. The proposed work combined with the results presented in chapter 6 may provide valuable insight into the future capabilities of catalytic oxidative pyrolysis.

BIBLIOGRAPHY

[1] J. M. Shuster, *Beyond fossil fools, the road map to energy independence by 2040*.

[2] "U. S. EIA Iternational Energy Statistics." 12-Jan-2012. Available Online. URL:www.eia.gov/cfapps/ipdbproject/IEDIndex3.cfm.

[3] J. L. Colby, PhD Thesis. pp. 1, University of Minnesota, 2010.

[4] "Meeting the world's demands for liquid fuels," presented at the EIA energy conference, Washington DC, 2009.

[5] "US department of energy on greenhouse gases." 24-Apr-2012. Available Online. URL: www1.eere.energy.gov/femp/program/greenhousegasese.html.

[6] "How Biomass Energy Works." Union of concerned scientists, 2012. Available Online. URL: www.ucsusa.org/clean_energy/our-energy-choices/renewable-energy/how-biomass-energy-works.html.

[7] J. C. Jenkins, R. A. Birdsey, and Y. Pan, "Biomass and NPP estimation for the mid-atlantic region (USA) using plot-level forest inventory data.," *Ecological Applications*, vol. 11, pp. 1174–1193, 2001.

[8] "VIASPACE Green Energy Inc. - Biomass Solutions." Available: http://www.viaspacegreenenergy.com/biomass.php, accessed: 06-May-2012.

[9] L. Schmidt, "CHEN5551 Renewable energy lecture notes," Fall Semester-2009.

[10] M. J. Skinner, E. L. Michor, W. Fan, M. Tsapatsis, A. Bhan, and L. D. Schmidt, "Ethanol dehydration to ethylene in a stratified autothermal millisecond reactor," *ChemSusChem*, vol. 4, no. 8, pp. 1151–1156, Aug. 2011.

[11] J. C. Serrano-Ruiz and J. A. Dumesic, "Catalytic routes for the conversion of biomass into liquid hydrocarbon transportation fuels," *Energy & Environmental*

Science, vol. 4, no. 1, pp. 83, 2011.

[12] J. Bedard, H. Chiang, and A. Bhan, "Kinetics and mechanism of acetic acid esterification with ethanol on zeolites," *Journal of Catalysis*, vol. 290, pp. 210–219, Jun. 2012.

[13] A. Weisman, *The World without Us*. NY: St. Martin's press, 2007.

[14] "Common Wastes and Materials: Plastics." U.S. Environmental Protection Agency, 16-Apr-2012. Available online. URL: www.epa.gov/osw/conserve/mat terials/plastics.html.

[15] P. Fimrite, "Environmentalists hunt wildlife-killing nurdles." Available:http://www.sfgate.com/cgi-bin/article.cgi?f=/c/a/2011/10/28/MNF91LN MLB.DTL, accessed: 14-May-2012.

[16] "Rational Energies to open in Plymouth - Lakeshore Weekly News - Wayzata, Minnesota."Available:http://www.weeklynews.com/main.asp?SectionID=26&Sub SectionID=37&ArticleID=9200, accessed: 27-Jul-2012.

[17] K. Myer, "Handbook of Materials Selection," John Wiley & Sons., 2002, pp. 341.

[18] R. Meyers, "Molecular biology and biotechnology: a comprehensive desk reference," Wiley-VCH, 1995, pp. 722.

[19] R. V. Lapshin, A. P. Alekhin, A. G. Kirilenko, S. L. Odintsov, and V. A. Krotkov, "Vacuum ultraviolet smoothing of nanometer-scale asperities of poly(methyl methacrylate) surface," *Journal of Surface Investifation. X-ray, Synchrotron and Neutron Techniques*, vol. 4, no. 1, pp. 1–11, 2010.

[20] W. Kaminsky and C. Eger, "Pyrolysis of filled PMMA for monomer recovery," *Journal of Analytical and Applied Pyrolysis*, vol. 58–59, pp. 781–787, 2001.

[21] E. Szabo, M. Olah, F. Ronkay, N. Miskolczi, and M. Blazso, "Characterization of the liquid product recovered through pyrolysis of PMMA–ABS waste," *ELSEVIER*, vol. 92, no. 1, pp. 19–24, 2010.

[22] K. Sundmacher and Z. Qi, "Multifunctional reactors," in *Chemical Engineering and Chemical Process Technology*, vol. 3, Encyclopedia of Life Support System (EOLSS).

[23] P. Dauenhauer, Ph.D. Thesis, pp.1-27, University of Minnesota, 2008.

[24] C. Wheeler, A. Jhalani, and L. D. Schmidt, "The water gas shift reaction at short times," *Journal of catalysis*, vol. 223, pp. 191–199, 2004.

[25] D. A. Hickman and L. D. Schmidt, “Production of syngas by direct catalytic oxidation of methane,” *Science*, vol. 259, no. 5093, pp. 343–346, Jan. 1993.

[26] J. Krummenacher, “Catalytic partial oxidation of higher hydrocarbons at millisecond contact times: decane, hexadecane, and diesel fuel,” *Journal of Catalysis*, vol. 215, no. 2, pp. 332–343, Apr. 2003.

[27] M. Huff and L. D. Schmidt, “Ethylene formation by oxidative dehydrogenation of ethane over monoliths at very short contact times,” *The Journal of Physical Chemistry*, vol. 97, no. 45, pp. 11815–11822, Nov. 1993.

[28] B. Dreyer, I. Lee, J. Krummenacher, and L. Schmidt, “Autothermal steam reforming of higher hydrocarbons: n-Decane, n-hexadecane, and JP-8,” *Applied Catalysis A: General*, vol. 307, no. 2, pp. 184–194, Jul. 2006.

[29] P. J. Dauenhauer, B. J. Dreyer, N. J. Degenstein, and L. D. Schmidt, “Millisecond reforming of solid biomass for sustainable fuels,” *Angewandte Chemie International Edition*, vol. 46, no. 31, pp. 5864–5867, Aug. 2007.

[30] J. zhang, Y. Wang, R. Ma, and D. Wu, “Characterization of alumina-supported Ni and Ni–Pd catalysts for partial oxidation and steam reforming of hydrocarbons,” *Appl. Catal., A Gen*, vol. 243, pp. 251–259, 2003.

[31] A. Qi, S. Wang, G. Fu, C. Ni, and D. Wu, “La–Ce–Ni–O monolithic perovskite catalysts potential for gasoline autothermal reforming system,” *Appl. Catal., A Gen*, vol. 281, pp. 233–246, 2005.

[32] B. S. Caglayan, A. K. Avci, Z. I. Onsan, and A. E. Aksoylu, “Production of hydrogen over bimetallic Pt–Ni/ɣ-Al_2O_3: I. Indirect partial oxidation of propane,” *Appl. Catal., A Gen*, vol. 280, pp. 181–188, 2005.

[33] C. Balonek, J. Colby, N. Persson, and L. D. Schmidt, “Rapid ablative pyrolysis of cellulose in an autothermal fixed-bed catalytic reactor,” *chemsuschem*, vol. 3, pp. 1355–1358, 2010.

[34] J. S. Church, N. W. Cant, and D. L. Trimm, “Stablisation of aluminas by rare earth and alkaline earth ions,” *Appl. Catal., A Gen*, vol. 101, pp. 105–116, 1993.

[35] A. Conazzi, B. Michael, and L. D. Schmidt, “Chemical and geometric effects of Ce and washcoat addition on catalytic partial oxidation of CH_4 on Rh probed by spatially resolved measurements,” *J. Catal.*, vol. 260, no. 2, pp. 270–275, 2008.

[36] N. J. Degenstein, R. Subramanian, and L. D. Schmidt, “Partial oxidation of n-hexadecane at short contact time: Catalyst and washcoat loading and catalyst

morphology," *Appl. Catal., A Gen*, vol. 305, pp. 146–159, 2006.

[37] "Database of Zeolite Structures." Available: http://www.iza-structure.org/databases/, accessed: 25-May-2012.

[38] A. Huang, Y. S. Lin, and W. Yang, "Synthesis and properties of A-type zeolite membranes by secondary growth method with vacuum seeding," *Journal of Membrane Science*, vol. 245, no. 1–2, pp. 41–51, Dec. 2004.

[39] M. Matsukata, N. Nishiyama, and K. Ueyama, "Synthesis of zeolites under vapor atmosphere," *Microporous Materials*, vol. 1, no. 3, pp. 219–222, Jun. 1993.

[40] X. Querol, A. Alastuey, A. López-Soler, F. Plana, J. M. Andrés, R. Juan, P. Ferrer, and C. R. Ruiz, "A fast method for recycling fly ash: microwave-assisted zeolite synthesis," *Environmental Science & Technology*, vol. 31, no. 9, pp. 2527–2533, Sep. 1997.

[41] A. Arafat, J. C. Jansen, A. R. Ebaid, and H. van Bekkum, "Microwave preparation of zeolite Y and ZSM-5," *Zeolites*, vol. 13, no. 3, pp. 162–165, Mar. 1993.

[42] L. Schmidt, "Millisecond chemical reactions and reactors," *Studies in catalysis and surface science*, vol. 130A, pp. 61–81.

[43] J. L. Colby, P. J. Dauenhauer, and L. D. Schmidt, "Millisecond autothermal steam reforming of cellulose for synthetic biofuels by reactive flash volatilization," *Green Chem.*, vol. 10, no. 7, pp. 773-783, 2008.

[44] 1. W.-H. cheng and H. H. Kung, *methanol production and use*. 1994.

[45] SCI counsulitng, "Methanol," report, Jan. 2009.

[46] A. C. Sofianos and M. S. Scurrell, "Conversion of synthesis gas to dimethyl ether over bifunctional catalytic systems," *Industrial & Engineering Chemistry Research*, vol. 30, no. 11, pp. 2372–2378, 1991.

[47] J.-H. Fei, M.-X. Yang, Z.-Y. Hou, and X.-M. Zheng, "Effect of the addition of manganese and zinc on the properties of copper-based catalyst for the Synthesis of syngas to dimethyl ether," *Energy Fuels*, vol. 18, no. 5, pp. 1584–1587, Sep. 2004.

[48] G. Cai, Z. Liu, R. Shi, H. Changqing, L. Yang, C. Sun, and Y. Chang, "Light alkenes from syngas via dimethyl ether," *Applied Catalysis A: General*, vol. 125, no. 1, pp. 29–38, Apr. 1995.

[49] T. Ogawa, N. Inoue, T. Shikada, and Y. Ohno, "Direct dimethyl ether synthesis,"

Journal of natural gas chemistry, vol. 12, no. 4, pp. 219–227, 2003.

[50] A. N. R. Bos, P. C. Borman, M. Kuczynski, and K. R. Westerterp, "The kinetics of the methanol synthesis on a copper catalyst: An experimental study," *Chemical Engineering Science*, vol. 44, no. 11, pp. 2435–2449, 1989.

[51] M. Takagawa, "Study on reaction rates for methanol synthesis from carbon monoxide, carbon dioxide, and hydrogen," *Journal of Catalysis*, vol. 107, no. 1, pp. 161–172, Sep. 1987.

[52] K. C. Waugh, "Methanol Synthesis," *Catalysis Today*, vol. 15, no. 1, pp. 51–75, May 1992.

[53] R. M. Agny and C. G. Takoudis, "Synthesis of methanol from carbon monoxide and hydrogen over a copper-zinc oxide-alumina catalyst," *Ind. Eng. Chem. Prod. Res. Dev.*, vol. 24, no. 1, pp. 50–55, Mar. 1985.

[54] K. Klier, "Catalytic synthesis of methanol from CO/H_2 IV. The effects of carbon dioxide," *Journal of Catalysis*, vol. 74, no. 2, pp. 343–360, Apr. 1982.

[55] P. Villa, P. Forzatti, G. Buzzi-Ferraris, G. Garone, and I. Pasquon, "Synthesis of alcohols from carbon oxides and hydrogen. 1. Kinetics of the low-pressure methanol synthesis," *Ind. Eng. Chem. Proc. Des. Dev.*, vol. 24, no. 1, pp. 12–19, Jan. 1985.

[56] G. Chinchen, P. Denny, J. Jennings, M. Spencer, and K. Waugh, "Synthesis of MethanolPart 1. Catalysts and Kinetics," *Applied Catalysis*, vol. 36, pp. 1–65, 1988.

[57] J. Skrzypek, M. Lachowska, and H. Moroz, "Kinetics of methanol synthesis over commercial copper/zinc oxide/alumina catalysts," *Chemical Engineering Science*, vol. 46, no. 11, pp. 2809–2813, 1991.

[58] R. Eijhoudt, John Geus, and J. Smit, "Process for the removal of metal carbonyl from a gaseous stream," U.S. Patent United States Patent 616542826-Dec-2000.

[59] R. Herman, "Catalytic synthesis of methanol from CO/H_2 I. Phase composition, electronic properties, and activities of the $Cu/ZnO/M_2O_3$ catalysts," *Journal of Catalysis*, vol. 56, no. 3, pp. 407–429, Mar. 1979.

[60] H. Ben Amor and V. L. Halloin, "Methanol synthesis in a multifunctional reactor," *Chemical Engineering Science*, vol. 54, no. 10, pp. 1419–1423, May 1999.

[61] S. Zhang, T. Li, B. Zhu, "Study of supercritical three-phase methanol synthesis with n-hexane atsupercritical state", *Chemical Engineering Science*

vol.61, pp.167-1173, 2006.

[62] M. Kuczynski, W. I. Browne, H. I. Fontein, K. R. Westerterp, “Methanol synthesis in a countercurrent gas—solid—solid trickle flow reactor. An experimental study” *Chemical Engineering Science*, vol.42, pp.1887-1898, 1987.

[63] K. R.Westerterp, M. Kuczynski, A model for a countercurrent gas—solid—solid trickle flow reactor for equilibrium reactions. The methanol synthesis, *Chemical Engineering Science*, vol.42, pp.1871-1886, 1987.

[64] A.V. Kruglov, “Methanol synthesis in a simulated countercurrent moving-bed adsorptive catalytic reactor” *Chemical Engineering Science*, vol. 49, pp. 4699-4716, 1994.

[65] M. Kuczynski, K. R.Westerterp, Hydrocarbon Processing, pp. 80-83, 1986.

[66] A. P. F. Leite, M. B. Grilo, R. R. D. Andrade, F. A. Belo, A. Meunier, "Experimental thermodynamic cycles and performance analysis of a solar-powered adsorptive icemaker in hot humid climate", *Renewable Energy*, vol. 32, pp. 697-712, 2007.

[67] A. O. Dieng, R. Z. Wang, Literature review on solar adsorption technologies for ice-making and air-conditioning purposes and recent developments in solar technology", *Renewable and Sustainable Energy Review*, vol. 5, pp. 313-342, 2001.

[68] L. Gordeeva, Y. Aristov, A. Freni, G. Restuccia, *Proc. Int. Sorption Heat Pump Conference*, 2002, September 24-27, Shanghai, CN, P. 625.

[69] I. Halasz, S. Kim, B. Marcus, "Uncommon adsorption isotherm of methanol on a hydrophobic Y-zeolite", *Journal of Physical Chemistry B.* vol. 105, pp. 10788-10796, 2001.

[70] (a)S. A. Mirji, S. B. Halligudi, N. Mathew, N. E. Jacob, K. R. Patil, A. B. Gaikward, " Adsorption of methanol on mesoporous SBA-15", *Materials Letters*, vol. 61, no. 1, pp. 88-92, 2007; (b)W. G. Shim, J. W. Lee, H. Moon, "Adsorption equilibrium and column dynamics of VOCs on MCM-48 depending on pelletizing pressure", *Microporous and Mesoporous Materials*, vol. 88, pp. 112-125, 2006.

[71] K. Jerbek, Z. Prokop, " Polymer adsorbents for methanol separation from a hydrocarbon stream", *Reactive Polymer*, vol. 18, no. 3, pp. 221-227,1992.

[72] J. Pires, A. Carvalho, M. B. De Carvalho, "Adsorption of volatile organic compounds in Y zeolites and pillared clays", *Microporous and Mesoporous Materials*, vol. 43, no. 3, pp. 277-287, 2001.

[73] L. G. Gordeeva, Y. I. Aristov, "Nanocomposites (salt inside porous matrix) for methanol sorption: design of phase composition and sorption properties, practical applications", *Sorbent: Properties, materials and applications*, Chapter 3, pp109-138.

[74] J. P. Breen and J. R. Ross, "Methanol reforming for fuel-cell applications: development of zirconia-containing Cu–Zn–Al catalysts," *Catalysis Today*, vol. 51, no. 3–4, pp. 521–533, Jul. 1999.

[75] D. Wang, Y. Han, Y. Tan, and N. Tsubaki, "Effect of H_2O on cu-based catalyst in one-step slurry phase dimethyl ether synthesis," *Fuel Processing Technology*, vol. 90, no. 3, pp. 446–451, 2009.

[76] D. Mao, W. Yang, J. Xia, B. Zhang, and G. Lu, "The direct synthesis of dimethyl ether from syngas over hybrid catalysts with sulfate-modified gamma-alumina as methanol dehydration components," *Journal of Molecular Catalysis. A, Chemical*, vol. 250, no. 1–2, pp. 138–144, 2006.

[77] M. Xu, J. H. Lunsford, D. W. Goodman, and A. Bhattacharyya, "Synthesis of dimethyl ether (DME) from methanol over solid-acid catalysts," *Applied Catalysis A, General*, vol. 149, no. 2, pp. 289–301, 1997.

[78] I. Sierra, M. Olazar, A. G. Gayubo, and A. T. Aguayo, "Deactivation of CuO-ZnO-Al_2O_3/ɣ-Al_2O_3 catalyst in the synthesis of Dimethyl Ether," *Ind. Eng. Chem. Res.*, vol. 47, no. 7, pp. 2238–2247, Apr. 2008.

[79] DeWitt, presented at the Global Methanol and MTBE conference, Bankok, 2007, pp. 12–14.

[80] M. Skinner, Master thesis. University of Minnesota, 2010.

[81] C. M. Balonek, J. L. Colby, and L. D. Schmidt, "Millisecond catalytic reforming of monoaromatics over noble metals," *AIChE Journal*, vol. 56, pp. 979-998, 2010.

[82] P. Dauenhauer, J. Salge, and L. Schmidt, "Renewable hydrogen by autothermal steam reforming of volatile carbohydrates," *Journal of Catalysis*, vol. 244, no. 2, pp. 238–247, Dec. 2006.

[83] V. Vishwanathan, K. W. Jun, J. W. Kim, and H. S. Roh, "Vapour phase dehydration of crude methanol to dimethyl ether over Na-modified H-ZSM-5 catalysts," *Applied Catalysis A, General*, vol. 276, no. 1–2, pp. 251–255, 2004.

[84] H. Schulz, "'Coking of zeolites during methanol conversion: Basic reactions of the MTO-, MTP- and MTG processes," *Catalysis Today*, vol. 154, no. 3–4, pp. 183–194, Sep. 2010.

[85] S. Meffe, A. Perkson, and O. Trass, "Coal beneficiation and organic sulfur removal," *Fuel*, vol. 75, no. 1, pp. 25–30, Jan. 1996.

[86] M. Stöcker, "Methanol-to-hydrocarbons: catalytic materials and their behavior," *Microporous and Mesoporous Materials*, vol. 29, no. 1–2, pp. 3–48, Jun. 1999.

[87] B. Traxel and K. Hohn, "Partial oxidation of methanol at millisecond contact times," *Applied Catalysis A: General*, vol. 244, no. 1, pp. 129–140, May 2003.

[88] D. A. Hickman, E. A. Haupfear, and L. D. Schmidt, "Synthesis gas formation by direct oxidation of methane over Rh monoliths," *Catalysis Letters*, vol. 17, no. 3–4, pp. 223–237, Sep. 1993.

[89] G. Panuccio and L. Schmidt, "Increasing olefins by H_2 and CH_4 addition to the catalytic partial oxidation of n-octane," *Applied Catalysis A: General*, vol. 313, no. 1, pp. 63–73, Sep. 2006.

[90] A. Bodke, D. Henning, and L. D. Schmidt, "A comparison of H_2 addition to 3 ms partial oxidation reactions," *Catalysis Today*, vol. 61, no. 1–4, pp. 65–72, Aug. 2000.

[91] A. Bodke, "Oxidative Dehydrogenation of Ethane at Millisecond Contact Times: Effect of H_2 Addition," *Journal of Catalysis*, vol. 191, no. 1, pp. 62–74, Apr. 2000.

[92] R. Horn, K. Williams, N. Degenstein, A. Bitschlarsen, D. Dallenogare, S. Tupy, and L. Schmidt, "Methane catalytic partial oxidation on autothermal Rh and Pt foam catalysts: Oxidation and reforming zones, transport effects, and approach to thermodynamic equilibrium," *Journal of Catalysis*, vol. 249, no. 2, pp. 380–393, Jul. 2007.

[93] F. Yaripour, M. Mollavali, S. M. Jam, and H. Atashi, "Catalytic dehydration of methanol to dimethyl ether catalyzed by aluminum phosphate catalysts," *Energy Fuels*, vol. 23, no. 4, pp. 1896–1900, Apr. 2009.

[94] G. Bercic and J. Levec, "Intrinsic and global reaction rate of methanol dehydration over gamma-alumina pellets," *Industrial & Engineering Chemistry Research*, vol. 31, no. 4, pp. 1035–1040, Apr. 1992.

[95] C. Weber, A. Farwick, F. Benisch, D. Brat, H. Dietz, T. Subtil, and E. Boles, "Trends and challenges in the microbial production of lignocellulosic bioalcohol

fuels," *Applied Microbiology and Biotechnology*, vol. 87, no. 4, pp. 1303–1315, Jun. 2010.

[96] V. García, J. Päkkilä, H. Ojamo, E. Muurinen, and R. L. Keiski, "Challenges in biobutanol production: How to improve the efficiency?," *Renewable and Sustainable Energy Reviews*, vol. 15, no. 2, pp. 964–980, Feb. 2011.

[97] S. Atsumi, T.-Y. Wu, E.-M. Eckl, S. D. Hawkins, T. Buelter, and J. C. Liao, "Engineering the isobutanol biosynthetic pathway in Escherichia coli by comparison of three aldehyde reductase/alcohol dehydrogenase genes," *Applied Microbiology and Biotechnology*, vol. 85, no. 3, pp. 651–657, Jul. 2009.

[98] S. Atsumi, T. Hanai, and J. C. Liao, "Non-fermentative pathways for synthesis of branched-chain higher alcohols as biofuels," *Nature*, vol. 451, no. 7174, pp. 86–89, Jan. 2008.

[99] C. Williams, M. A. Makarova, L. V. Malysheva, E. A. Paukshtis, K. I. Zamaraev, and J. M. Thomas, "Mechanistic studies of the catalytic dehydration of isobutyl alcohol on NaH-ZSM-5," *Journal of the Chemical Society, Faraday Transactions*, vol. 86, no. 20, pp. 3473-3485, 1990.

[100] B. Shi, H. A. Dabbagh, and B. H. Davis, "Catalytic dehydration of alcohols. kinetic isotope effect for the dehydration of t-butanol," *Topics in Catalysis*, vol. 18, pp. 259–264, 2002.

[101] D. Zhang, R. Al-Hajri, S. A. I. Barri, and D. Chadwick, "One-step dehydration and isomerisation of n-butanol to iso-butene over zeolite catalysts," *Chemical Communications*, vol. 46, no. 23, p. 4088-4090, 2010.

[102] J. Houzvicka, "The shape selectivity in the skeletal isomerisation of n-butene to isobutene," *Journal of Catalysis*, vol. 167, no. 1, pp. 273–278, Apr. 1997.

[103] Z. Cheng, "Selective Isomerization of butene to isobutene," *Journal of Catalysis*, vol. 148, no. 2, pp. 607–616, Aug. 1994.

[104] W.-Q. Xu, Y.-G. Yin, S. L. Suib, J. C. Edwards, and C.-L. OYoung, "n-Butene skeletal isomerization to isobutylene on shape selective catalysts: Ferrierite/ZSM-35," *The Journal of Physical Chemistry*, vol. 99, no. 23, pp. 9443–9451, Jun. 1995.

[105] V. Macho, M. Králik, E. Jurecekova, J. Hudec, and L. Jurecek, "Dehydration of C_4 alkanols conjugated with a positional and skeletal isomerisation of the formed C_4 alkenes," *Applied Catalysis A: General*, vol. 214, no. 2, pp. 251–257, Jun. 2001.

[106] J. Q. Bond, D. M. Alonso, D. Wang, R. M. West, and J. A. Dumesic, "Integrated

catalytic conversion of valerolactone to liquid alkenes for transportation fuels," *Science*, vol. 327, no. 5969, pp. 1110–1114, Feb. 2010.

[107] A. Mantilla, F. Tzompantzi, G. Ferrat, A. López-Ortega, S. Alfaro, R. Gómez, and M. Torres, "Oligomerization of isobutene on sulfated titania: Effect of reaction conditions on selectivity," *Catalysis Today*, vol. 107–108, pp. 707–712, Oct. 2005.

[108] R. J. Quann, L. A. Green, S. A. Tabak, and F. J. Krambeck, "Chemistry of olefin oligomerization over ZSM-5 catalyst," *Industrial & Engineering Chemistry Research*, vol. 27, no. 4, pp. 565–570, Apr. 1988.

[109] D. S. J. Jones and P. R. Pujado, "Handbook of petroleum processing," Spingerlink, 2006, pp. 356–360.

[110] H. Sun and L. D. Schmidt, "Methanol dehydration to dimethyl ether in a staged autothermal millisecond residence time reactor," *Applied Catalysis A: General*, vol. 404, pp. 81-86, Jul. 2011.

[111] R. J. J. Nel and A. de Klerk, "Fischer−tropsch aqueous phase refining by catalytic alcohol dehydration," *Industrial & Engineering Chemistry Research*, vol. 46, no. 11, pp. 3558–3565, May 2007.

[112] J. Kruger, Ph.D thesis. pp. 48-54, pp.154-175, University of Minnesota, Aug-2011.

[113] B. C. Michael, D. N. Nare, and L. D. Schmidt, "Catalytic partial oxidation of ethane to ethylene and syngas over Rh and Pt coated monoliths: Spatial profiles of temperature and composition," *Chemical Engineering Science*, vol. 65, no. 12, pp. 3893–3902, Jun. 2010.

[114] B. C. Michael, A. Donazzi, and L. D. Schmidt, "Effects of H_2O and CO_2 addition in catalytic partial oxidation of methane on Rh," *Journal of Catalysis*, vol. 265, no. 1, pp. 117–129, Jul. 2009.

[115] D. Zhang, S. A. I. Barri, and D. Chadwick, "n-Butanol to iso-butene in one-step over zeolite catalysts," *Applied Catalysis A: General*, vol. 403, no. 1–2, pp. 1–11, Aug. 2011.

[116] M. Guisnet, "Skeletal Isomerization ofn-Butenes I. Mechanism of n-Butene Transformation on a Nondeactivated H-Ferrierite Catalyst," *Journal of Catalysis*, vol. 158, no. 2, pp. 551–560, Feb. 1996.

[117] B. de Ménorval, P. Ayrault, N. S. Gnep, and M. Guisnet, "n-Butene skeletal isomerization over HFER zeolites: Influence of Si/Al ratio and of carbonaceous deposits," *Applied Catalysis A: General*, vol. 304, pp. 1–13, May 2006.

[118] M. Makarova, “Dehydration of n-butanol on zeolite H-ZSM-5 and amorphous aluminosilicate: setailed mechanistic study and the effect of pore confinement,” *Journal of Catalysis*, vol. 149, no. 1, pp. 36–51, Sep. 1994.

[119] M. A. Makarova, C. Williams, K. I. Zamaraev, and J. M. Thomas, “Mechanistic study of sec-butyl alcohol dehydration on zeolite H-ZSM-5 and amorphous aluminosilicate,” *Journal of the Chemical Society, Faraday Transactions*, vol. 90, no. 14, p. 2147-2153, 1994.

[120] M. A. Makarova, E. A. Paukshtis, J. M. Thomas, C. Williams, and K. I. Zamaraev, “In situ FTIR kinetic studies of diffusion, adsorption and dehydration reaction of tert-butanol on zeolite NaH-ZSM-5,” *Catalysis Today*, vol. 9, no. 1–2, pp. 61–68, Mar. 1991.

[121] C. Williams, “Kinetic studies of catalytic dehydration of tert-butanol on zeolite NaHZSM-5,” *Journal of Catalysis*, vol. 127, no. 1, pp. 377–392, Jan. 1991.

[122] H. Chiang and A. Bhan, “Catalytic consequences of hydroxyl group location on the rate and mechanism of parallel dehydration reactions of ethanol over acidic zeolites,” *Journal of Catalysis*, vol. 271, no. 2, pp. 251–261, May 2010.

[123] H. Chiang and A. Bhan, “Catalytic consequences of hydroxyl group location on the kinetics of n-hexane hydroisomerization over acidic zeolites,” *Journal of Catalysis*, vol. 283, no. 1, pp. 98–107, Oct. 2011.

[124] J. Macht, R. T. Carr, and E. Iglesia, “Consequences of acid strength for isomerization and elimination catalysis on solid acids,” *Journal of the American Chemical Society*, vol. 131, no. 18, pp. 6554–6565, May 2009.

[125] C. K. Gonçalves, J. A. S. Tenório, Y. A. Levendis, and J. B. Carlson, “Emissions from premixed combustion of polystyrene,” *Energy & Fuels*, vol. 22, no. 1, pp. 354–362, Jan. 2008.

[126] D. S. Scott, S. R. Czernik, J. Piskorz, and D. S. A. G. Radlein, “Fast pyrolysis of plastic wastes,” *Energy & Fuels*, vol. 4, no. 4, pp. 407–411, Jul. 1990.

[127] G. S. Darivakis, J. B. Howard, and W. A. Peters, “Release rates of condensables and total volatiles from rapid devolatilization of polyethylene and polystyrene” *Combustion Science and Technology*, vol. 74, no. 1–6, pp. 267–281, Nov. 1990.

[128] H. Bockhorn, A. Hornung, and U. Hornung, “Gasification of polystyrene as initial step in incineration, fires, or smoldering of plastics,” *Symposium (International) on Combustion*, vol. 27, no. 1, pp. 1343–1349, Jan. 1998.

[129] W. Kaminsky, M. Predel, and A. Sadiki, “Feedstock recycling of polymers by pyrolysis in a fluidised bed,” *Polymer Degradation and Stability*, vol. 85, no. 3, pp. 1045–1050, Sep. 2004.

[130] P. T. Williams and E. A. Williams, “Interaction of plastics in mixed-plastics pyrolysis,” *Energy & Fuels*, vol. 13, no. 1, pp. 188–196, Jan. 1999.

[131] J. S. Kruger, D. C. Rennard, T. R. Josephson, and L. D. Schmidt, “Effect of functional groups on autothermal partial oxidation of bio-oil. Part 2: role of homogeneous and support-mediated reactions,” *Energy & Fuels*, vol. 25, no. 7, pp. 3172–3185, Jul. 2011.

[132] G. J. Panuccio and L. D. Schmidt, “Species and temperature profiles in a differential sphere bed reactor for the catalytic partial oxidation of n-octane,” *Applied Catalysis A: General*, vol. 332, no. 2, pp. 171–182, Nov. 2007.

[133] K. L. Hohn and L. D. Schmidt, “Partial oxidation of methane to syngas at high space velocities over Rh-coated spheres,” *Applied Catalysis A: General*, vol. 211, no. 1, pp. 53–68, Mar. 2001.

[134] G. A. Deluga, “Renewable hydrogen from ethanol by autothermal reforming,” *Science*, vol. 303, no. 5660, pp. 993–997, Feb. 2004.

[135] J. Warnatz, M. D. Allendorf, R. J. Kee, and M. E. Coltrin, “A model of elementary chemistry and fluid mechanics in the combustion of hydrogen on platinum surfaces,” *Combustion and Flame*, vol. 96, no. 4, pp. 393–406, Mar. 1994.

[136] A. Bitsch-Larsen, N. J. Degenstein, and L. D. Schmidt, “Effect of sulfur in catalytic partial oxidation of methane over Rh–Ce coated foam monoliths,” *Applied Catalysis B: Environmental*, vol. 78, no. 3–4, pp. 364–370, Feb. 2008.

[137] A. S. Bodke, “High selectivities to ethylene by partial oxidation of ethane,” *Science*, vol. 285, no. 5428, pp. 712–715, Jul. 1999.

[138] D. Castner, B. Sexton, and G. Somorjai, “Leed and thermal desorption studies of small molecules (H_2, O_2, CO, CO_2, NO, C_2H_4, C_2H_2 AND C) chemisorbed on the rhodium (111) and (100) surfaces,” *Surface Science*, vol. 71, no. 3, pp. 519–540, Feb. 1978.

[139] J. L. Colby, T. Wang, and L. D. Schmidt, “Steam reforming of benzene as a model for biomass-derived syngas tars over Rh-based cCatalysts,” *Energy & Fuels*, vol. 24, no. 2, pp. 1341–1346, Feb. 2010.

[140] J. R. Pereira and P. H. Calderbank, “Mass transfer in the spinning catalyst basket

reactor," *Chemical Engineering Science*, vol. 30, no. 2, pp. 167–175, Feb. 1975.

[141] C.-F. Chang and S.-C. Lee, "Adsorption behavior of pesticide methomyl on activated carbon in a high gravity rotating packed bed reactor," *Water Research*, vol. 46, no. 9, pp. 2869–2880, Jun. 2012.

[142] X. Peng, "Kinetic understanding of the chemical synergy under LPDMETM conditions-once-through applications," *Chemical Engineering Science*, vol. 54, no. 13–14, pp. 2787–2792, Jul. 1999.

[143] J. Erena, R. Garona, J. Arandes, A. T. Aguayo, and J. Bilbao, "Direct synthesis of dimethyl ether from (H_2+CO) and (H_2+CO_2) feeds. effect of feed composition," *International Journal of Chemical and Reactor Engineering*, vol. 3, no. 3, pp. 1295-1312, 2005.

[144] S. P. Naik, H. Du, H. Wan, V. Bui, J. D. Miller, and W. W. Zmierczak, "A comparative study of ZnO-CuO-Al_2O_3/SiO_2-Al_2O_3 composite and hybrid catalysts for direct synthesis of dimethyl ether from syngas," *Ind. Eng. Chem. Res.*, vol. 47, no. 23, pp. 9791–9794, Dec. 2008.

[145] J. Kim, "DME synthesis from synthesis gas on the admixed catalysts of Cu/ZnO/Al_2O_3 and ZSM-5," *Applied Catalysis A: General*, vol. 264, no. 1, pp. 37–41, Jun. 2004.

[146] V. Vishwanathan, K.-W. Jun, J.-W. Kim, and H.-S. Roh, "Vapour phase dehydration of crude methanol to dimethyl ether over Na-modified H-ZSM-5 catalysts," *Applied Catalysis A: General*, vol. 276, no. 1–2, pp. 251–255, Nov. 2004.

[147] Y. Lv, T. Wang, C. Wu, L. Ma, and Y. Zhou, "Scale study of direct synthesis of dimethyl ether from biomass synthesis gas," *Biotechnology Advances*, vol. 27, no. 5, pp. 551-554, 2009.

[148] Y. Li, T. Wang, X. Yin, C. Wu, L. Ma, H. Li, Y. Lv, and L. Sun, "100t/a-Scale demonstration of direct dimethyl ether synthesis from corncob-derived syngas," *Renewable Energy*, vol. 35, no. 3, pp. 583–587, Mar. 2010.

[149] Q. Ge, Y. Huang, F. Qiu, and S. Li, "Bifunctional catalysts for conversion of synthesis gas to dimethyl ether," *Applied Catalysis A, General*, vol. 167, no. 1, pp. 23–30, 1998.

[150] O. S. Joo, K. D. Jung, and S. H. Han, "Modification of H-ZSM-5 and gamma-alumina with formaldehyde and its application to the synthesis of dimethyl ether from syn-gas," *Bullentin-Korean Chemical Society*, vol. 23, no. 8, pp. 1103–1105, 2002.

[151] M. Mollavali, F. Yaripour, S. Mohammadi-Jam, and H. Atashi, “Relationship between surface acidity and activity of solid-acid catalysts in vapour phase dehydration of methanol,” *Fuel Processing Technology*, vol. 90, no. 9, pp. 1093–1098, 2009.

[152] J. Erena, R. Garona, J. Arandes, A. Aguayo, and J. Bilbao, “Effect of operating conditions on the synthesis of dimethyl ether over a CuO-ZnO-Al_2O_3/NaHZSM-5 bifunctional catalyst,” *Catalysis Today*, vol. 107–108, pp. 467–473, Oct. 2005.

[153] X. D. Peng, A. W. Wang, B. A. Toseland, and P. J. A. Tijm, “Single-step syngas-to-dimethyl ether processes for optimal productivity, minimal emissions, and natural gas-eerived syngas,” *Ind. Eng. Chem. Res.*, vol. 38, no. 11, pp. 4381–4388, Nov. 1999.

[154] J. Erena, J. M. Arandes, R. Garona, A. G. Gayubo, and J. Bilbao, “Study of the preparation and composition of the metallic function for the selective hydrogenation of CO_2 to gasoline over bifunctional catalysts,” *J. Chem. Technol. Biotechnol.*, vol. 78, no. 2–3, pp. 161–166, Feb. 2003.

[155] V. M. Mysov, S. I. Reshetnikov, V. G. Stepanov, and K. G. Ione, “Synthesis gas conversion into hydrocarbons (gasoline range) over bifunctional zeolite-containing catalyst: experimental study and mathematical modelling,” *Chemical Engineering Journal*, vol. 107, no. 1–3, pp. 63–71, 2005.

[156] J. Erena, J. M. Arandes, J. Bilbao, A. T. Aguayo, and H. I. de Lasa, “Study of physical mixtures of Cr_2O_3- ZnO and ZSM-5 catalysts for the transformation of syngas into liquid hydrocarbons,” *Ind. Eng. Chem. Res*, vol. 37, no. 4, pp. 1211–1219, 1998.

[157] J. Ereña, “Conversion of syngas to liquid hydrocarbons over a two-component (Cr2O3–ZnO and ZSM-5 zeolite) catalyst: Kinetic modelling and catalyst deactivation,” *Chemical Engineering Science*, vol. 55, no. 10, pp. 1845–1855, May 2000.

[158] C. Chang, “A kinetic model for methanol conversion to hydrocarbons,” *Chemical Engineering Science*, vol. 35, no. 3, pp. 619–622, 1980.

[159] M. Fujiwara, R. Kieffer, H. Ando, and Y. Souma, “Development of composite catalysts made of Cu-Zn-Cr oxide/zeolite for the hydrogenation of carbon dioxide,” *Applied Catalysis A, General*, vol. 121, no. 1, pp. 113–124, 1995.

[160] M. Bjørgen, F. Joensen, M. Spangsberg Holm, U. Olsbye, K.-P. Lillerud, and S. Svelle, “Methanol to gasoline over zeolite H-ZSM-5: Improved catalyst performance by treatment with NaOH,” *Applied Catalysis A: General*, vol. 345, no.

1, pp. 43–50, Jul. 2008.

[161] H. Zaidi, “Catalytic conversion of methanol to gasoline range hydrocarbons,” *Catalysis Today*, vol. 96, no. 3, pp. 155–160, Oct. 2004.

[162] H. Schiweck, M. Munir, K. M. Rapp, B. Schneider, and M. Vogel, “Carbohydrates as organic saw materials. New developments in the use of sucrose as an industrial bulk chemical,” Germany: Wiley-VCH, 1991, pp. 57–94.

[163] B. F. M. Kuster, “5-Hydroxymethylfurfural (HMF). a review focussing on its manufacture,” *Starch - Stärke*, vol. 42, no. 8, pp. 314–321, 1990.

[164] J. Lewkowski, “Synthesis, chemistry and application of 5-hydroxymethyl-furfural and its derivatives,” *Arkivoc*, vol. i, pp. 17–54, 2001.

[165] H. E. van Dam, A. P. G. Kieboom, and H. van Bekkum, “The conversion of fructose and glucose in acidic media: formation of hydroxymethylfurfural,” *Starch - Stärke*, vol. 38, no. 3, pp. 95–101, 1986.

[166] A. I. Torres, P. Daoutidis, and M. Tsapatsis, “Continuous production of 5-hydroxymethylfurfural from fructose: a design case study,” *Energy & Environmental Science*, vol. 3, no. 10, pp. 1560-1572, 2010.

[167] E. S. Olson, R. K. Sharma, and T. R. Aulich, “Higher-alcohols biorefinery: improvement of catalyst for ethanol conversion,” *Applied Biochemistry and Biotechnology*, vol. 115, no. 1–3, pp. 0913–0932, 2004.

[168] P. L. Burk, R. L. Pruett, and K. S. Campo, “The rhodium-promoted guerbet reaction,” *Journal of Molecular Catalysis*, vol. 33, no. 1, pp. 1–14, Oct. 1985.

[169] P. L. Burk, R. L. Pruett, and K. S. Campo, “The rhodium-promoted guerbet reaction,” *Journal of Molecular Catalysis*, vol. 33, no. 1, pp. 15–21, Oct. 1985.

[170] W. Ueda, T. Kuwabara, T. Ohshida, and Y. Morikawa, “A low-pressure guerbet reaction over magnesium oxide catalyst,” *Journal of the Chemical Society, Chemical Communications*, no. 22, pp. 1558-1559, 1990.

[171] T. Tsuchida, S. Sakuma, T. Takeguchi, and W. Ueda, “Direct synthesis of n-butanol from ethanol over nonstoichiometric hydroxyapatite,” *Industrial & Engineering Chemistry Research*, vol. 45, no. 25, pp. 8634–8642, Dec. 2006.

[172] T. Tsuchida, J. Kubo, T. Yoshioka, S. Sakuma, T. Takeguchi, and W. Ueda, “Reaction of ethanol over hydroxyapatite affected by Ca/P ratio of catalyst,” *Journal of Catalysis*, vol. 259, no. 2, pp. 183–189, Oct. 2008.

[173] N. Miskolczi, “Chapter: kinetic model of the chemical and catalytic recycling of waste polyethylene into fuels,” in *Feedstock Recycling and Pyrolysis of Easte Plastics: Converting Waste Plastics into Diesel and Other Fuels*, John Wiley & Sons., 2006, pp. 225–247.

[174] K.-H. Lee, “Chapter: thermal and catalytic degradation of waste HDPE,” in *Feedstock Recycling and Pyrolysis of Easte Plastics: Converting Waste Plastics into Diesel and Other Fuels*, John Wiley & Sons., 2006, pp. 129–160.

[175] C. M. Balonek, Ph.D Thesis, pp.65-83, University of Minnesota, 2011.

[176] C. G. Jung and A. Fontana, “Production of gaseous and liquid fuels by pyrolysis and gasification of plastics: tehnology approach,” in *Feedstock Recycling and Pyrolysis of Easte Plastics: Converting Waste Plastics into Diesel and Other Fuels*, John Wiley & Sons., 2006, pp. 251–283.

[177] P. T. Williams, “Yield and composition of gases and oils/waxes from the feedstock recycling of waste plastic,” in *Feedstock Recycling and Pyrolysis of Easte Plastics: Converting Waste Plastics into Diesel and Other Fuels*, John Wiley & Sons., 2006, pp. 285–313.

[178] W. Kaminsky and J. Franck, “Monomer recovery by pyrolysis of poly(methyl methacrylate) (PMMA),” *Journal of Analytical and Applied Pyrolysis*, vol. 19, pp. 311–318, Jul. 1991.

[179] H. Arisawa and T. B. Brill, “Kinetics and mechanisms of flash pyrolysis of poly(methyl methacrylate) (PMMA),” *Combustion and Flame*, vol. 109, no. 3, pp. 415–426, May 1997.

[180] M. Bradford, “Preparation, characterization and application of Cr_2O_3/ZnO catalysts for methanol synthesis,” *Fuel Processing Technology*, vol. 83, no. 1–3, pp. 11–25, Sep. 2003.

[181] G. Moradi, J. Ahmadpour, M. Nazari, and F. Yaripour, “Effects of feed composition and space velocity on direct synthesis of dimethyl ether from syngas,” *Ind. Eng. Chem. Res.*, vol. 47, no. 20, pp. 7672–7679, Oct. 2008.

Appendix A

Calculations for methanol synthesis in a multifunctional reactor

Calculations of Presence of Radial Diffusion from Condenser to Catalyst Bed

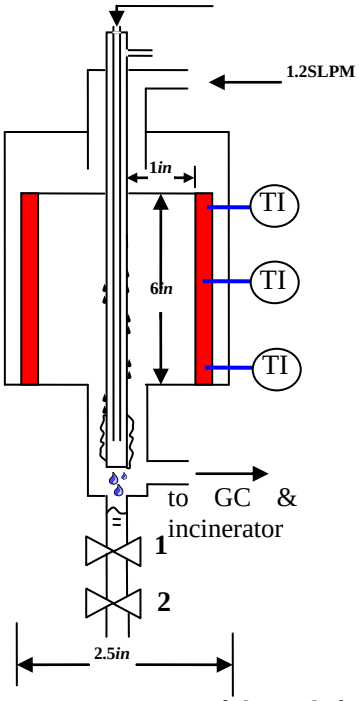

Figure A1 Geometry of the multifunctional reactor, shade: catalyst. TI: thermocouples.

Estimate diffusion coefficient (50 bar, 230 ºC, gas phase):

$$D \propto T^{3/2}P^{-1}; D = \frac{0.1cm^2/s * (\frac{230+273}{25+273})^{3/2}}{50/1} = 0.00439cm^2/s$$

The distance from condenser to catalyst bed: $1inch = 2.54cm$

Axial velocity near condenser

$$= \frac{\text{volumetric flow rate (50 bar, approximately 50 °C)}}{\text{cross sectional area}}$$

$$= \frac{(1.2L/\min) * (\frac{273+50}{273})/(50/1)}{\pi * (\frac{2.5in}{2} * 0.254\frac{dm}{in})^2} = 0.089709\frac{dm}{\min} = 0.014951\frac{cm}{s}$$

There were temperature gradients in the axial and radial directions in the reactor after condenser was turned on. The estimated average temperature in the reactor is 180ºC. The density of reactants was around 40 kg/m^3 and the viscosity was around 1.612 kg/m.s. These values are calculated by the online density and viscosity calculator.

$$\text{Re} = \frac{\rho vD}{\mu} = \frac{40kg/m^3 * 0.01495cm/s * 2.5in}{1.612kg/m.s} = 0.0003$$

$$E = \frac{v^2d^2}{192D} = \frac{(0.014951cm/s)^2(2.5in)^2}{192 * 0.00439cm^2/s} = 0.01069cm^2/s$$

Since Reynolds number is small, dispersion is very small and it is mainly due to the diffusion. The calculated dispersion and diffusion are comparable as well. E is used to calculate the time scale of reactants reaching the catalyst bed from condenser in the radial direction.

$$time = \frac{l^2}{E} = \frac{(2.54cm)^2}{0.01069cm^2/s} = 10.0586\min$$

Height of the catalyst bed = 6 *inch* = 15.24 *cm*

Time to reach the bottom at the reactor = $\frac{15.24cm}{0.014951cm/s} = 16.99\min$

The time scale of reactants reaching catalyst bed from condenser is comparable to the

time scale of reactants reaching the bottom of the reactor. This shows it is possible to have radial diffusion back to the catalyst bed form condenser. However, this is just a rough estimation and the flow pattern in the reactor is non-ideal. There might be channeling in the reactor which contributes to increase the conversion after the condenser is turned on.

Appendix B

Calculations of Methanol dehydration in an Autothermal Staged Reactor

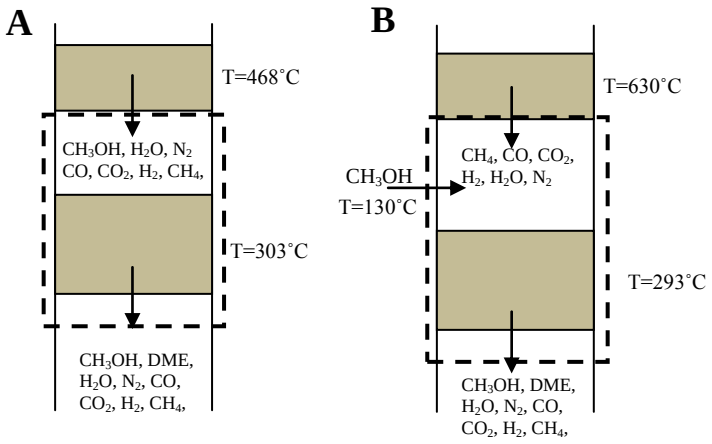

B1 Control volume for methanol dehydration in autothermal staged reactor**.** (A) methanol top feed configuration, (B) methanol side feed configuration.

The dash line is the control volume (CV), streams coming in and out the CV are labeled in the figure. The energy lost is 9.42 J/s and 10.43 J/s for top feed and side feed configuration, respectively. The energy flux is 0.368 and 0.337 J/cm^{2}·s for top feed and side feed configuration. The equations are listed below.

$$\frac{dU_{\Omega}}{dt} = \dot{Q} + \dot{W} + \sum_{k=1}^{Nin}\sum_{i=1}^{Ns} \dot{n}_{ik}^{in}\overline{H}_{ik}^{in} - \sum_{k=1}^{N_{out}}\sum_{i=1}^{Ns} \dot{n}_{ik}^{out}\overline{H}_{ik}^{out} + \Delta H_{rxn} rV \quad (5)$$

$$-\dot{Q} = \sum_{k=1}^{Nin}\sum_{i=1}^{Ns} \dot{n}_{ik}^{in}\overline{H}_{ik}^{in} - \sum_{k=1}^{N_{out}}\sum_{i=1}^{Ns} \dot{n}_{ik}^{out}\overline{H}_{ik}^{out} + \Delta H_{rxn}\Delta\dot{n}_{CH_3OH} \quad (6)$$

$$\overline{H}_{ik} = \tilde{H}_{ik} \quad (7)$$

$$-\dot{Q} = \sum_{k=1}^{Nin}\sum_{i=1}^{Ns} \dot{n}_{ik}^{in}\tilde{H}_{ik}^{in} - \sum_{k=1}^{N_{out}}\sum_{i=1}^{Ns} \dot{n}_{ik}^{out}\tilde{H}_{ik}^{out} + \Delta H_{rxn}\Delta\dot{n}_{CH_3OH} \quad (8)$$

$$-\dot{Q} = \sum_{k=1}^{Nin}\sum_{i=1}^{Ns} \dot{n}_{ik}^{in}(\Delta H_{f298} + \int_{T_{298}}^{T_{final}} C_p(T)dT)_{ik}^{in} - \sum_{k=1}^{N_{out}}\sum_{i=1}^{Ns} \dot{n}_{ik}^{out}(\Delta H_{f298} + \int_{T_{298}}^{T_{final}} C_p(T)dT)_{ik}^{out} + \Delta H_{rxn}\Delta\dot{n}_{CH_3OH} \quad (9)$$

U_{Ω} :Total energy across the system boundary

$\dot{Q}$:Heat flow rate across the system boundary

$\dot{W}$:Work across the system boundary per time

$\overline{H}_{ik}^{in}$:Partial moalr enthylpy of species i in stream k coming in the system

$\tilde{H}_{ik}^{in}$:Pure species molar enthalpy of species i in stream k coming in the system

$\dot{n}_{ik}^{in}$:Molar flow rate of species I in stream k coming in the system

ΔH_{298}: Heat of formation at 25˚C (298K)

$\Delta\dot{n}_{CH_3OH}$: CH_3OH reacted in the reactor (molar flow rate)

$C_p(T)$: Heat capaticity of pure species as function of temperature, corresponding calue was obtained from Perry's chemical engineering hand

Appendix C

Catalyst Preparation Methods

Catalysts Preparation for Direct Gasoline Synthesis from Syngas

Cr_2O_3-ZnO catalyst for methanol synthesis reaction is synthesized as reported by co-precipitation method [180]. $Cr(NO_3)_3 \cdot 9H_2O$ and $Zn(NO_3)_2 \cdot 3H_2O$ is added to deionized water to form 0.14 M cation solution. This solution is added into a stirred beaker of deionized water together with a 0.5 M solution of $(NH_4)_2CO_3$ at 65°C and the pH value is maintained at $7.0 \leq pH \leq 7.5$. The solid is recovered by filtration. It is washed with deionnized water for several times and dried at 110°C. The Cr_2O_3-ZnO catalyst is calcined at 200°C for 2 h. The ZSM-5 part is available commercially and should be purchased.

HZSM-5 (Si/Al=46, 154) could be purchased commercially from Sud-Chemie Co. (sample no. 304 H/06) [181]. HZSM-5 is treated with 0.2 M NaOH solution (about 20 ml/g) for 4 h at 75ºC, followed by washing with deionized water for 1 h at 75 ºC. Sample is filtered after first 4 h and is treated with NaOH at the same condition for another 4 h. The solution is dried at room temperature overnight and the sample is ion exchanged with a 1 M NH_4NO_3 for 3X2h at 75ºC. The sample is calcined at 550ºC for 24 h [160].

ZnO doped HZSM-5 is prepared by standard impregnation method. NH_4OH solution is added to HZSM-5 in the solution of zinc nitrate to increase pH to 5. The solution is stirred for 12 h. The catalyst is transferred to a rotary evaporator to remove excess water. The sample is dried at 120ºC for 12 h. The product is calcined at 550ºC for 5 h [161].